

國立交通大學

電機學院 電子與光電學程

碩 士 論 文

利用大氣電漿對有機半導體
之介電層表面做改質研究

**Modify Surface of dielectric layer on polymer thin-film
transistors by atmospheric-pressure Plasma technology**

研 究 生：洪柏誠

指 導 教 授：張國明 教授

中 華 民 國 一 百 年 七 月

利用大氣電漿對有機半導體
之介電層表面做改質研究

**Modify Surface of dielectric layer on polymer thin-Film
transistors by atmospheric-pressure plasma technology**

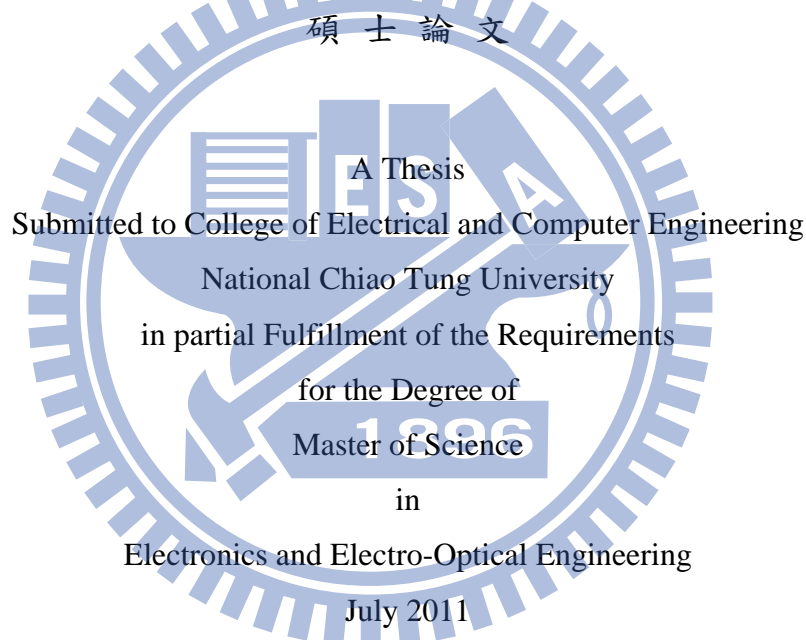
研究生：洪柏誠

Student：Hung Po Cheng

指導教授：張國明

Advisor：Kow-Ming Chang

國立交通大學
電機學院 電子與光電學程
碩士論文



Hsinchu, Taiwan, Republic of China

中華民國一百年七月

利用大氣電漿對有機半導體之介電層表面做改質研究

學生：洪柏誠

指導教授：張國明 博士

國立交通大學 電機學院 電子與光電學程 碩士班

摘 要

本論文研製之利用旋塗方式沉積有機薄膜電晶體對於元件製作有大面積且低成本的好處。由於有機薄膜電晶體的效能跟半導體與介電層之間的介面特性有很大的關係，所以此篇論文的研究目標是藉控制半導體與介電層之間的化學特性，並呈現有機薄膜電晶體的改良特性。而因為二氧化矽的製作及介面改質容易，在此我們選擇熱氧化方式的二氧化矽作為我們的介電層。高規則度聚(3-烷基噻吩P₃HT)具有較高的結晶排列特性，能夠提供薄膜電晶體元件較高的電子遷移率，因此選用作為元件半導體層。經由六甲基二矽氮烷的自組裝層所處理的氧化層介面，P₃HT薄膜電晶體將獲得明顯的改善。我們將使用常壓式電漿來實現介面處理。而常壓電漿系統是可使用在大氣壓之下，同時製程溫度在 120 度以下。在本文可以看到這些表面處理過後的電氣特性。處理過後的臨界電壓可被降至-9 伏特以內，載子遷移率也由原先的 $1.9 \times 10^{-3} \text{cm}^2/\text{Vs}$ 提升至 $2.62 \times 10^{-2} \text{cm}^2/\text{Vs}$ 。在本文中，可驗證常壓式電漿系統，可提供低溫且高效率的有機薄膜電晶體介面改質製程。

Modify Surface of dielectric layer on polymer thin-Film transistors by atmospheric-pressure plasma technology

student : Hung Po Cheng

Advisors : Dr. Kow-Ming Chang

Degree Program of Electrical and Computer Engineering
National Chiao Tung University

ABSTRACT

A procedure is using the spin coat way twists the organic thin film transistor can gain the advantage which is large area and lower cost in manufacturing. Because there is a close relations among the organic thin film transistor's potency, the semiconductor and the dielectric level's interface characteristic.

Therefore the research objective of the study is to present the improvement characteristic of the organic thin film transistor by the affiliation control semiconductor and the dielectric level chemical characteristic. And because the silicon dioxide manufacture and the interface change the nature is easy, we choose the thermal oxidization, the silicon dioxide, to be our dielectric level. High regioregularity poly(3-hexylthiophene) has the high crystallization arrangement characteristic, will provide the thin transistor part high electronic mobility, therefore it is selected to be the part semiconductor level. Through hexamethyldisilazane (HMDS) the oxide layer interface which will process from the assembly level institute, the P3HT thin film transistor will obtain the distinct improvement. We will use the to atmospheric-pressure plasma technology (APPT) to realize interface processing. And atmospheric-pressure plasma technology (APPT) can be used under the atmospheric pressure, simultaneous regulation temperature below 120 °C. May see these surface treatment from now on electrical specification in this article. Processing from now on threshold voltage may drop to the - 9 volts, field-effect mobility also to promote by original $1.9 \times 10^{-3} \text{cm}^2/\text{Vs}$ to $2.62 \times 10^{-2} \text{cm}^2/\text{Vs}$. That can confirm the atmospheric pressure plasma system, can provide the low temperature, and the high efficiency's organic thin film transistor interface to change the nature system regulation.

Acknowledgements

首先，我要感謝指導教授張國明老師，老師認真的教學精神和開明的教學態度，使我這幾幾年研究生涯獲益匪淺，在此致上最深的謝意。

謝謝黃士軒學長在碩士班幾年間給予我的建議及協助，使我的實驗能順利完成。也要謝謝張庭嘉學長、黃菘宏學長、林志祥學長、呂成家同學，有了他們的協助及指導，使得研究能夠更加完整。

感謝我的口試委員：王水進老師、鄧一中老師、吳建宏老師，由於你們的指導，使我的論文內容更加完備。

感謝所有指導過我的老師，學長，同學，雖然我們相識不久，但是你們的熱情，讓我感覺到交通大學這個大家庭，是充滿溫暖的，不單單只是求學的地方。

謝謝交大奈米中心、國家奈米實驗室提供各種機台設備，讓我可以進行實驗；同時感謝所有工程師的技術指導。

最後，更感謝我的父母，洪建和先生與吳英祝女士，感謝他們對我從小到大的養育及栽培，在生活上給我無微不至的關心，讓我得以全心完成學業。我相信他們會以我為榮。

Contents

Chinese Abstract	i
English Abstract	ii
Acknowledgements	iii
Contents	iv
Table Captions	vi
Figure Captions	vii
Chapter 1 Introduction	1
1.1 General Background and Motivation	1
1.2 Thesis Organization	3
Chapter 2 Property of P ₃ HT	6
2.1 Introduction of Poly(3-hexylthiophene) P ₃ HT	6
2.1.1 P ₃ HT molecular structure	6
2.1.2 Conduction Mechanism	7
2.1.3 P ₃ HT alignment	8
2.2 Solution processed deposition	9
2.2.1 OTFT method manufacture	9
2.2.2 The Motivation for Spin-Coat	10
2.2.3 Polymer morphology and resolver function	11
2.3 Contact Resistance of P ₃ HT OTFT	12
2.4 Operation of Organic Thin Film Transistors	13
Chapter 3 Influence of APPT for OTFT	24
3.1 Oxide compound surface revision	24
3.2 Introduction of APPT	25
3.2.1 Introduction of plasma	25
3.2.2 Applications of APPT	26
3.2.3 Surface modification by plasma	27
3.3 Fabrication of OTFT	30
3.4 Determination of Thershold voltage and Mobility	31
3.5 Results and discussion	31
3.5.1 The influence of APPT	32
3.5.2 Spin-coating and evaporated of HMDS-treated SiO ₂	34

3.5.3 Hysteresis	35
3.5.4 Anomalous leakage	37
3.5.5 Crystallization behavior of P ₃ HT	37
3.5.6 XRD and UV-vis for highly oriented crystals of P ₃ HT	38
Chapter 4 Conclusions and Future work	77
4.1 Conclusions	79
4.2 Future work	81
4.2.1 In-situ passivation layer for protecting the P3HT film	81
4.2.2 Novel method for depositing P3HT thin films	82
4.2.3 Thermal stability of P ₃ HT OTFT	82
4.2.4 Use APPT Grows SiO ₂ and the surface treatment	82
References	83



Table Captions

Chapter 1

Table 1-1 Highest field-effect mobility (μ) values measured from OTFT as reported in the literature annually from 1986 through 2000[12].

Chapter 2

Table 2-1:Field-effect mobility and ON/OFF ratio of samples prepared from different solvents and process condition [14]. Condition 1, cast , vacuum pumped for 24 h; condition 2, spin-coated; condition 3, treated with NH_3 for 10 h; condition 4, heated to $100\text{ }^\circ\text{C}$ under N_2 for 5 min; condition 5, heated to $150\text{ }^\circ\text{C}$ under N_2 for 35 min.

Chapter 3

Table 3-1:Electrical parameters of the OTFTs in this study.

Table 3-2:Comparison of contact angle and surface roughness with different scanning times by APPT

Table 3-3:The different methods of surface treatment

Table 3-4:The different methods of surface treatment

Table 3-5: T_m and ΔH of P_3HT in Run first and second time with difference pre-heating temperature.

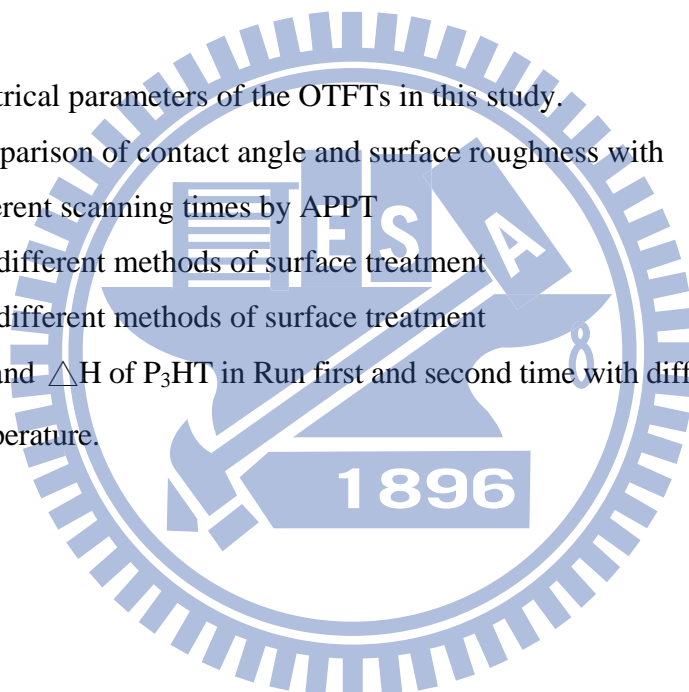


Figure Captions

Chapter 1

Figure 1-1: Semilogarithmic plot of the highest field-effect mobility (μ)

Reported for OTFT fabricated from the most promising polymeric and oligomeric semiconductors versus year from 1986 to 2000[12]

Chapter 2

Figure 2-1: The structure of the polymer chain of P₃HT

Figure 2-2: Two different orientations of ordered P₃HT (a) Edge-on orientation
(b) Face-on orientation

Figure 2-3: The molecular structure of P₃HT s for High RR (d_{b-b}^{100} and d_{b-b}^{100} are the a-direction and b-direction chain-stacking spacings, respectively) The a-direction and b-direction are parallel and perpendicular to the thiophene ring plane, respectively (see the chemical structures within the ovals as well as the schematic illustration for lamella folding and ordering on a substrate).

Figure 2-4: (a) charge carrier transport in conjugated polymers (b) charge transport mechanisms in solid

Figure 2-5: Schematic of operation of organic thin film transistor, showing a lightly doped semiconductor; + indicates a positive charge in semiconductor; - indicates a negatively charge in semiconductor. (a) No-bias (b) Depletion mode (c) Accumulation mode (d) Non-uniform charge density (e) Pinch-off of channel (f) and (g) Growth of the depletion zone

Chapter 3

Figure 3-1: (a) The structure of APPT (b) The diagram of plasma surface treatment

Figure 3-2: (a) APP system of ITRI (b) The other APP systems

Figure 3-3: Two basic structures of OTFT

Figure 3-4: Process flow of top-contact OTFT

Figure 3-5: Surface treatment of APPT HMDS 1 for OTFT (a) I_D - V_G curve and (b) I_D - V_D curve (W/L = 2000 μ m/500 μ m)

Figure 3-6: Surface treatment of APPT HMDS 2 for OTFT (a) I_D - V_G curve and (b) I_D - V_D curve (W/L = 2000 μ m/500 μ m)

Figure 3-7: Surface treatment of APPT HMDS 4 for OTFT (a) I_D - V_G curve and (b) I_D - V_D curve (W/L = 2000 μ m/500 μ m)

Figure 3-8:Surface treatment of APPT HMDS 8 for OTFT(a) I_D-V_G curve (b) I_D-V_D curve ($W/L = 2000 \text{ um}/500 \text{ um}$)

Figure 3-9 :The comparison of (a), (b) I_D-V_G and (c), (d) I_D-V_D with different scanning times by APPT

Figure 3-10:Comparison of threshold voltage and saturation mobility with different scanning times by APPT

Figure 3-11:Contact angle vs. different scanning times by APPT

Figure 3-12:Contact angle of (a) No treatment ($<10^\circ$) (b) APP1(68.9°) (c) APP2 (76.3°) (d) APP4 (90.5°) (e) APP8 (90.9°)

Figure 3-13:AFM micrography of (a) No treatment (b) APP1 (c) APP2 (d) APP4 (e)APP8

Figure 3-14: (a) I_D-V_G curve and(b) I_D-V_D curve with spin-coating HMDS for OTFT

Figure 3-15: (a) I_D-V_G curve and(b) I_D-V_D curve with evaporated HMDS for OTFT

Figure 3-16:Comparison of threshold voltage and saturation mobility with different methods of surface treatment

Figure 3-17:Contact angle of (a) spin-coating HMDS (65.49°) and(b) evaporated HMDS (75.28°)

Figure 3-18:AFM photography of (a) Spin-coating HMDS and(b) evaporated HMDS

Figure 3-19:The comparison of (a), (b) I_D-V_G and (c), (d) I_D-V_D with different methods of surface treatment

Figure 3-20 Comparison of contact angle and surface roughness with different methods of surface treatment

Figure 3-21 Comparison of surface roughness and mobility with different methods of surface treatment.

Figure 3-22:Comparison of contact angle and mobility with different methods of surface treatment and different scanning times by APPT

Figure 3-23:Comparison of contact angle and roughness with different methods of surface treatment and different scanning times by APPT.

Figure 3-24:Comparison of roughness and mobility with different methods of surface treatment and different scanning times by APPT.

Figure 3-25: A typical hysteresis curve.

Figure 3-26:Hysteresis of P_3HT OTFTs with no surface treatment.

Figure 3-27:Hysteresis of P_3HT OTFTs with spin-coating surface treatment

- Figure 3-28:**Hysteresis of P₃HT OTFTs with evaporation surface treatment.
- Figure 3-29:**Hysteresis of P₃HT OTFTs with APP 1 times surface treatment.
- Figure 3-30:**Hysteresis of P₃HT OTFTs with APP 2 times surface treatment.
- Figure 3-31:**Hysteresis of P₃HT OTFTs with APP 4 times surface treatment.
- Figure 3-32:**Hysteresis of P₃HT OTFTs with APP 8 times surface treatment.
- Figure 3-33:**ID versus VG for various surface treatment processes and the gate leakage currents in VG approaches 0 V.
- Figure 3-34:**ID versus VG for different numbers of APP scans and the gate leakage currents in VG approaches 0 V.
- Figure 3-35:**TGA thermograph of P₃HT. 5 % weight loss is about 500 °C .
- Figure 3-36:**DSC thermograph of P₃HT was pre-heating at the temperature of 70 °C for 3 min.
- Figure 3-37:**DSC thermograph of P₃HT was pre-heating at the temperature of 90 °C for 3 min.
- Figure 3-38:**DSC thermograph of P₃HT was pre-heating at the temperature of 110 °C for 3 min.
- Figure 3-39:**DSC thermograph of P₃HT was pre-heating at the temperature of 130 °C for 3 min.
- Figure 3-40:** DSC thermograph of P₃HT was pre-heating at the temperature of 150 °C for 3 min.
- Figure 3-41:**T_m and ΔH of P₃HT in Run first time with difference pre-heating temperature.
- Figure 3-42:**T_m and ΔH of P₃HT in Run second time with difference pre-heating temperature.
- Figure 3-43:**X-ray analysis of deposition of P₃HT on SiO₂ dielectric layer with various surface treatments.
- Figure 3-44:**UV-VIS absorption spectra of P₃HT films that are deposited on SiO₂ dielectric layers following various surface treatments, normalized to the maxima of the spectra.

Chapter 1

Introduction

1.1 General Background and Motivation

In the last few years, Today's microelectronics is based on the use of highly pure and high performance semiconductors like Si, Ge, GaAs, and InP, etc. These materials can provide carrier mobility (μ) in the order 10^3 cm²/Vs at room temperature, offer long lifetime, can be precisely doped and patterned with accuracy better than 100 nm. In this way, they profit at best of the device speed and manufacture complex systems on chip that are capable to receive, memorize, elaborate and transmit enormous quantity of information, making possible like PCs, mobile phones and almost every commercial products around our daily life.

Organic thin-film transistors (OTFT) using organic semiconductors have attracted a great deal of interest for use in lightweight, low-cost, large-area and flexible electronic products such as flat-panel displays, sensors, smart cards, and radio-frequency identification (RFID) tags. OTFT are more compatible with polymeric substrates than conventional silicon-based transistors because they can fabricated with a low-temperature process. Therefore, OTFT on polymeric substrates have been developed to construct organic integrated circuits [1,2,3], electric papers, active-matrix liquid crystal displays (AMLCDs) [4,5], and active matrix organic electroluminescent displays [6].

Organic thin-film transistors (OTFT) based on conjugated polymers, oligomers, or other molecules have been envisioned as a viable alternative to more traditional, mainstream thin-film transistors (TFT) based on inorganic

materials. Because of the relatively low mobility of the organic semiconductor layers, OTFT can't rival the performance of field-effect transistors based on single-crystalline inorganic semiconductors, such as Si, Ge, GaAs, and InP, which have charge carrier mobilities about three orders of magnitude higher [7].

The performance of OTFT has steadily improved in the last two decades as a result of the development of new organic semiconductors, the optimization of deposition conditions and gate dielectric surface treatments [8,9,10,11]. We presented a semilogarithmic plot of the highest yearly reported field-effect mobility value measured from thin-film transistors based on specific organic semiconductors, beginning in 1986. An update of that plot is shown in Figure 1-1, which is based on Table 1-1.

Solution-processable conjugated polymers are among the most promising candidates for a cheap electronic and optoelectronic technology on plastic substrates. The technology that is believed to have the potential to produce the highest impact on manufacturing costs is the use of soluble organic semiconductor, both polymers and oligomers, combined with large area coating employed in OTFT is the fact that can be deposited using very low cost procedures such as spin-coating. This is the case of soluble polymers such as regioregular polythiophenes we used in experiments. Spin-coating procedures are also thermally compatible with plastic substrates, because they are carried out at the room temperature.

Therefore, here we employ the poly-3-hexylthiophene (P_3HT), solution processable conjugated materials, as active layers in OTFT. Atmospheric-pressure plasma technology (APPT) will be adopted to treat the surface of dielectric of OTFT and discuss the influence.

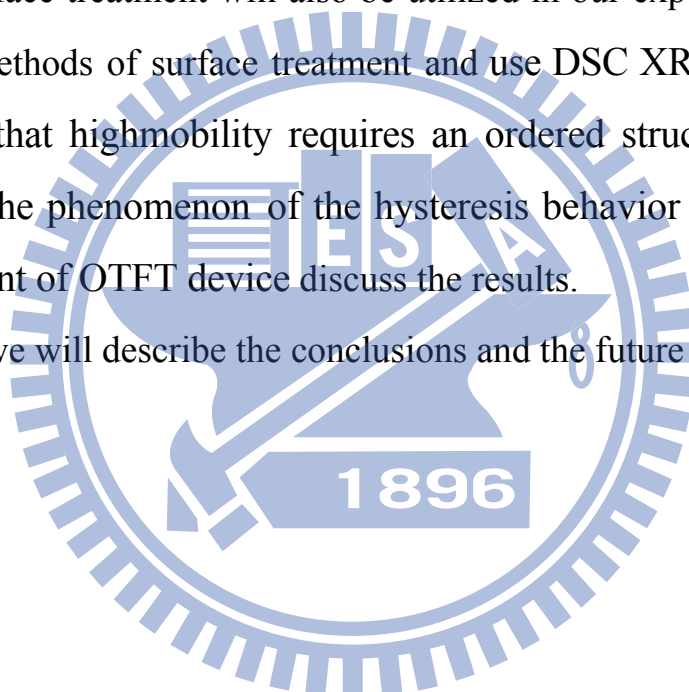
1.2 Thesis Organization

In chapter 1, we describe our background and motivation of our study.

In chapter 2, we will introduce the characteristic of P₃HT and methods for OTFT fabrication.

In chapter 3, we adopt a new process, APPT, which can be operated under low temperature and atmospheric ambient. And APPT will make use of modify surface of dielectric layer SiO₂ for our experiment. In addition, the other methods of HMDS surface treatment will also be utilized in our experiment. we compare the various methods of surface treatment and use DSC XRD and UV-VIS to demonstrate that high mobility requires an ordered structure. And we also explain that the phenomenon of the hysteresis behavior and the anomalous leakage current of OTFT device discuss the results.

In chapter 4, we will describe the conclusions and the future works.



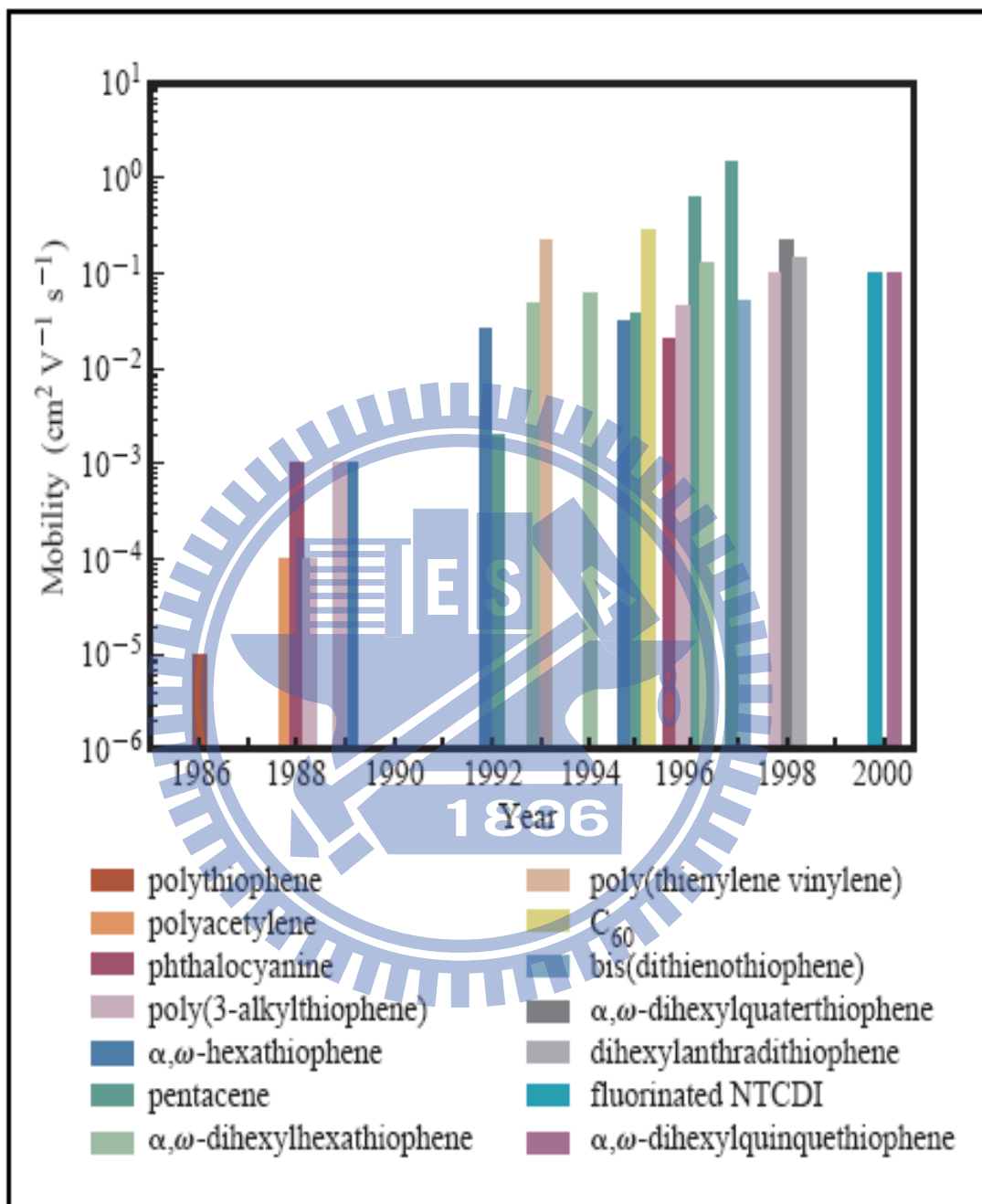


Figure 1-1: Semilogarithmic plot of the highest field-effect mobility(μ) Reported for OTFT fabricated from the most promising polymeric and oligomeric semiconductors versus year from 1986 to 2000 [12]

Year	Mobility ($\text{cm}^2 \text{V}^{-1} \text{s}^{-1}$)	Material (deposition method) (v) = vacuum deposition (s) = from solution	$I_{\text{on}}/I_{\text{off}}^*$	W/L	Reference
1983	Minimal, not reported (NR)	Polyacetylene (s) (demonstration of field effect in an OTFT)	NR	200	[16]
1986	10^{-5}	Polythiophene (s)	10^3	NR	[17]
1988	10^{-4}	Polyacetylene (s)	10^5	750	[18]
	10^{-3}	Phthalocyanine (v)	NR	3	[19]
	10^{-4}	Poly(3-hexylthiophene) (s)	NR	NR	[20]
1989	10^{-3}	Poly(3-alkylthiophene) (s)	NR	NR	[21]
	10^{-3}	α - ω -hexathiophene (v)	NR	NR	[22]
1992	0.027	α - ω -hexathiophene (v)	NR	100	[23]
	2×10^{-3}	Pentacene (v)	NR	NR	ibid.
1993	0.05	α - ω -di-hexyl-hexathiophene (v)	NR	100–200	[24]
	0.22 [†]	Polythiénylenevinylene (s)	NR	1000	[25]
1994	0.06	α - ω -dihexyl-hexathiophene (v)	NR	50	[26]
1995	0.03	α - ω -hexathiophene (v)	$>10^6$	21	[27]
	0.038	Pentacene (v)	140	1000	[28]
	0.3	C_{60} (v)	NR	25	[29]
1996	0.02	Phthalocyanine (v)	2×10^5	NR	[30]
	0.045	Poly(3-hexylthiophene) (s)	340	20.8	[31]
	0.13	α - ω -dihexyl-hexathiophene (v)	$>10^4$	7.3	[15]
	0.62	Pentacene (v)	10^8	11	[32]
1997	1.5	Pentacene (v)	10^8	2.5	[33]
	0.05	Bis(dithienothiophene) (v)	10^8	500	[34]
1998	0.1	Poly(3-hexylthiophene) (s)	$>10^6$	20	[35]
	0.23	α - ω -dihexyl-quaterthiophene (v)	NR	1.5	[36]
	0.15	Dihexyl-anthradithiophene	NR	1.5	[37]
2000	0.1	n-decapentafluoroheptyl-methyl- naphthalene-1,4,5,8-tetracarboxylic diimide (v)	10^5	1.5	[38]
	0.1	α - ω -dihexyl-quinquethiophene (s)	NR	NR	[38]

*Values for $I_{\text{on}}/I_{\text{off}}$ correspond to different gate voltage ranges and thus are not readily comparable to one another. The reader is encouraged to read the details of the experiments in the cited references.

†This result has not yet been reproduced.

Table1-1 Highest field-effect mobility(μ) values measured from OTFT as reported in the literature annually from 1986 through 2000 [12].

Chapter 2

Property of P₃HT

2.1 Introduction of Poly(3-hexylthiophene) P₃HT

2.1.1 P₃HT molecular structure

The field-effect mobility of P(3-hexylthiophene) P₃HT is strongly influenced by the structure of the polymer chain and the direction of intermolecular π - π stacking. The structure of the polymer chain of P₃HT is shown in Fig 2-1. The 3-alkylsubstituents can be incorporated into a polymer chain with two different regioregularities: head to tail (HT) and head to head (HH) [13,14].

R represents the alkyl side chain (C₆H₁₃ for P₃HT), which allows P₃HT to be dissolved in solvents like chloroform. This solution processability enables simple film deposition. A regiorandom P₃HT consists of both HH and HT 3-hexylthiophene in a random pattern while a regioregular has only one kind of 3-hexylthiophene, either HH and HT. This type of order is known as regioregularity and has been shown to give much higher field-effect mobility values over regiorandom material [15]. In our experiments, regioregular P₃HT (HT regioregularity of 98.5%) and high grade solvent, chloroform, were purchased from Aldrich Chemical Company. A dramatic increase in mobility was observed relative to regiorandom poly-3-alkylthiophenes [16] when regioregular P₃HT consisting of 98.5% head to tail (HT) linkages, so we did not

perform further purification to these chemicals in our experiments. After being deposited on the substrate, P₃HT backbones may form two different morphologies, edge-on or face-on of lamella structure as shown in Fig 2-2. The higher mobility is given by edge-on structure since the carriers can move more efficiently through intra-chain transport along the direction of π - π stacking. Two different methods are applied to deposit the P₃HT film, one is spin-coating and while the other is dip-casting. The mobility of dip-coated films is usually higher than that of the spin-coating that's maybe due to the evaporation rate of solvents. Lower evaporation rate results in a slower crystal growth with better ordered polymer structure [16,17]. In spite of that method provide the higher field effect mobility, the dip-coating method can not be applied for coverage of a large area. Therefore, in all of our experiments, we used spin-coating technique as a key process of organic layer deposition.

2.1.2 Conduction Mechanism

The weak intermolecular interaction forces in organic semiconductors, most usually van der Waals interactions with energies smaller than 10 Kcal mol⁻¹, may be responsible for such small carriers mobility. In contrast, in inorganic semiconductors such as Si and Ge, the atoms are tied together with very strong covalent bonds, which for the case of Si have energies as high as 76 Kcal mol⁻¹. In these semiconductors, charge carrier flows like highly delocalized plane waves in the wide bands and have very high mobility. On the other hand, inorganic semiconductors usually have high order lattice structures and there are fewer traps than organic ones. This is another reason to explain the poor electrical characteristics of organic electronics.

However, for conjugated organic materials, the polymer chains are weakly bound by van der Waals force. These polymer typically have narrow energy bands, highest occupied molecular orbit (HOMO) and lowest occupied molecular orbit (LUMO), which can easily be disrupted by disorder. Due to disorder structures, band transport is not applicable to organic semiconductors; in which carrier transport take place by hopping[18] between localized state like Fig 2-4. Transport from one molecular to another is much more difficult due to a small energetic coupling between molecules held by weak van der Waals force of $\sim 10 \text{ Kcal mol}^{-1}$. Another characteristic of organic material is that most polymers conduct one kind of carrier only, either electron or hole (P_3HT is p-type that majority carriers are holes). Because of the nature of large band gap (e.g. E_g of $P_3HT = 2.2 \text{ eV}$), the active layer cannot be inverted by thermal energy at room temperature (i.e. slow generation rate of inversion layer). Therefore, OTFTs operate in the accumulation mode at its ON state and depletion at its OFF state.

P_3HT are semi-crystalline in nature, and their conduction mechanism is complex. The crystalline portion can conduct through intra-chain and inter-chain transport, whereas the amorphous portion conducts current through hopping processes.

2.1.3 P_3HT alignment

3-Alkyl substituents can be incorporated into the poly(3-hexylthiophene) polymer in two arrangements (Fig.2-1) - head to tail (HT) and head to head (HH). A regiorandom P_3HT has both HH and HT 3-hexylthiophenes in a random pattern while a regioregular P_3HT has only one 3-alkylthiophene -either HH or HT.

Structure-controlled syntheses of P₃HT have been recently developed, and regioregular P₃HT with HT linkages of greater than 98.5% can be obtained [19,20]. Most interestingly, these polymers have been shown to have very different properties from their corresponding regiorandom polymers, such as smaller band gaps, better ordering and crystallinity in their solid state, as well as markedly improved electroconductivities. Highly regioregular P₃HT self-orient into a well-ordered lamellar structure with an edge-on orientation of the thiophene rings relative to the substrate. In samples with a high regioregularity (>91%), the preferential orientation of ordered domains is with the (100)-axis normal to the film and the (010)-axis in the plane of the film (Figs. 2-2 and 2-3). In contrast, low regioregularity (81% head-to-tail linkages) is associated with lamellae with a face-on orientation, and crystallites that are preferentially oriented along the (100)-axis in the plane and the (010)-axis normal to the film. In another work [21], Prosa et al. presented the different intensity distributions of the (100) reflections that are associated with the lamella layer structure and the (010) reflections that are associated with $\pi - \pi$ interchain stacking. Therefore, in this study, highly regioregular (98.5%) P₃HT is adopted as the active layer, and the above characteristics are exploited to provide P₃HT alignment.

2.2 Solution processed deposition

2.2.1 OTFT method manufacture

There are four methods to form organic semiconductor film: (1) solution-processed deposition, (2) electro-polymerization, (3) vacuum

evaporation, and (4) Langmuir-Blodgett Technique [22]. Recently, many researchers extensively use solution-processed deposition to fabricate organic semiconductor film. For solution-deposited organic semiconductor film, one kind of the organic semiconductor material such as poly (3-hexylthiophene) are dissolved in solvent such as chloroform. In our experiment, we use P₃HT as the semiconductor because P₃HT has many potential advantages for use the semiconductor layer in field-effect transistors. (1) P₃HT is a well-known polymer as an organic semiconductor and has shown the effect mobility from 10⁻⁴ cm²/Vs in 1988 to 0.2 cm²/Vs in 2003. [12,23]. (2) P₃HT has high solvent selectiveness, can dissolve in toluene, xylene, chloroform and so on. (3) P₃HT is solution processed, therefore can be processed by spin-coating .

2.2.2 The Motivation of Spin-Coat

The organic semiconductors that exhibit the best mobility, ON/OFF Current ratio, uniformity over large areas, and devices reproducibility have been deposited by vacuum sublimation. However the need for expensive vacuum chambers and lengthy pump-down cycles is unavoidable. Since the organic semiconductors have the relatively low mobility of organic semiconductors as described in chapter 1, OTFT cannot rival the performance of based on single crystalline inorganic semiconductors, such as Si, Ge, and GaAs. However, the unique processing characteristics and demonstrated performance of OTFT suggest that they can be competitive candidates for existing or novel thin film transistor applications requiring large area coverage, structural flexibility, low temperature processing, and especially low cost. Some recent efforts in the field have focused on processes for solution deposition of small molecule [24] and

polymers, as well as integration of these process with other non-lithographic device fabrication technique [25]. To realize truly the advantages (i.e., processability and low cost) of organic materials in device applications, liquid phase processing technique by spin-coating is strongly desired. In all of our experiments, we used spin-coating technique as a key process of organic layer fabrication.

2.2.3 Polymer morphology and resolver function

The molecular structure of the P₃HT greatly influences the charge carrier mobility and related current-voltage (I-V) characteristics of OTFT.

A comparison study of P₃AT (A = hexyl, octyl, dodecyl, hexadecyl) with side chains ranging from butyl to decyl showed that field-effect mobility decreases with increasing chain length [26].

Under different processing conditions, the field effect mobility of OTFT is highly anisotropic. For example, Karl et al [27] observed that the field effect mobility was highly anisotropic, with the larger mobility along the direction in which the polymer chain axis aligned.

The molecular structure obtained by using spin-coating films is usually lower than that of the cast films [16]. This is perhaps because in the cast films, the rate of solvent evaporation is slower and has slower crystal growth, and hence better ordering, and large grain size.

The choice of solvents and polymers has a very significant impact on the electrical characteristics of OTFT. In a recent publication, Bao et al [18]. Observed that when chloroform was used as a solvent to make poly-(3-hexylthiophene)-based transistors, the field-effect mobility was $0.1 \text{ cm}^2\text{Vs}^{-1}$.

However when Tetra hydrofuran (THF) was used as the solvent, the value of field-effect mobility is only $0.0006 \text{ cm}^2\text{Vs}^{-1}$. Table 2-1 shows the performance of various devices made from casting poly(3-hexylthiophene) films using different solvents with different process conditions [14].

Sirringhaus et al., [18] observed that the mobility could differ by a factor of 100 depending on the direction of $\pi - \pi$ stacking in which efficient inter-chain transport is happened. The polymer solution we used is regioregular P₃HT in chloroform with high purity. From Table 2-1, the mobility is typically in the range 10^{-3} which matches the result obtained in our experiment.

2.3 Contact Resistance of P₃HT OTFT

There are many parameters will impact the performance of OTFT. The contact resistance between the source/drain electrodes and the organic semiconductor is an important one of them [28-30]. The contact resistance between the source/drain electrodes and the semiconductor becomes increasingly important to device performance. The contact resistance dominates the overall device resistance.

Material of source/drain electrodes and the structure both affect the contact characteristics between the source/drain electrode and the organic semiconductors. Unlike the FET of single-crystalline silicon, polycrystalline silicon, or hydrogenated amorphous silicon, the P₃HT material cannot be optimized easily by semiconductor doping or silicide formation. Such properties of organic semiconductors deteriorate the performance of devices; moreover, the chemical compound always increase the contact resistance between the source/drain electrode and the organic semiconductor [31,32]. It is a

straightforward method to find a suitable electrode material which forms ohmic contact with the organic active layer and thus to improve the performance of OTFT. P₃HT can form an ohmic contact with material for its work function larger than 4.5eV because the work function of P₃HT is 4.5eV. Work functions of all materials we used are larger than 4.5eV; they include Ni(5.1eV), Pt(5.65eV), and Cr(4.5eV).

2.4 Operation of Organic Thin Film Transistors

Refer to [33], the operation of the P₃HT which bases on OTFT is described below. Organic thin-film transistors are opposed to the usual inversion mode operation of silicon MOSFETs and primarily operated as a P-type accumulation-mode enhancement type transistor. There are four basic modes which will be described later.

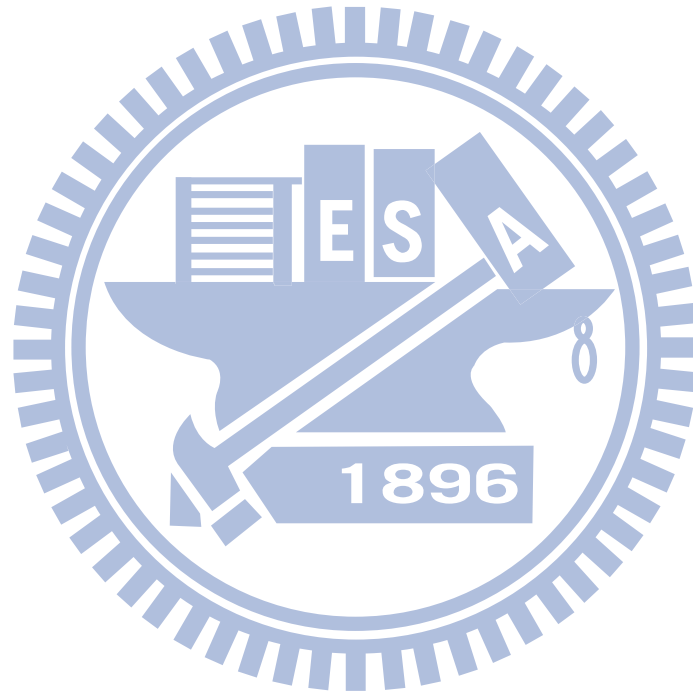
Mode (I): When zero bias is applied to three electrodes of OTFT. The schematic diagram is shown in Fig 2-5(a), it is called cut-off. If applied a small drain bias, V_d , and the source-current, I_{ds} , will be small and ohmic.

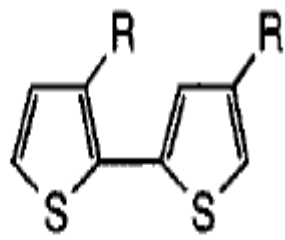
Mode (II): When a positive bias applied, the bend bending will occur in the interface between dielectric layer and semiconductor layer. Negative charges will locate at interface and form the depletion region. The schematic diagram is shown in Fig 2-5(b). The channel resistance is so large that the current will smaller than that of mode (I). Because of the large band gap, inversion layer cannot be observed in the organic thin-film transistor.

Mode (III): When gate bias is negative, the schematic diagram is shown in Fig 2-5(c), the voltage is dropped over the insulator and over the semiconductor near the interface between dielectric layer and semiconductor layer. More

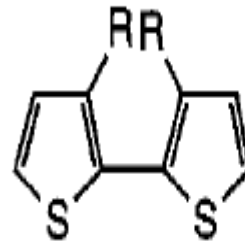
positive charges will be accumulated in the accumulate region. When a small bias is applied to drain, the source-drain current will be larger than that of Mode (I), the schematic diagram is shown in Fig 2-5(d).

Mode (IV): When drain voltage is negative enough that the voltage difference of gate and drain, V_{gd} , which is lower than $V_{th}(<0)$, therefore, the depletion region will form near drain and pitch-off (Fig 2-5(e)). If drain voltage is more negative, the depletion region will grow and approach source. The schematic diagram is shown in Fig 2-5(f)(g).





head-to-tail
(HT)



head-to-head
(HH)

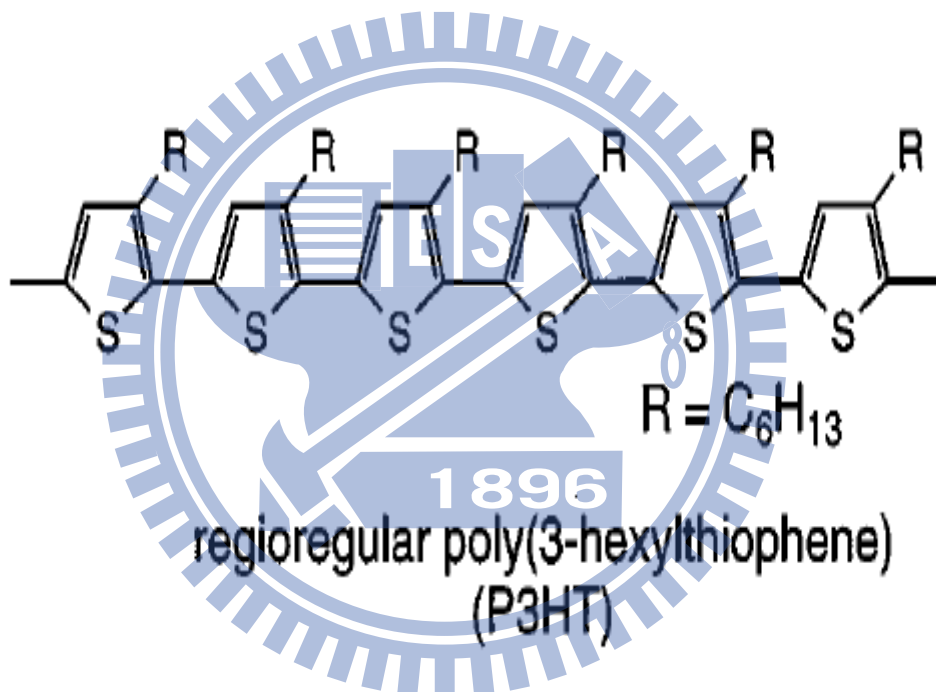
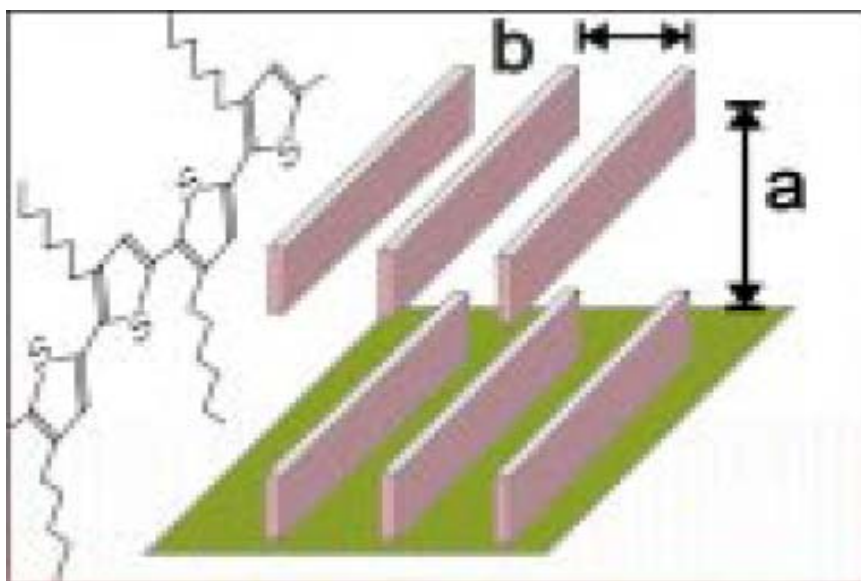
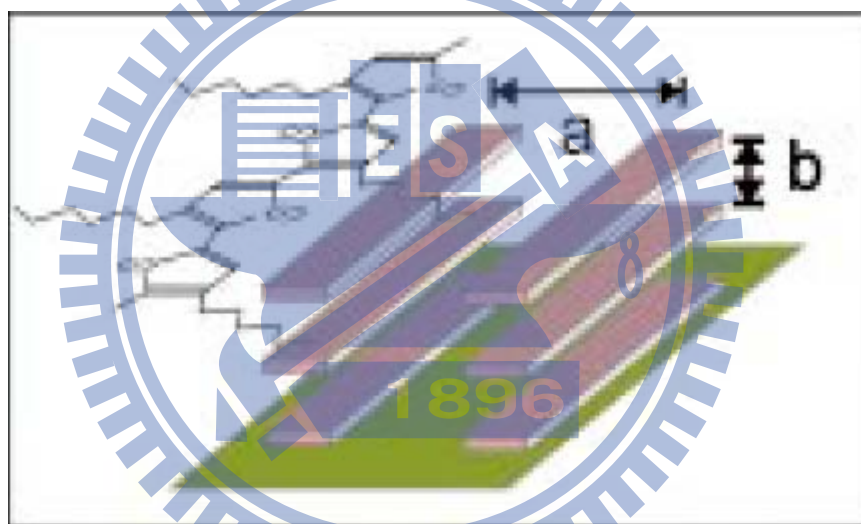


Figure 2-1: The structure of the polymer chain of P₃HT



(a)



(b)

Figure 2-2: Two different orientations of ordered P₃HT

(a)Edge-on orientation (b)Face-on orientation

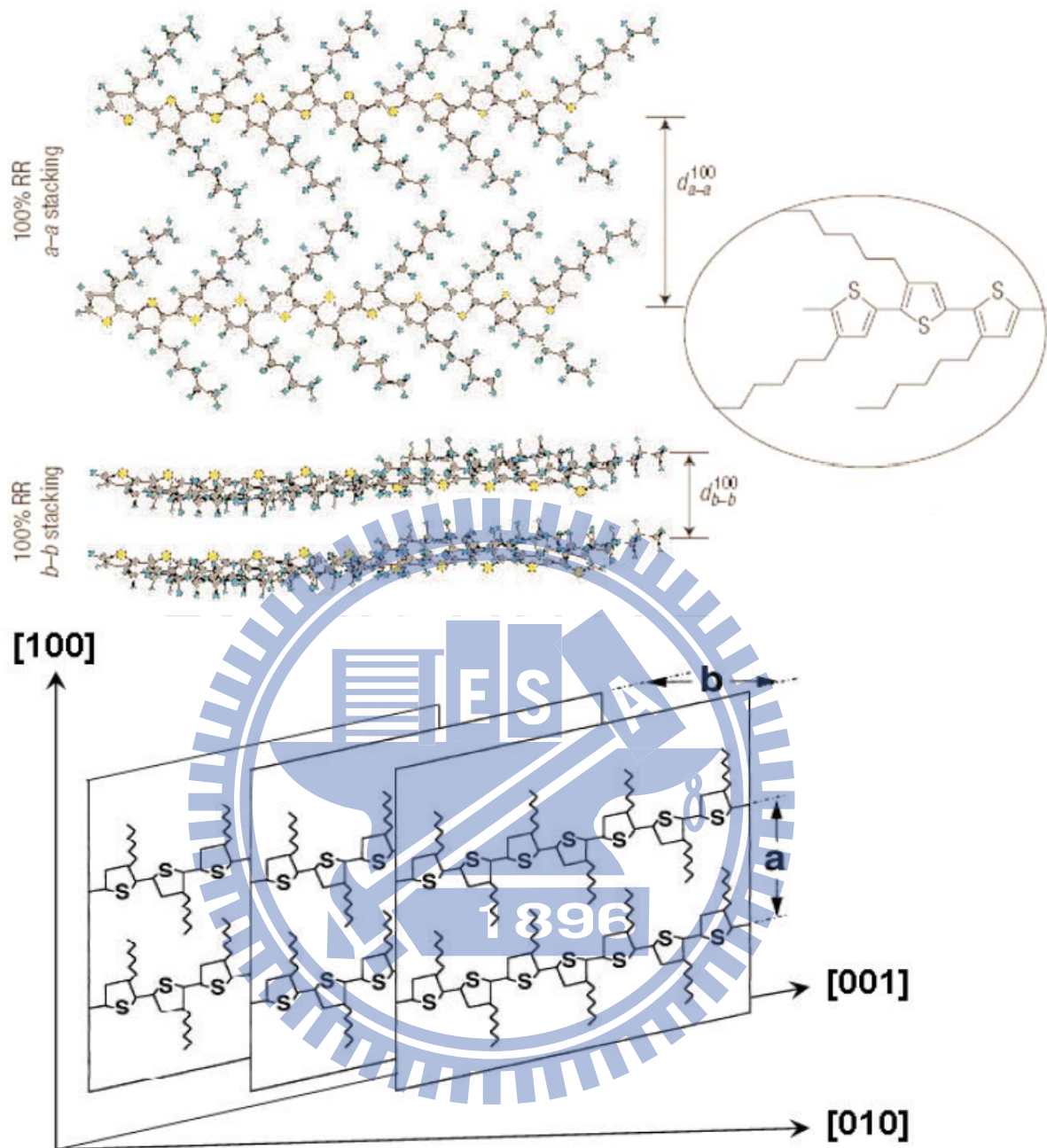


Figure 2-3: The molecular structure of P₃HT s for High RR (d_{b-b}^{100} and d_{a-a}^{100} are the a-direction and b-direction chain-stacking spacings, respectively) The a-direction and b-direction are parallel and perpendicular to the thiophene ring plane, respectively (see the chemical structures within the ovals as well as the schematic illustration for lamella folding and ordering on a substrate).

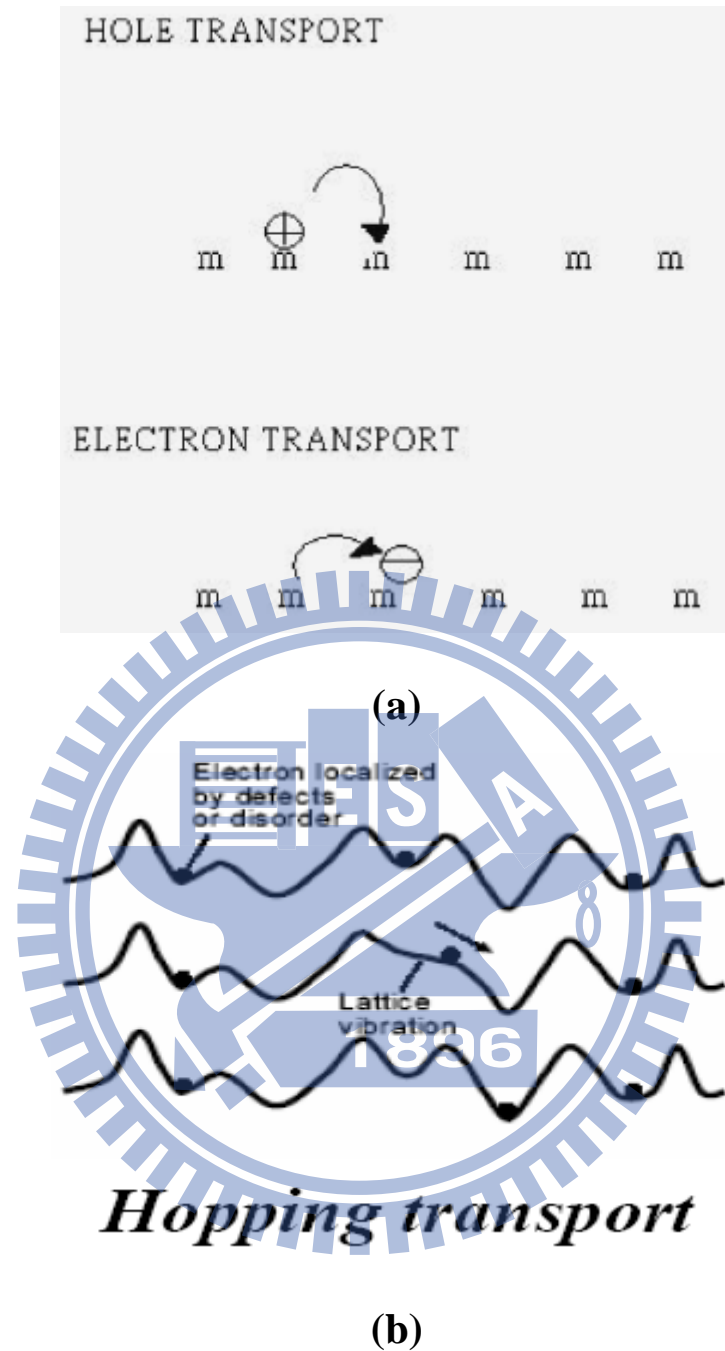


Figure 2-4: (a) charge carrier transport in conjugated polymers and
 (b) charge transport mechanisms in solid

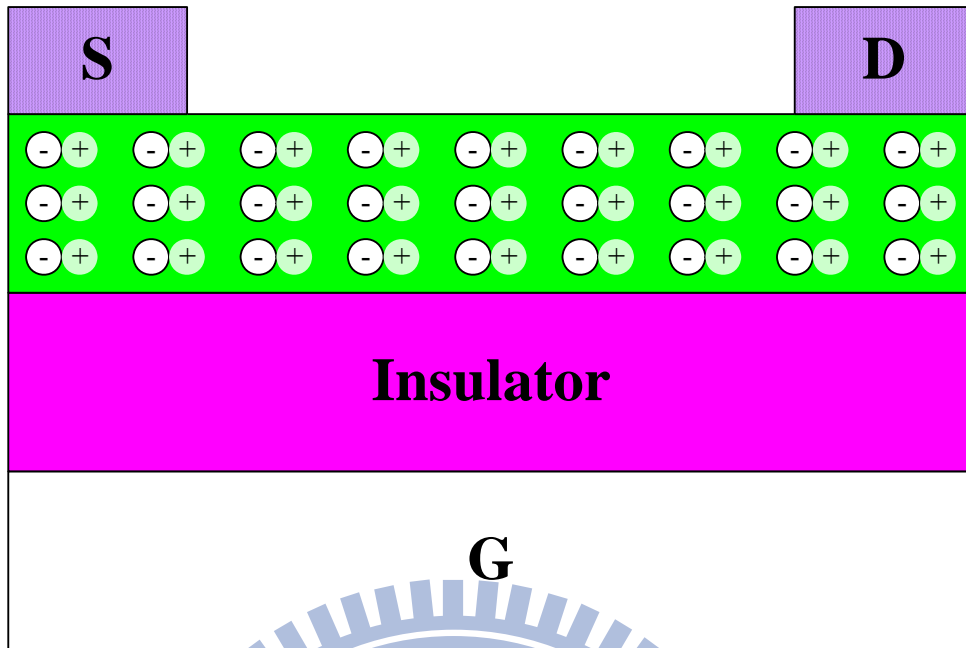
Entry	Solvent	Condition	Mobility ($\text{cm}^2/\text{V s}$) ^a	On/off ratio ^b
1	THF	1	6.2×10^{-4}	10
2	<i>p</i> -xylene	1	1.9×10^{-3}	40
3		2	1.9×10^{-5}	2
4	Toluene	1	3.6×10^{-3}	10
5		2	3.2×10^{-3}	25
6	Chlorobenzene	1	4.7×10^{-3}	10
7		entry 6 condition 3	4.7×10^{-3}	80
8		2	6.9×10^{-4}	72
9	1,1,2,2-tetrachloroethylene	1	6.8×10^{-3}	35
10	1,1,2,2-tetrachloroethane	1	2.4×10^{-2}	6
11		entry 10 condition 4	1.4×10^{-2}	35
12		entry 11 condition 5	3.3×10^{-3}	15
13	Chloroform	2	9.2×10^{-3}	80
14		1	4.5×10^{-2}	340
15		entry 14 condition 3	2.1×10^{-2}	9000

^aField-effect mobility for the accumulation-mode operation.

^bOn/off ratio is calculated for enhancement-mode operation only, and it is ten times higher for enhancement-depletion operation.

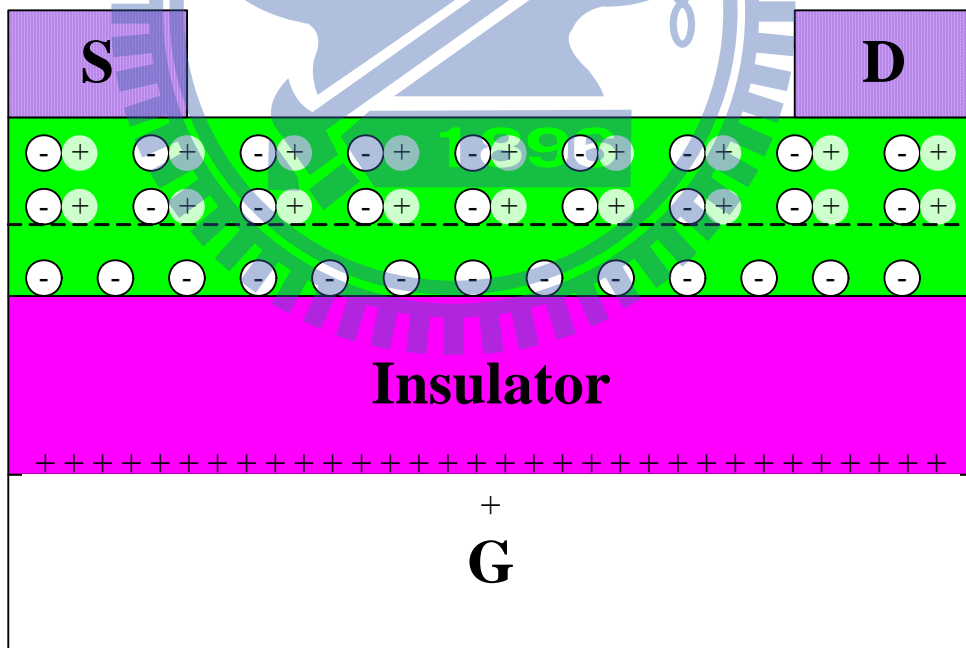
Table 2-1: Field-effect mobility and ON/OFF ratio of samples prepared from different solvents and process condition [14]. Condition 1, cast, vacuum pumped for 24 h; condition 2, spin-coated; condition 3, treated with NH_3 for 10 h; condition 4, heated to 100°C under N_2 for 5 min; condition 5, heated to 150°C under N_2 for 35 min.

$$V_G = V_S = V_D = 0$$



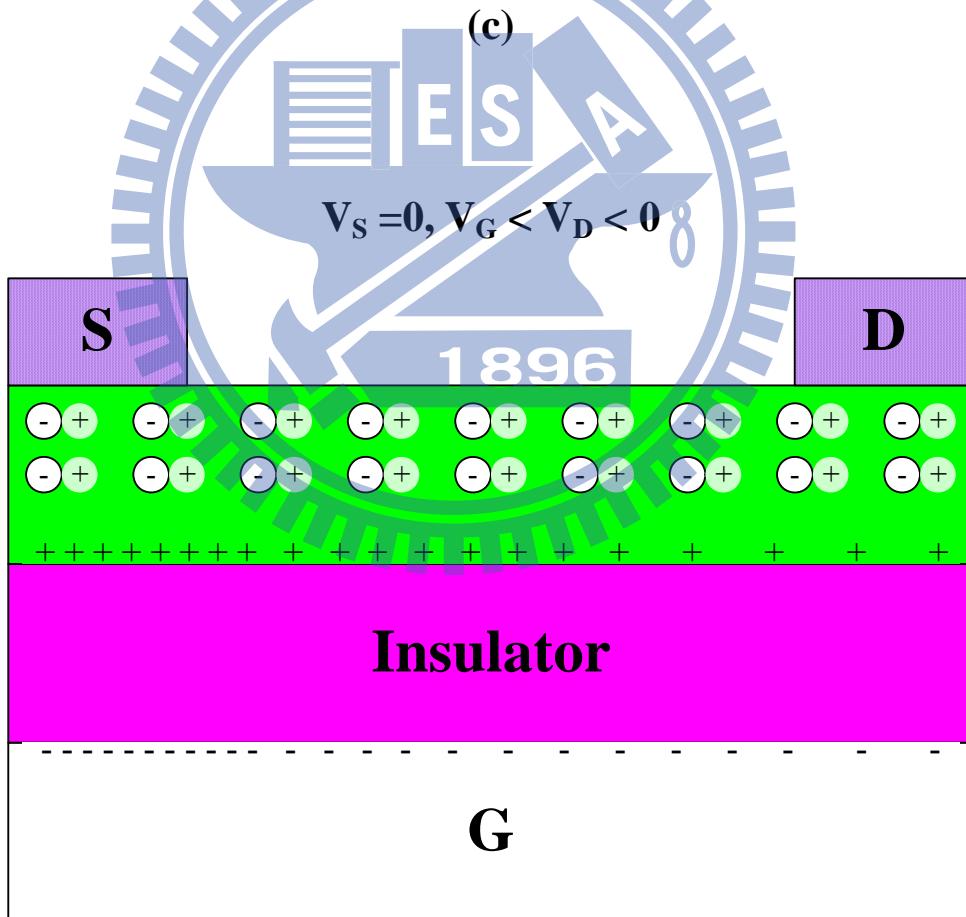
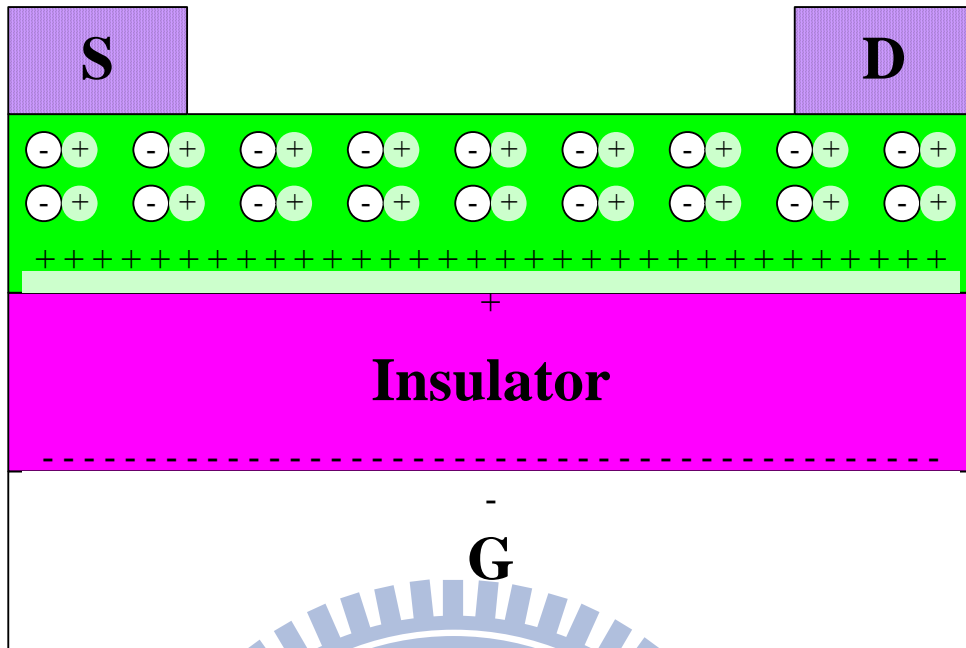
(a)

$$V_S = V_D = 0, V_G > 0$$



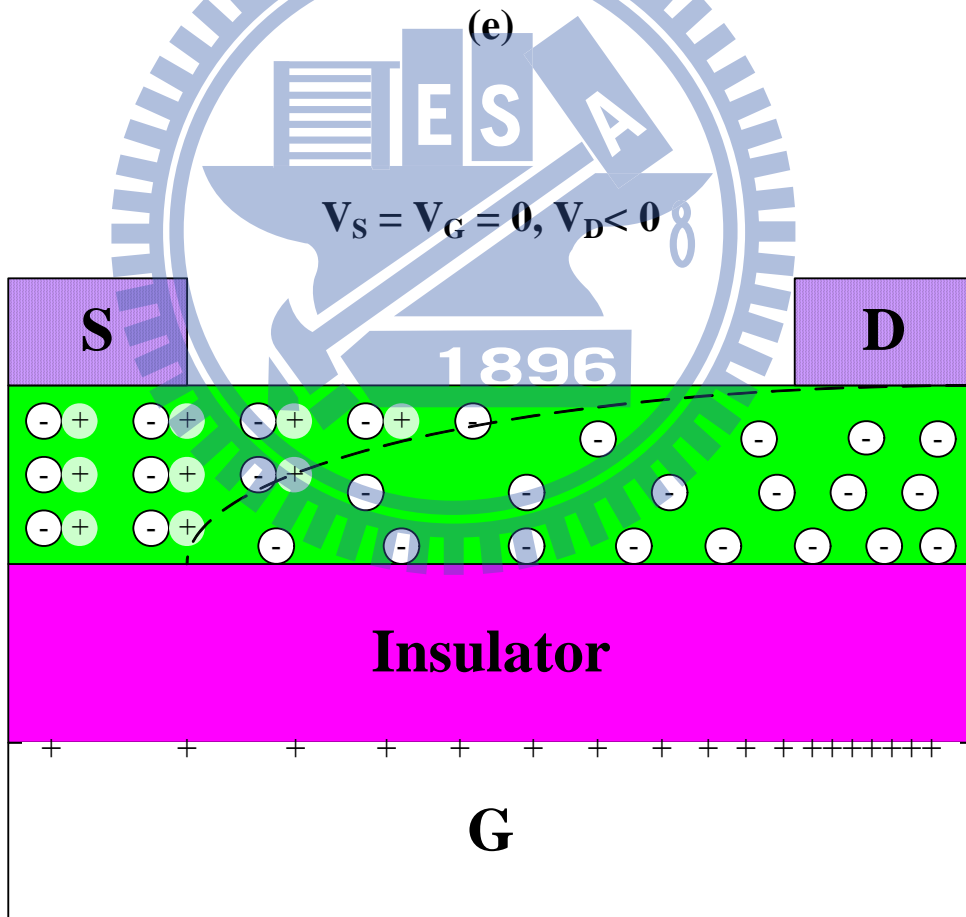
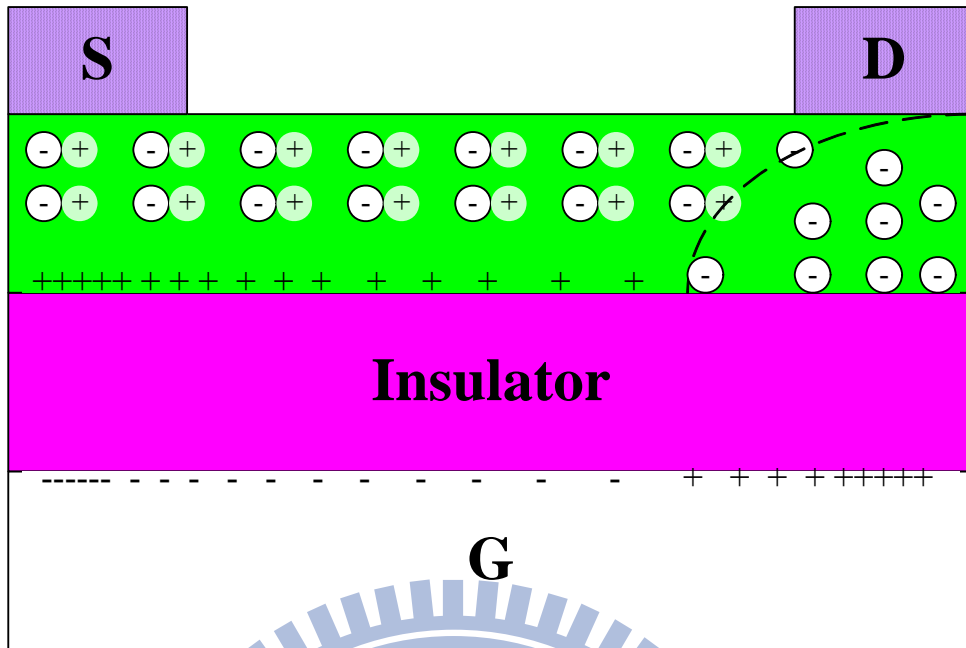
(b)

$$V_S = V_D = 0, V_G < 0$$



(d)

$V_S = 0, V_D < V_G < 0$



(f)

$V_S = V_G = 0, V_D \ll 0$

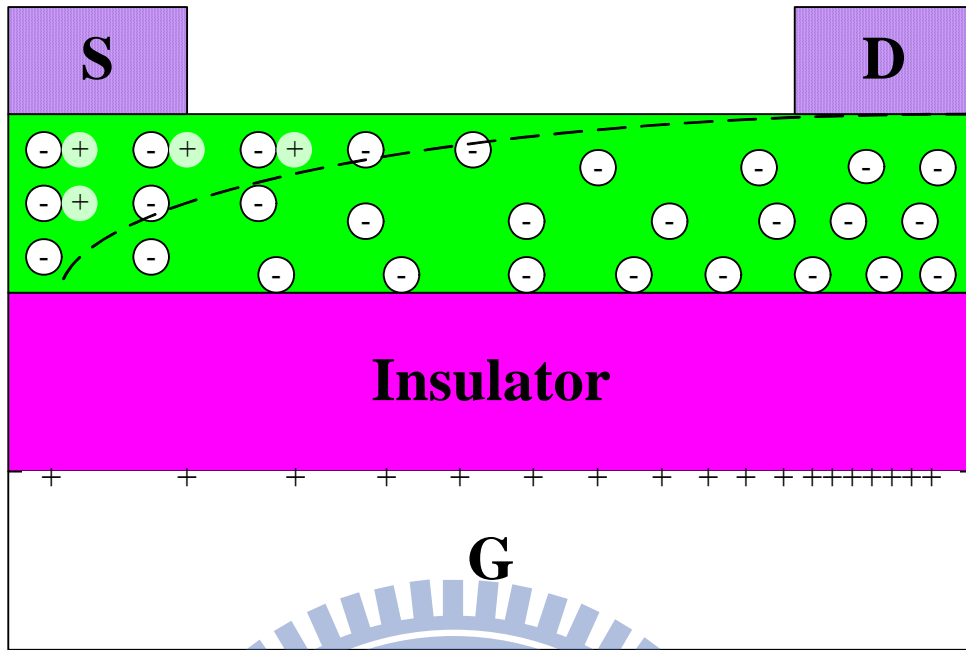


Figure 2-5: Schematic of operation of organic thin film transistor, showing a lightly doped semiconductor; + indicates a positive charge in semiconductor; - indicates a negative charge in semiconductor. (a) No-bias (b) Depletion mode (c) Accumulation mode (d) Non-uniform charge density (e) Pinch-off of channel (f) and (g) Growth of the depletion zone

Chapter 3

Influence of APPT for OTFT

3.1 Oxide compound surface revision

The interface between an organic material and dielectric layer is a critical factor for device performance. This is because the surface of the dielectric strongly influences the quality of the dielectric/channel interface and the crystalline organic channel. The quality of the interface and the organic channel, as well as the electrical properties of the gate dielectric itself, play a major role in determining the device performance of an OTFT [34-36]. Although several methods have been recently proposed to improve the condition of the interface states, only a few have been proved to be reliable and robust. One of the proposed methods is the use of a self-assembly monolayer (SAM), such as octadecyltrichlorosilane (OTS) [37] and hexamethyldisilazane (HMDS) [38], have been extensively studied. A dielectric surface treatment with OTS is found to improve the mobility of OTFTs. Another dielectric surface treatment technique is O₂ plasma cleaning and subsequent HMDS deposition on dielectrics [38]. A problem owing to O₂ plasma cleaning, which is applied to remove residues generated from previous photolithography processes, was found to be the generation of a large number of trap states during the cleaning process by assisting OH termination at the SiO₂ surface [39]. Although a HMDS layer subsequently applied is expected to reduce the number of traps and act as a SAM, the time-consuming wet processes used to apply a SAM on the interface are unreliable and can cause other undesirable contaminations of the device. Surface treatments using an ion beam have been widely studied in other research fields. It is well known that ion implantation techniques can change the surface conditions or thin-film properties [40]. In the LCD fabrication process, for example, Ar ion beam treatment has been

considered as a viable option as a surface treatment method to replace conventional contact-based treatment such as rubbing [41]. One of the advantages of Ar ion beam treatment is that because argon is an inert gas, it can clean the surface effectively without affecting the chemical structure of the dielectric layer.

3.2 Introduction of APPT

3.2.1 Introduction of plasma

Plasma can be defined as a partially or wholly ionized gas with a roughly equal number of positively and negatively charged particles. Some scientists have dubbed plasma the "fourth state of matter" because while plasma is neither gas nor liquid, its properties are similar to those of both gases and liquids.

There are two types of plasma - high temperature and low temperature. A good example of naturally occurring high temperature plasma is lightning. This type of plasma can be artificially generated using a high voltage, high temperature arc, which is the basis for the corona discharge process and for the plasma torch used to vaporize and redeposit metals. Low temperature plasmas, used in surface modification and organic cleaning, are ionized gases generated at pressures between 0.1 and 2 torr. These types of plasmas work within a vacuum chamber where atmospheric gases have been evacuated typically below 0.1 torr. Low pressure allows for a relatively long free path of accelerated electrons and ions. Since the ions and neutral particles are at or near ambient temperatures and the long free path of electrons, which are at high temperature or electron volt

levels, have relatively few collisions with molecules at this pressure the reaction remains at low temperature.

3.2.2 Applications of APPT

Therefore this has been occupied for several years with developing atmospheric pressure plasma processes for surface coating and treatment. Table 3-1 shows the type of atmospheric pressure plasma.

Atmospheric pressure plasma is particularly suited for the large-area surface treatment of flat substrates (Fig. 3-1). This forms between two electrodes on application of an alternating current if at least one dielectric barrier or insulator obstructs the current. Gases are activated in these micro discharges by electronic excitation, ionization and dissociation to form very chemically reactive species. Thus the average gas temperature in the discharge gap rises only a few degrees Kelvin. Since the discharge in effect remains "cold" even temperature-sensitive substrates can be treated. Despite the filament of the discharge, with appropriate process control it is normal to achieve a very uniform surface treatment.

The atmospheric-pressure plasma technology (APPT) is useful for treating and modifying the surface properties of organic and inorganic materials. The APT apparatus does not require any vacuum systems, produces a high density plasma, and provides treatment of various substrates at low temperatures while operating open to the atmosphere. The plasma system has used for a wide variety of applications including treatment of polymer films, paper, wood, and foils; plasma grafting and plasma polymerization; ash various materials in the microelectronics industry; barrier layer deposition for the packaging industry;

and sterilizing biologically contaminated materials. For polymer films, the technique offers the following advantages:

- Uniform treatment and No backside treatment.
- Improved surface energy with concomitant improved wettability, printability, and adhesion
- No additional vacuum system and low cost
- Continuous fabrication available and high speed for production
- High plasma density

As shown in Fig 3-1(a), we exhibited the atmospheric-pressure plasma system which was used in our experiment, and also showed the other atmospheric-pressure plasma systems in Fig 3-1(b).

3.2.3 Surface modification by plasma

Fig 3-2 shows the mechanisms of plasma surface modification, a glow discharge plasma is created by evacuating a reaction chamber and then refilling it with a low-pressure gas. The gas is then energized by one of the following types of energy: radio frequency, microwaves, and alternating or direct current. The energetic species in gas plasma include ions, electrons, radicals, metastables, and photons in the short-wave ultraviolet (UV) range. Surfaces in contact with the gas plasma are bombarded by these energetic species and their energy is transferred from the plasma to the solid. These energy transfers are dissipated within the solid by a variety of chemical and physical processes to result in a unique type of surface modification that reacts with surfaces in depths from

several hundred angstroms to 10 μ m without changing the bulk properties of the material.

A wide variety of parameters can greatly affect the physical characteristics of the plasma and subsequently affect the surface chemistry obtained by plasma modification. Processing parameters, such as gas types, treatment power, treatment time and operating pressure, can be varied by the user; however system parameters, such as electrode location, reactor design, gas inlets and vacuum are set by the design of the plasma equipment. This broad range of parameters offers greater control over the plasma process than that offered by most high-energy radiation processes.

Plasma treatment is aiming for various goals as for example:

- Improved adhesion
- Removal of the "water skin"
- Activation of the substrate surface
- Modification of the substrate surface
- Cleaning of substrate surfaces

Since the organic film of OTFT is fabricated on to the dielectric layer under the influence of the physical and chemical interactions between organic and dielectric layer, the OTFT performance strongly depends on the semiconductor /dielectric interface. The purpose of this work is to show the improvement of OTFT performance by controlling the surface treatments of dielectric/polymer interface. The surface properties such as frictional or abrasion, permeability, insulating properties, wettability and chemical reactivity are strongly dependent on a molecular aggregation state of the surface [33,34]. Therefore, the control of

a molecular aggregation state in the film is important to construct a highly functionalized surface. One of the most effective ways of studying surface properties is contact angle measurement. The contact angle is the angle between the tangent to the drop's profile and the tangent to the surface at the interaction of the vapor, the liquid, and the solid. The contact angle is an index of the wettability of the solid surface. A low contact angle between solid surface water-drop indicates that the surface is hydrophilic and has a high surface energy. On the contrary, a high contact angle means that the surface is hydrophobic and has a low surface energy. The surface free energy was traditionally quantified by contact angle measurements [42,43]. In our work, we investigated the electrical properties of the OTFT using by APPT. Hexamethyldisilane ((CH₃)₃-Si-O-Si-(CH₃)₃) (HMDS) have already been widely used for oxide-based dielectric [45]. Oxide surfaces were treated with hexamethyldilazane to improve the adhesion between polymer chain and oxide surfaces. Modification of the substrate surface prior to deposition of regioregular P₃HT has also been found to influence film morphology. For example, treatment of SiO₂ with hexamethyldilazane (HMDS) or an alkyltrichlorosilane replaces the hydroxyl groups at the SiO₂ surface with methyl or alkyl groups. The apolar nature of these groups apparently attracts the hexyl side chains of P₃HT, favoring lamellae with an edge-on orientation [18]. According to [18], the mobility of OTFT with an edge-on orientation P₃HT film is higher than the one with a face-on orientation.

And so HMDS would be adopted in our experiment. We will discuss and analyze the effects of APPT surface treatments latter, and find the optimum parameters in our experiments.

3.3 Fabrication of OTFT

There are two kinds of basic structures which are adopted generally, bottom contact (BC) and top contact (TC) were shown in Fig 3-3.

Top-contact device is favorable compared to deposition onto prefabricated source and drain electrodes bottom-contact device, yielding mobilities that are typically larger by a factor of 2 [45,46].

First, an n-type bare silicon wafer was cleaned by the standard RCA cleaning process. After that, phosphorous atoms were diffused into an n-type silicon wafer by POCl_3 to form a common gate electrode. We used dilute HF to remove SiO_2 after diffusing. Before the insulating layer of silicon dioxide was deposited, the n+ silicon wafer must be cleaned by the standard RCA cleaning again. An insulating layer of silicon dioxide was grown by thermal oxidation 5hr at 1000°C . The thickness of silicon dioxide was 200nm measured by n&k system. The wafers was taken to remove silicon dioxide of backside, then gate dielectric layer was formed. The “top-contact” OTFT structures were treated by different surface treatments before deposition of the P_3HT active layer. The surface treatments were to control chemical and physical characteristics of surface by different ways. In our experiments, we adopted three methods of surface treatments and compared the difference of them.

(1) Spin-coating HMDS adopted at 800rpm for 3 sec as step one,

1500 rpm for 35 sec as step two, and baking at 150°C for 30 min.

(2) Evaporated HMDS at 150°C

(3) Atmospheric pressure plasma technology (APPT) was operated at

50W of plasma power, 0.1 sccm of He-gas flow, below 120°C , and

various scanning times which are one, two, four, and eight times.

After finishing surface treatments, active layer P₃HT was spun-coated at 1500 rpm 35sec and baked 130 °C for 3min on hot plate. The P₃HT (with head-to-tail linkages greater than 98.5 %) and the high purity solvent (chloroform) used in this study were obtained from the Aldrich Chemical Company. The solutions of P₃HT in chloroform were made with weight concentration of 0.3 %, and filtered through a 0.2 μm pore-size PTFE filter. Finally, deposition of S/D contacts was formed by sputter system, Ion Tech Microvac 450CB, and patterned through the shadow mask. The thickness of Ni contacts was 1000Å. W(2000 μm) is the channel width, L(500μm) is the channel length. The process flow is shown in Fig 3-4.

3.4 Determination of Thershold voltage and Mobility

The linear regime field effect mobility can be obtained by the calculation described below. At low V_D, I_D increases linearly with V_D (linear regime) and is approximately determined by the following equation:

$$I_D = \frac{W\mu_n C_{ox}}{2L} [2(V_G + V_T)V_D - V_D^2] \quad (3-1)$$

where L is the channel length, W is the channel width, C_{ox} is the capacitance per unit area of the insulating layer, V_T is the threshold voltage, and μ is the field effect mobility, which can be calculated in the linear regime from the transconductance,

$$G_m = \frac{\partial I_D}{\partial V_G} = \frac{Z}{L} \mu_n C_{ox} V_D \quad (3-2)$$

by plotting I_D versus V_G at a constant low V_D, with -V_D << -(V_G - V_T), and equating the value of the slope of this plot to G_m, then find G_{m,max} which can

gain the value of threshold voltage (V_T) and linear mobility. For the known values included C_{ox} , V_T , and W/L , the value of saturation mobility can be obtained from equation (3-3)

$$I_D (sat) = \frac{W\mu_n C_{ox}}{2L} (V_G + V_T)^2 \quad (3-3)$$

3.5 Results and discussion

3.5.1 The influence of APPT

Here we focus on the influence of APPT under varied conditions which have different scanning times of APPT. They are one, two, four, eight scanning times respectively. We define that one time as APP1, two times as APP2 and so on.

As shown from Fig 3-5 to Fig 3-8, plot of drain current I_D versus gate voltage V_G at various drain voltage V_D and drain current I_D versus gate voltage V_D at various drain voltage V_G with different scanning times.

In all figures of APP0 to APP8, we can observe that APP4 has best electrical characteristic about I_D - V_G and I_D - V_D . Additionally, we plotted the comparison of I_D - V_G and I_D - V_D in the same figure due to observe clearly, they were shown in Fig 3-9. For magnitude of current at the same operating voltage, $APP4 > APP8 > APP2 > APP1 > APP0$. Furthermore, threshold voltage and mobility would be calculated by taking measured data into Eq.(3-1) ~ (3-3). Arrangement of threshold voltage and mobility is shown in Table 3-2 (labeled as APP 0, APP 1, APP 2, APP 4, and APP 8) and Fig 3-10. The mobility in the saturation region and the threshold voltage of the OTFT are $1.9 \times 10^{-3} \text{ cm}^2/\text{Vs}$ and -21.7V ,

respectively. On the other hand, the values of field-induced current at the same gate voltage for APP4 has almost ten times higher than without treatment, as shown in Table 3-1 and Fig 3-10. After surfacing treatment, threshold voltage reduce down to -8.3V and field-effect mobility ($\mu_{\text{sat}} = 2.6 \times 10^{-2} \text{cm}^2/\text{Vs}$) which is 15-fold improvement over the mobility on bare silicon oxide.

In order to further analyze the phenomenon about surface treatment of APPT, we used atomic force microscope (AFM) to observe the surface morphology. Contact angle was measured to judge the surface state. The contact angle and surface roughness of SiO_2 with different scanning times of APPT, as shown in Table 3-2. After surface treatment of APPT, the surface of SiO_2 (contact angle $< 10^\circ$) will approach hydrophobic state. With increasing times of surface treatment, contact angle will present an increasing trend. When scanning times are more than four times, the increasing trend of contact angle will be flattened gradually, as shown in Fig 3-11. In the AFM micrography, the rms values of surface roughness increases with increasing scanning times of APPT. The rms value of surface roughness changes from 6.07 nm for APP4 to 10.42 nm for APP8. The surface roughness will become more smooth after spin-coating P_3HT , as shown in Table 3-2.

In general, most inorganic oxide surface including SiO_2 shows hydrophilic state while most of organic semiconductor (P_3HT in this case) shows hydrophobic states. Therefore, this mismatch has bad influence on crystalline formation of organic semiconductor fabricated on oxide substrates [47]. So it could result in good influence on increment of crystallinity and also increase field-effect mobility. After surface treatment of APPT, surface of SiO_2 becomes more hydrophobic (increment of contact angle), as shown in Fig 3-11. It obtains

the improvement of field-effect mobility in our experiment. We observe the contact angle of APP4 and APP8 which are similar, but field-effect mobility of APP8 is somewhat decay compared with APP4. It is speculated that APP8 is too rough so that cause scattering effect [48].

Detailed photography of contact angle and AFM under different conditions, as shown in Fig 3-12 and Fig 3-13.

3.5.2 Spin-coating and evaporated of HMDS-treated SiO₂

As mentioned in previous section, we only emphasized on surface treatment of APPT. Here, we provide another two methods of surface treatment which were spin-coating HMDS and evaporated HMDS. Many reaserchs about spin-coating HMDS could be refer to [47,49]. We will compare the difference about the three methods, and discuss the relationship of them.

As shown in Fig 3-14 and Fig 3-15, plot of drain current I_D versus gate voltage V_G at various drain voltage V_D and drain current I_D versus gate voltage V_G at various drain voltage V_D . Fig 3-14 shows the realthionship of I-V about spin-coating HMDS, and Fig 3-15 shows the realthionship of I-V about evaporated HMDS. The same calculation for threshold voltage and mobility in saturation region is listed in Table 3-3 (labeled as APP 0, Spin-coating, Evaporation, and APP4) .

Additional measured values such as contact angle and surface roughness also are shown in Table 3-3. The two methods have obvious improvement in our experiment. The mobility in the saturation region was 4-fold for spin-coating HMDS ($\mu_{sat} = 7.8 \times 10^{-3} \text{ cm}^2/\text{Vs}$) and 11-fold for evaporated HMDS ($\mu_{sat} = 2.2 \times 10^{-2} \text{ cm}^2/\text{Vs}$) higher than no treatment ($\mu_{sat} = 1.9 \times 10^{-3} \text{ cm}^2/\text{Vs}$). In Table3-3, for HMDS-treated SiO₂ has larger contact angle certainly, hence HMDS play an

important role in the interface between SiO_2 and P_3HT . Threshold voltage also decreases after HMDS-treated SiO_2 referred to [47]. Comparison of field-effect mobility and threshold voltage is shown in Fig 3-16. The plot of measured contact angle for spin-coating and evaporation is shown Fig 3-17, and Fig 3-18 shows the AFM photography. Surface of SiO_2 remains smooth after spin-coating and evaporated HMDS. Comparison of $I_D\text{-}V_G$ and $I_D\text{-}V_D$ is shown in Fig 3-19. For magnitude of current at the same operated voltage, APP4 > Evaporation > Spin-coating > No treatment. So APPT is still better than the other methods of HMDS-treated SiO_2 in our experiment.

3.5.3 Hysteresis

Figure 3-25 plots a typical hysteresis curve. This curve depicts the response of the polarization, P , to the externally applied electric field, E . The hysteresis curve saturates at P_{sat} when the maximum alignment of the spontaneous polarization occurs. When the electric field is removed instantaneously after reaching P_{sat} , the electronic polarization associated with the linear capacitance component decreases to zero, and the spontaneous polarization, P_S , remains.

Then, within milliseconds usually, the polarization decays to the remnant polarization, P_r . For much longer times, the polarization is observed to decay linearly with the log of time for many orders of magnitude of time [50].

The current that flows through the gate-dielectric/channel interface is widely believed to be dominant during the operation of OTFTs. Therefore, electronic conduction at the interface is expected directly to affect the TFT performance. This effect is directly related to the hysteresis behavior, which

is induced by the trap sites at the interface in OTFTs. P₃HT films that are deposited on the gate dielectric have many trap sites, depending on the surface state of the gate dielectric. Undoubtedly, if the gate dielectric contains trap sites inside the bulk, then these trapped charges may also induce hysteresis. The hysteresis of gate dielectrics represents a potential problem that can limit their range of applications, because this hysteresis leads to instability of the threshold voltage in OTFTs. Various studies of hysteretic behavior observed in OTFTs have been published [51,52]. However, in this work, the effects of oxide trapping are assumed to be weaker than those of interface trapping. This assumption is similar to that made in previous investigations and is supported by changes in the extent of hysteresis with the use of various surface modification protocols [53,54]. In recent reports, -OH groups have been identified as the origin of the electron trapping sites that are largely responsible for the hysteretic behavior observed in OTFTs [55,56]. Since the dielectric layer (SiO₂) in this work is an -OH-rich surface, the hysteretic behavior is very serious (Fig.3-26). Therefore, when the surface is transformed from an -OH-rich surface into a CH₃-terminated surface by HMDS surface treatment, the hysteresis behavior decreases (Figs 3-27~3-32). Furthermore, the formation of well-defined orientation of P₃HT grains markedly reduces the hysteresis by reducing the number of grain boundaries, such as when the surface is treated by evaporation, APP 4 and APP 8 (Figs. 3-28, 3-31 and 3-27). Treatment of the surface by evaporation yields less hysteresis than the other methods: perhaps evaporation forms the flattest surface. In one investigation [57], the surface roughness caused strong variations in the local field with associated scattering of carriers and the possible formation of carrier traps. These results offer clear evidence that -OH groups, the

orientation of P₃HT and the surface roughness of the gate dielectric surface, are responsible for the hysteresis behavior that is observed in OTFTs.

3.5.4 Anomalous leakage current

According to the ID-VG plots in Fig 3-33, current increases as VG approaches 0 V, especially following surface treatment by APP. For the APP process (Fig 3-34), the magnitude of the current as VG approaches 0 V follows the order APP 4 > APP 8 > APP 2 > APP 1, perhaps because of an anomalous leakage current. The gate leakage current increase may have two causes – weak points [51], and the higher channel conductance of the OTFTs [58]. The poor uniformity and roughness of the surfaces are the main sources of the “weak points, which act as local high-electric-field regions where breakdown occurs.

These weak points enhance carrier injection and further increase the leakage current. As presented in Fig 3-33, surface treatment by APP increased the leakage current, because the surface became rougher. However, although the surface of APP 8 is rougher, the leakage current is smaller than that of APP 4. APP 4 surface treatment may enlarge the crystalline domain of P₃HT, causing the high channel conductance. In the future, to improve the anomalous leakage current will be studied.

3.5.5 Crystallization behavior of P₃HT

Isothermal crystallization and melting was monitored using a Seiko

SSC-5200 differential scanning calorimeter (DSC), and the temperature was calibrated using indium. About 5 mg of the polymer (P₃HT) sample was weighed very accurately. It was pre-heated at 70 °C, 90 °C, 110°C, 130 °C and 150 °C for 3 min and then cooled to room temperature at a rate of 20 °C /min. The sample was subsequently reheated to 300 °C (Run 1), cooled to room temperature and then reheated to 300 °C (Run 2) to study its melting behavior.

The heating rate and the cooling rate were 20 /min. All measurements were made in a nitrogen atmosphere, and each sample was used only once to mitigate any effect of thermal degradation after treatment at high temperature. The thermogravimetric analysis (TGA) indicated that the thermal degradation temperature of P₃HT was approximately 500 °C (Fig. 3-35). Figures 3-36~3-40 plot the melting temperature (T_m) and crystallization enthalpy (ΔH) of P₃HT for various pre-heating temperatures. These data were collated in in Figs. 3-41 (Heat Run 1) and 3-42(Heat Run 2) and Table 3-5. The melting temperature did not vary in Run 1 or Run 2, but the enthalpy in Run 1 increased with the pre-heating temperature up to 130°C . The greater enthalpy of crystallization indicated a higher degree of crystallinity - because the higher temperature gave the molecular chain enough kinetic energy to increase the overall crystallinity of P₃HT. However, an excessive temperature caused the molecular chain to move too fast, reducing the strength of its orientation. Hence, the P₃HT baking condition herein was set to 130 for 3 min. The enthalpy in Run 2 did not markedly fluctuate, because the

P₃HT became amorphous after Run 1 at up to 300°C. The crystallization effect of pre-heating disappeared, and the enthalpy in Run 2 was almost the same in various pre-heating temperatures.

3.5.6 XRD and UV-VIS for highly oriented crystals of P₃HT

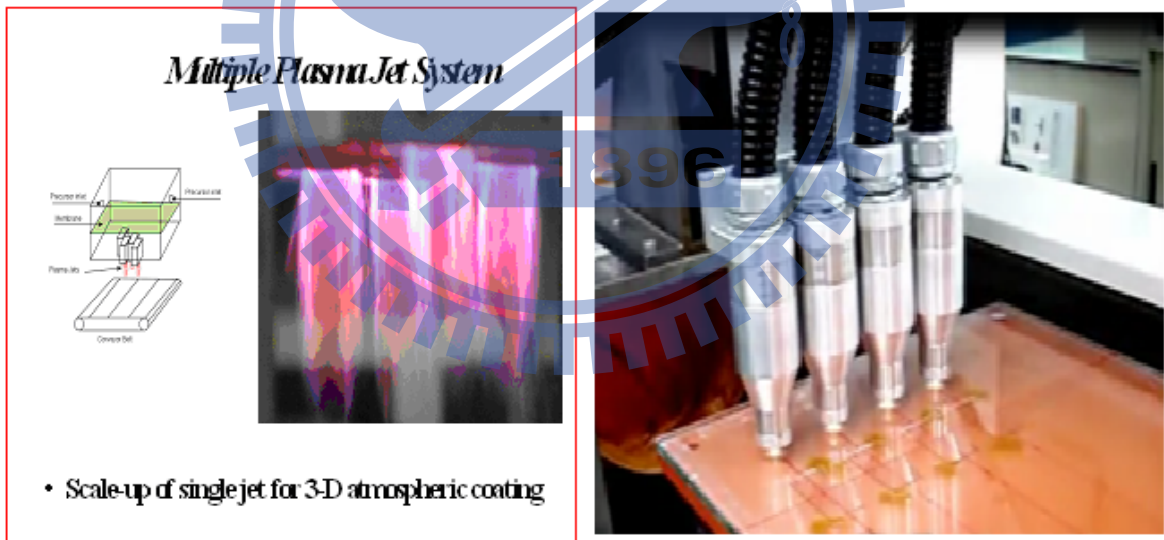
X-ray analysis indicates that the polymer films were composed of microcrystalline domains that were embedded in an amorphous matrix, and inside these microcrystalline regions, the polymers π stack in one direction such that use the analysis with UV-VIS, because P₃HT is a single bond duplet bond arranges the conjugate structure alternately, the high polymer chain's conjugate long is longer, (Lamda max) will be bigger to the ultraviolet ray absorption wave length, moreover, the position rule higher will also have the same phenomenon UV-VIS absorption spectra reveal π - π absorption, and lamella of the interlocking side chains in the other direction [59,60]. In another investigation [61], XRD data and UV-VIS absorption spectra suggest that the molecules are oriented such that their long axis is almost normal to the film, and the π - π stacking direction is parallel to the substrate. XRD [62,63] and UV-VIS absorption [64,65] have been adopted in many studies to identify the P₃HT crystal. Wang et al [66] thought that the lowest energy (long wave length) absorbs the peak the relative strength to be higher, represents P₃HT in thin film structure order, the manufacture the organic thin film transistor original part can obtain high carries the child transport ratio, and this long wave often the absorbancy relatively strong reason lies in correlation strong relations between the P₃HT member chain's, i.e. mean distance between the P₃HT chain's are few phenomenon which creates. When the P₃HT is deposited on the SiO₂ surface, interchain stacking occurs in the molecular chain, so the molecules are ordered in a two-dimensional lamella structure [18]. If the

molecular structure of P₃HT exhibits high regioregularity (which is the percentage of stereoregular head-to-tail attachments of the hexyl side chains to the 3-position of the thiophene rings), then this lamellar structure will have the edge-on orientation, its (100)-axis will be normal to the film and the (010)-axis will be in the plane of the film. Previous research has verified that good ordering is a basic requirement of improved transistor performance (better field-effect mobility) [67,68]. Figure 3-43 shows the XRD diagrams obtained following various surface treatments, including a strong and sharp diffraction peak at 5.3φ (especially after treatment with APP 4), corresponding to an intermolecular spacing of 1.636 nm in the well-organized lamellar structure, which value is consistent with the literature. The intensity of the diffraction at the same diffraction angle follows the order APP 4 > Eva > Spin > No treatment. This result was consistent with the mobility of OTFT. The surface is predicted to be more hydrophobic after APP treatment, such that the P₃HT has more ordered domains along the (100)-axis and the mobility of OTFT is therefore higher.

Figure 3-44 presents the UV-VIS absorption spectra in the region of the π - π absorption regioregular P₃HT. The magnitude of the absorption peak at 610nm follows the order APP 4 > APP 8 > APP 2 > APP 1 > Spin > No treatment. This result was consistent with the mobility of OTFT. The figure indicates that modifying the surface with APP 4 increases the absorption peak at 610 nm, revealing increases in chain extension and chain alignment. In this chapter, XRD and UV-VIS were adopted to demonstrate that high mobility requires an ordered structure.

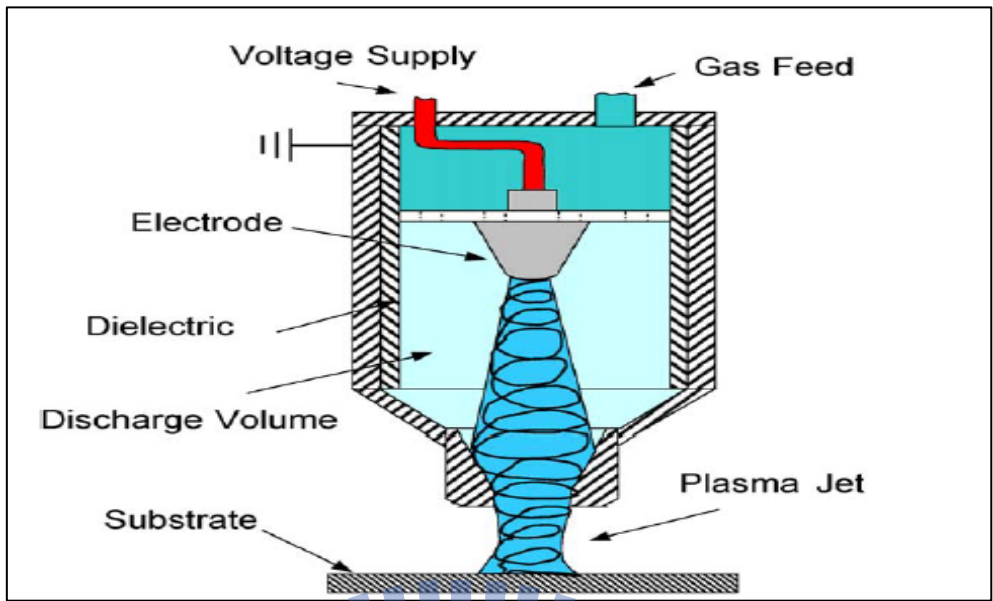


(a)

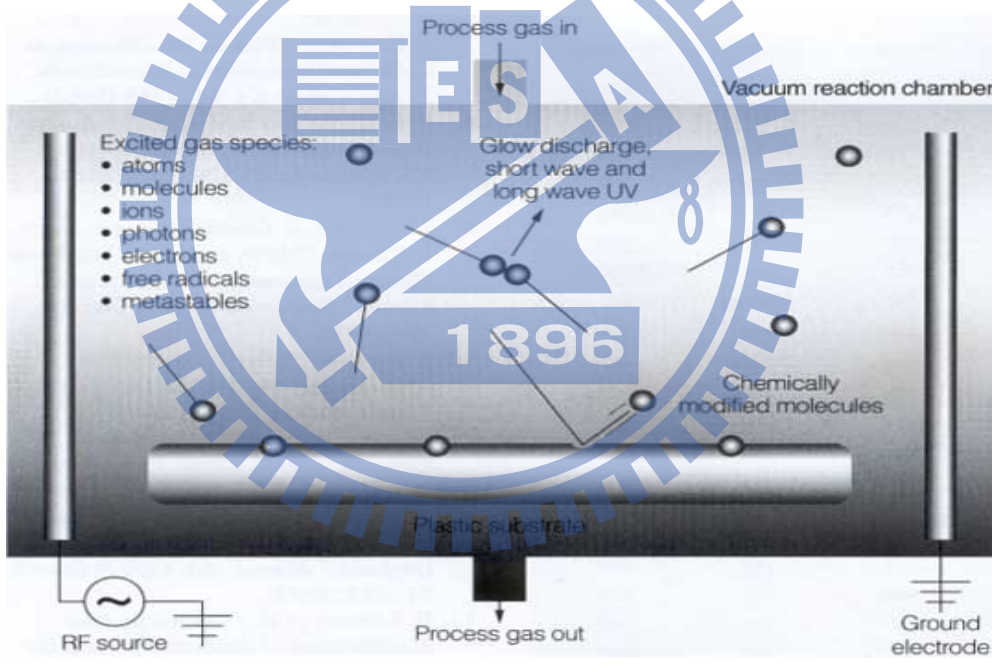


(b)

Figure 3-1: (a) The structure of APPT (b) The diagram of plasma surface treatment

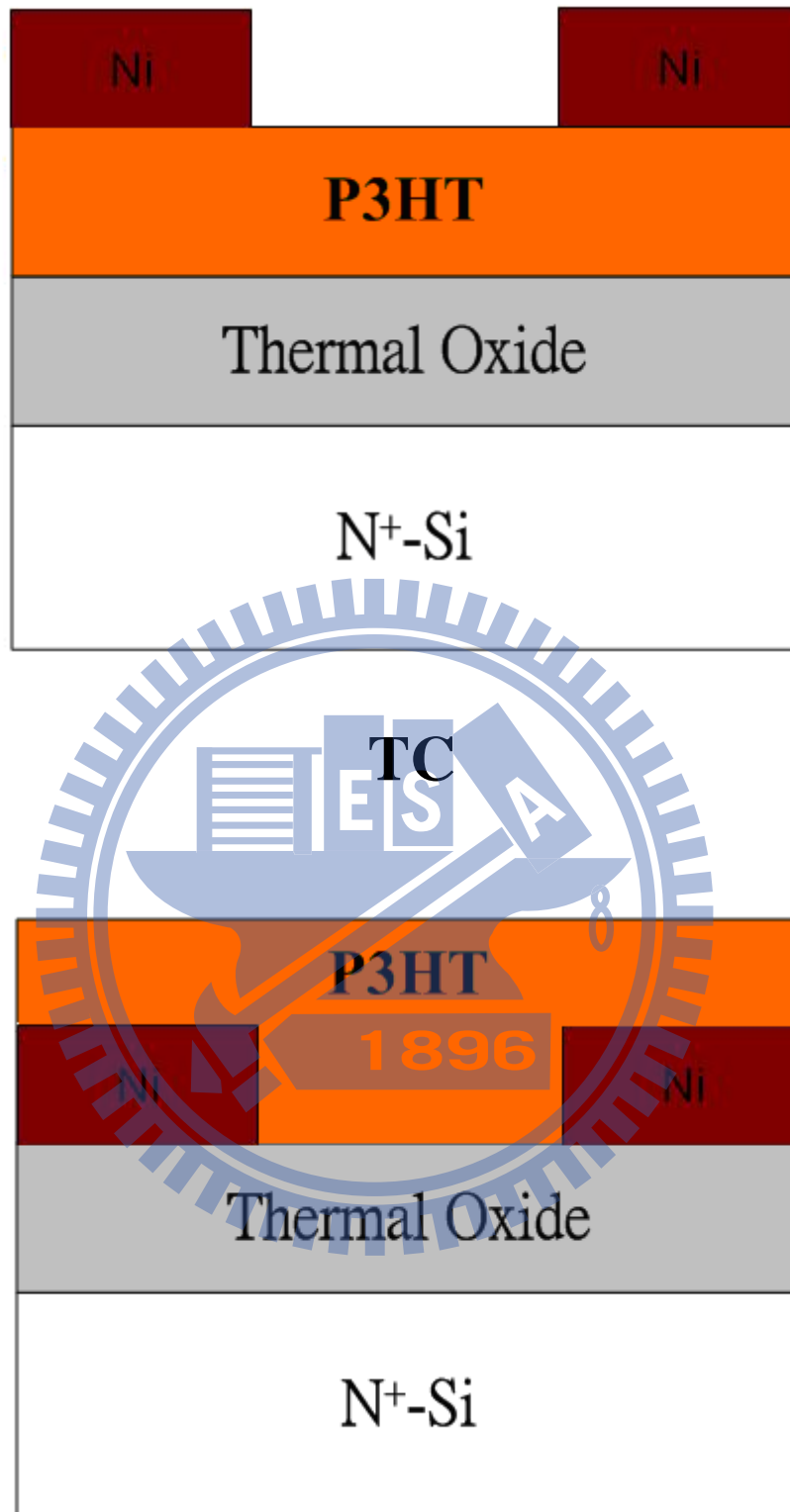


(a)



(b)

Figure 3-2: (a) APP system of ITRI (b) The other APP systems



BC

Figure 3-3: Two basic structures of OTFT

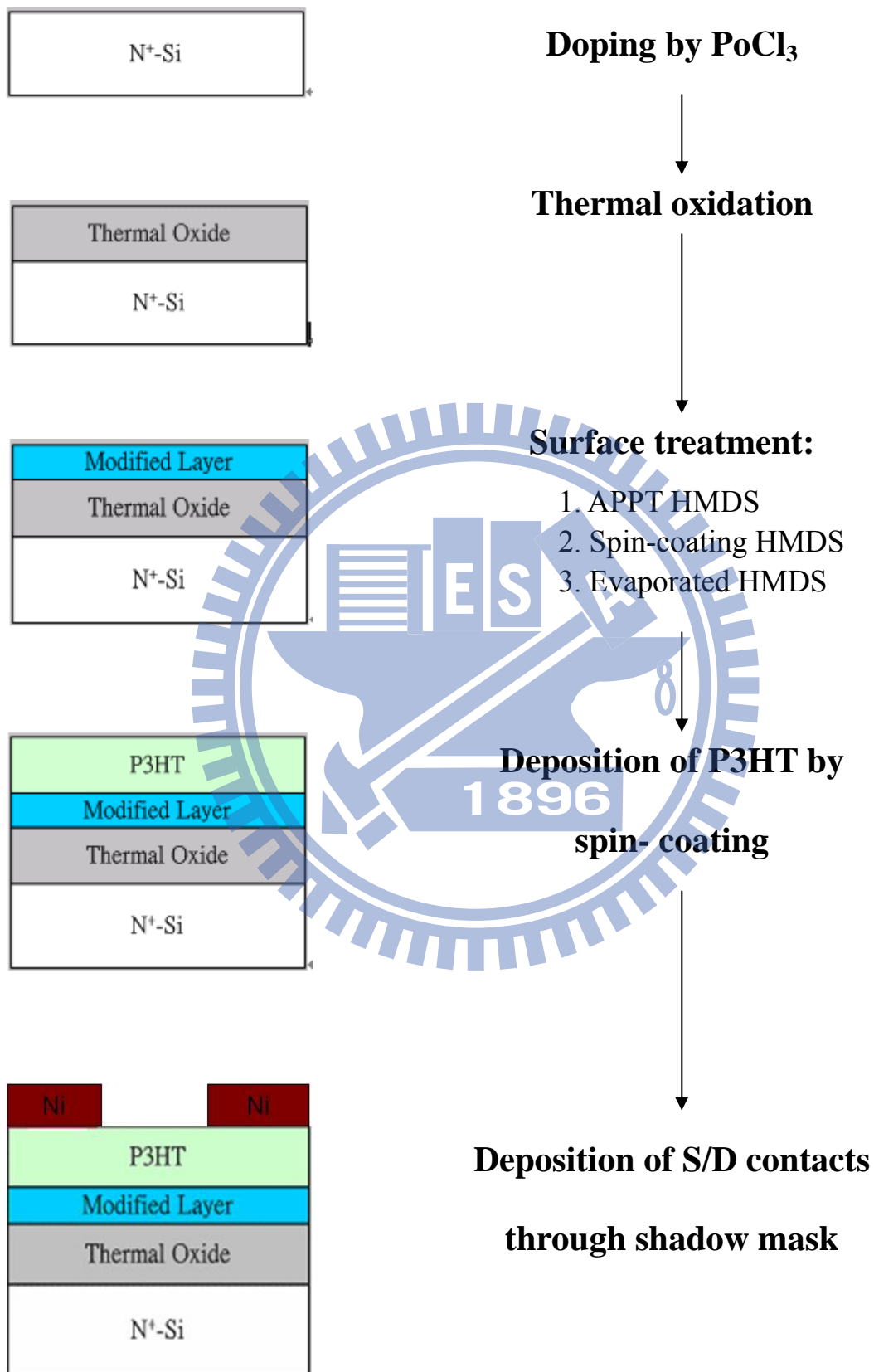
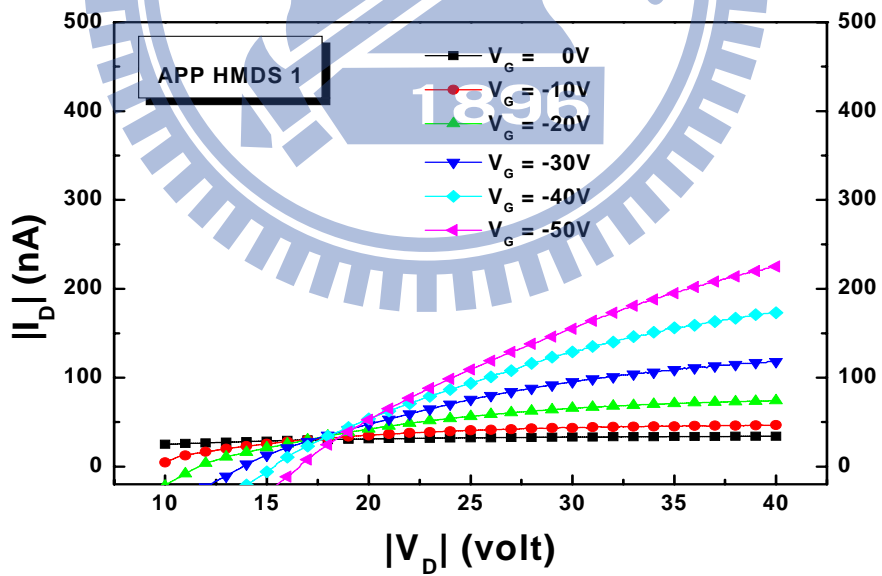
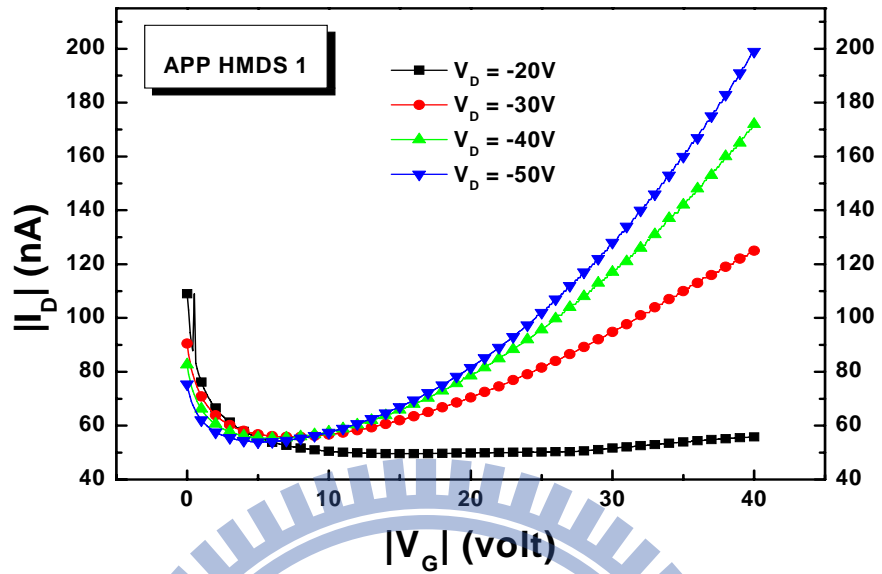


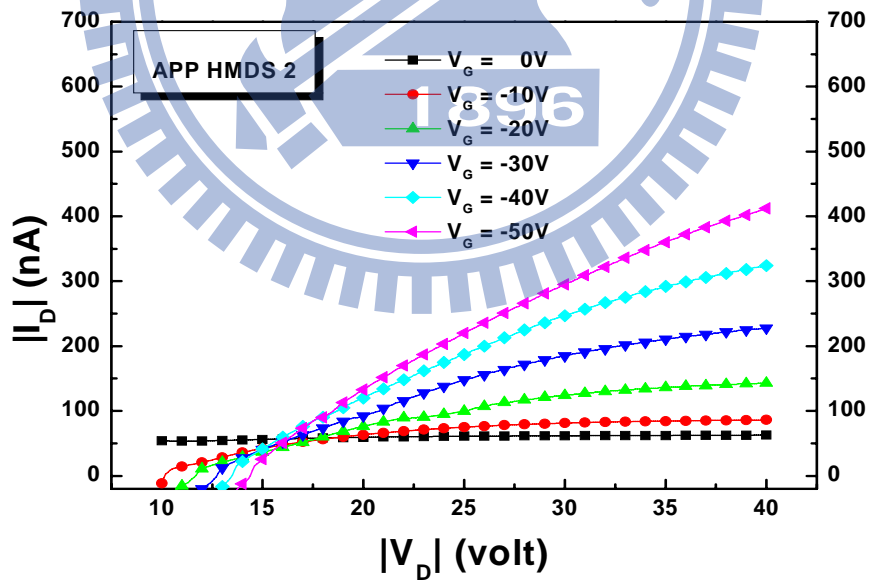
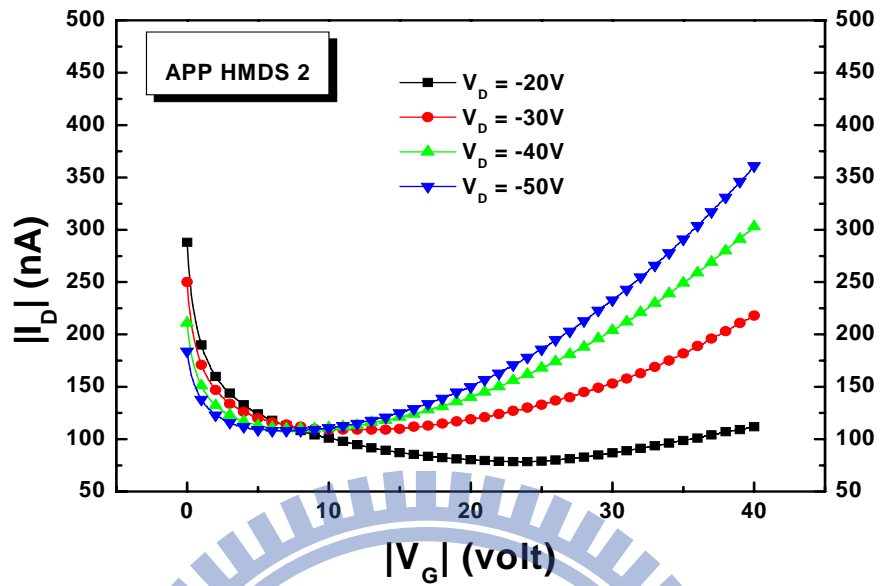
Figure 3-4: Process flow of top-contact OTFT



(b)

Figure 3-5: Surface treatment of APPT HMDS 1 for OTFT

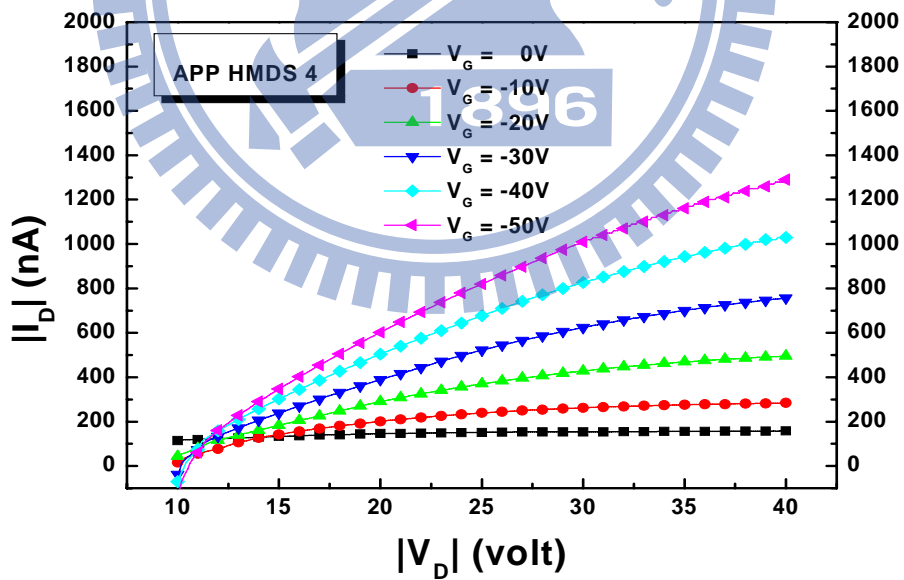
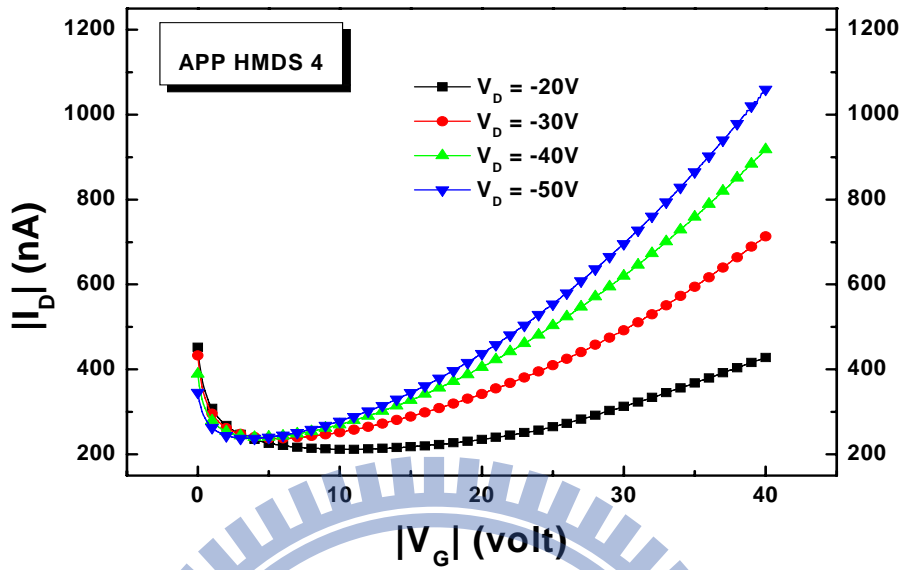
(a) I_D - V_G curve (b) I_D - V_D curve ($W/L = 2000 \text{ um}/500 \text{ um}$)



(b)

Figure 3-6: Surface treatment of APPT HMDS 2 for OTFT

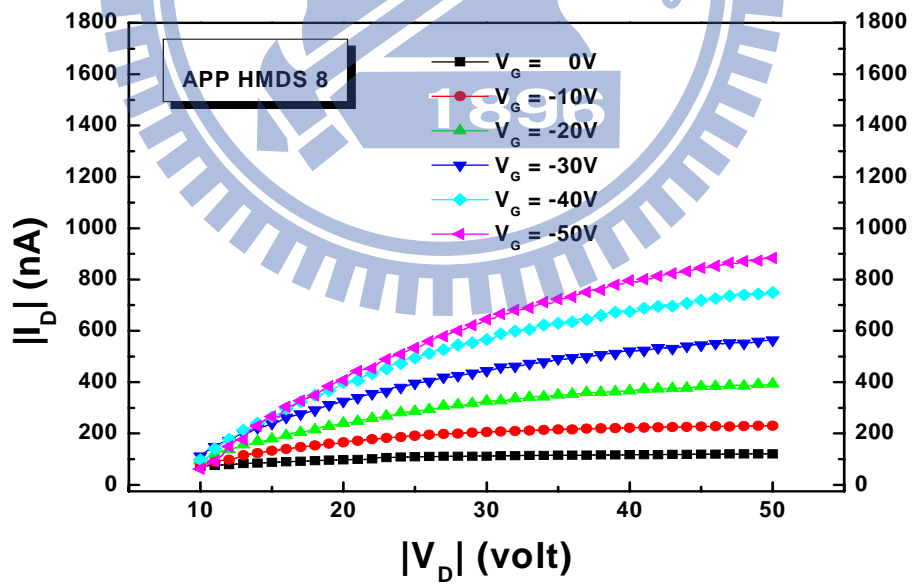
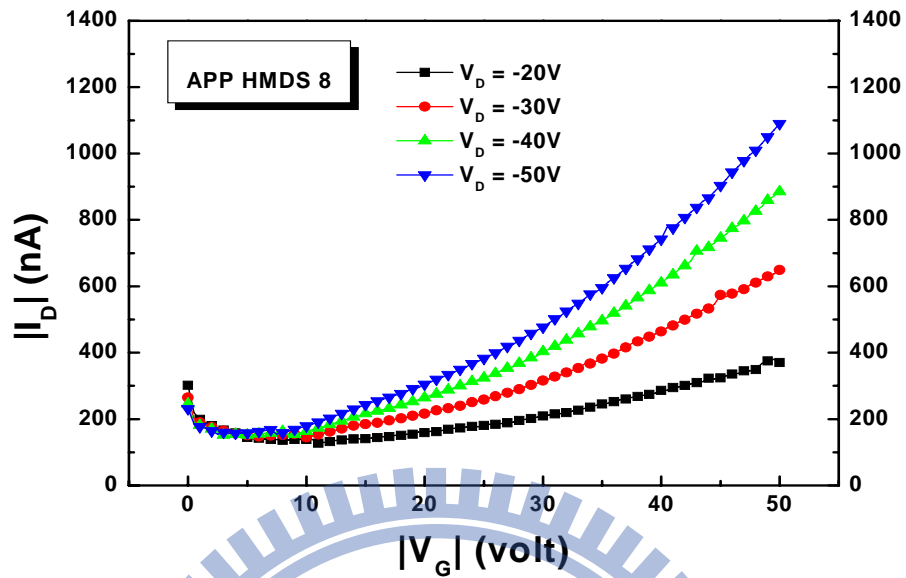
(a) I_D - V_G curve (b) I_D - V_D curve ($W/L = 2000 \text{ um}/500 \text{ um}$)



(b)

Figure 3-7: Surface treatment of APPT HMDS 4 for OTFT

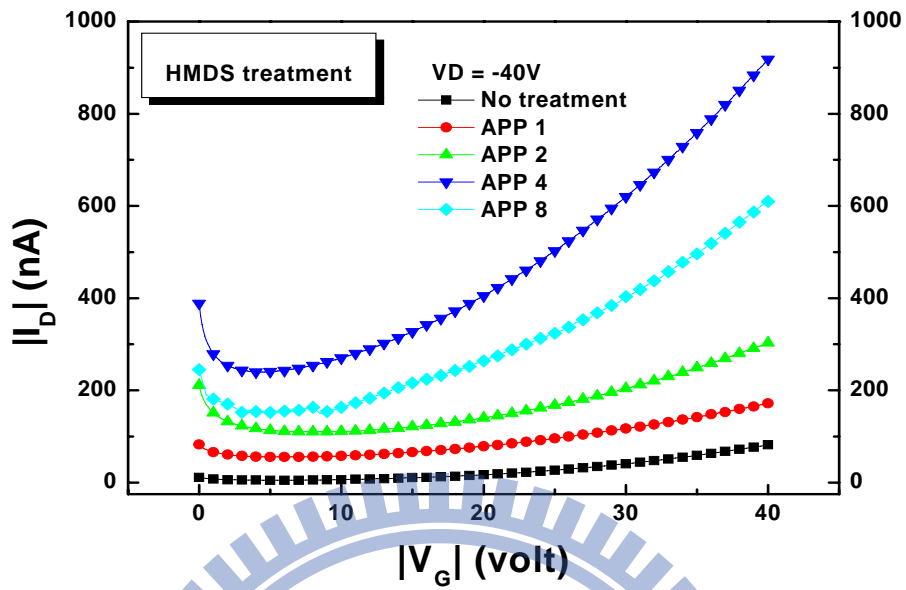
(a) I_D - V_G curve (b) I_D - V_D curve ($W/L = 2000 \text{ um}/500 \text{ um}$)



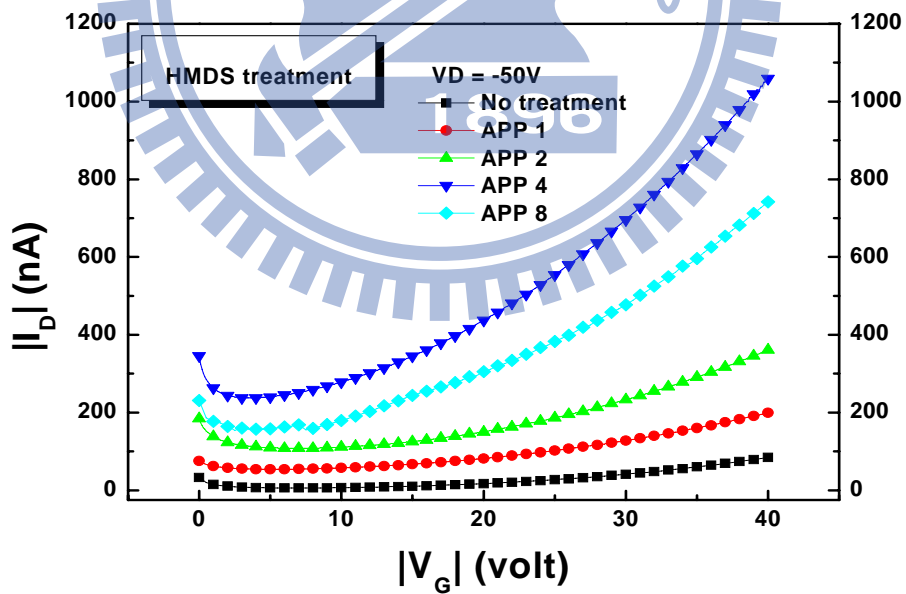
(b)

Figure 3-8: Surface treatment of APPT HMDS 8 for OTFT

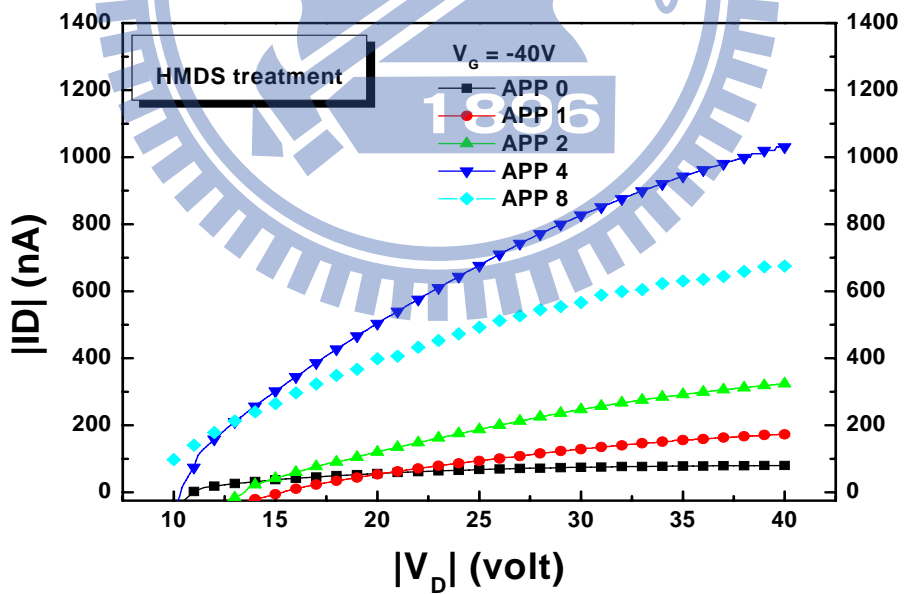
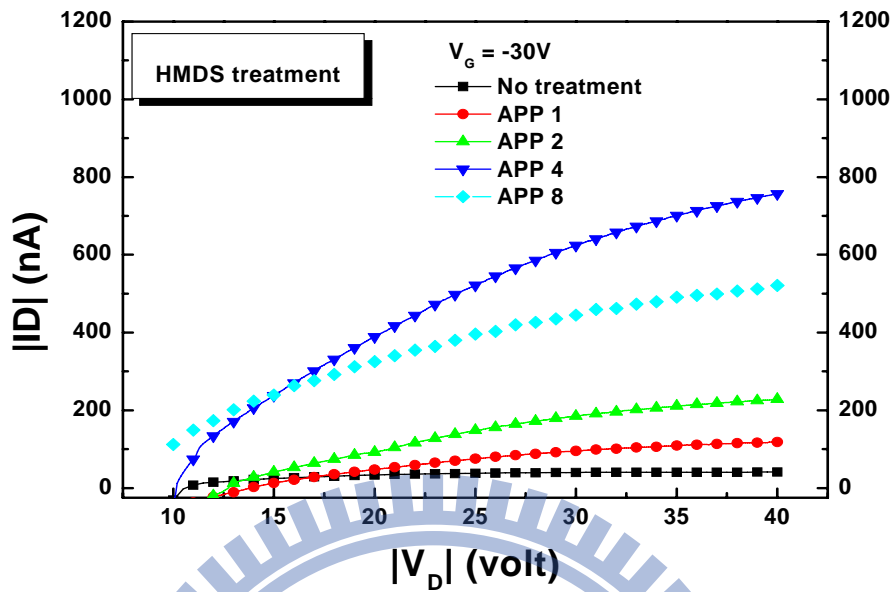
(a) I_D - V_G curve (b) I_D - V_D curve ($W/L = 2000 \text{ um}/500 \text{ um}$)



(a)



(b)



(d)

Figure 3-9: The comparison of (a), (b) I_D - V_G and (c), (d) I_D - V_D with different scanning times by APPT

Table 3-1: Electrical parameters of the OTFTs in this study.

Surface treatment	Mobility μ_{lin} (cm ² /Vs)	Mobility μ_{sat} (cm ² /Vs)	Threshold voltage V_{th} (V)
No treatment	1.2×10^{-3}	1.9×10^{-3}	-21.7
APPT-HMDS-1	3.5×10^{-3}	4.3×10^{-3}	-5.3
APPT-HMDS-2	4.2×10^{-3}	8.0×10^{-3}	-7.8
APPT-HMDS-4	1.7×10^{-2}	2.6×10^{-2}	-8.3
APPT-HMDS-8	1.3×10^{-2}	2.0×10^{-2}	-7.7

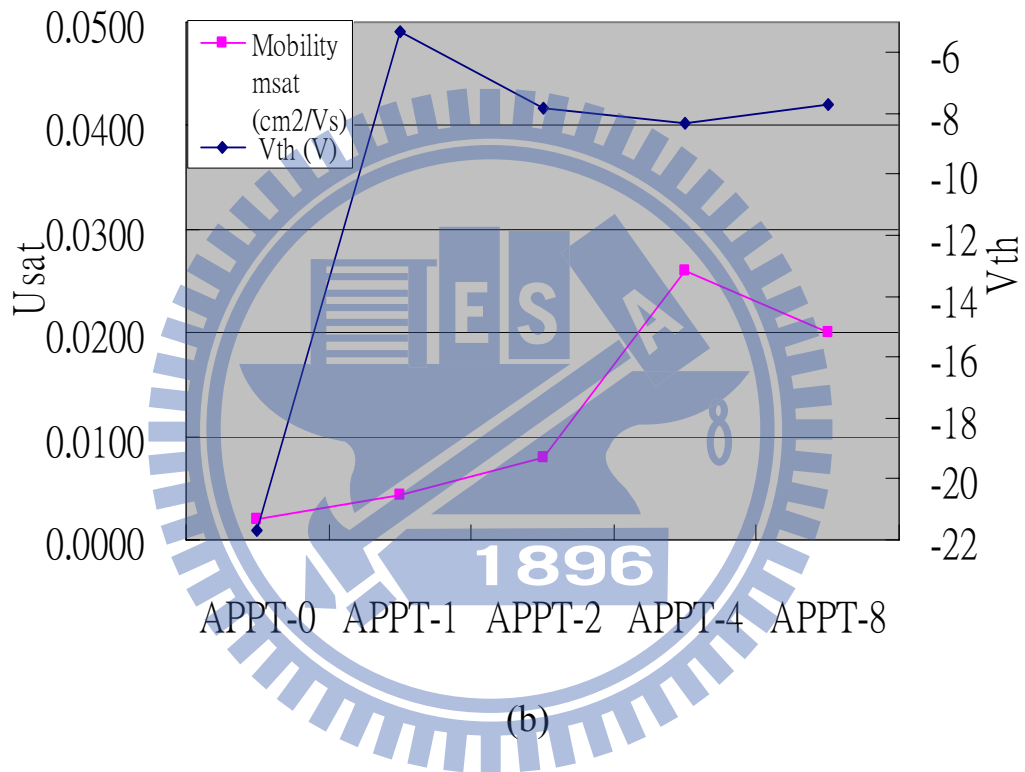


Figure 3-10: Comparison of threshold voltage and saturation mobility with different scanning times by APPT

Table 3-2: Comparison of contact angle and surface roughness with different scanning times by APPT

Surface treatment	Contact angle	Surface roughness (nm)	P ₃ HT surface roughness (nm)
No treatment	<10°	1.58	1.32
APPT-HMDS-1	68.9°	4.32	2.42
APPT-HMDS-2	76.3°	4.47	2.56
APPT-HMDS-4	90.5°	6.07	3.73
APPT-HMDS-8	90.9°	10.42	4.26

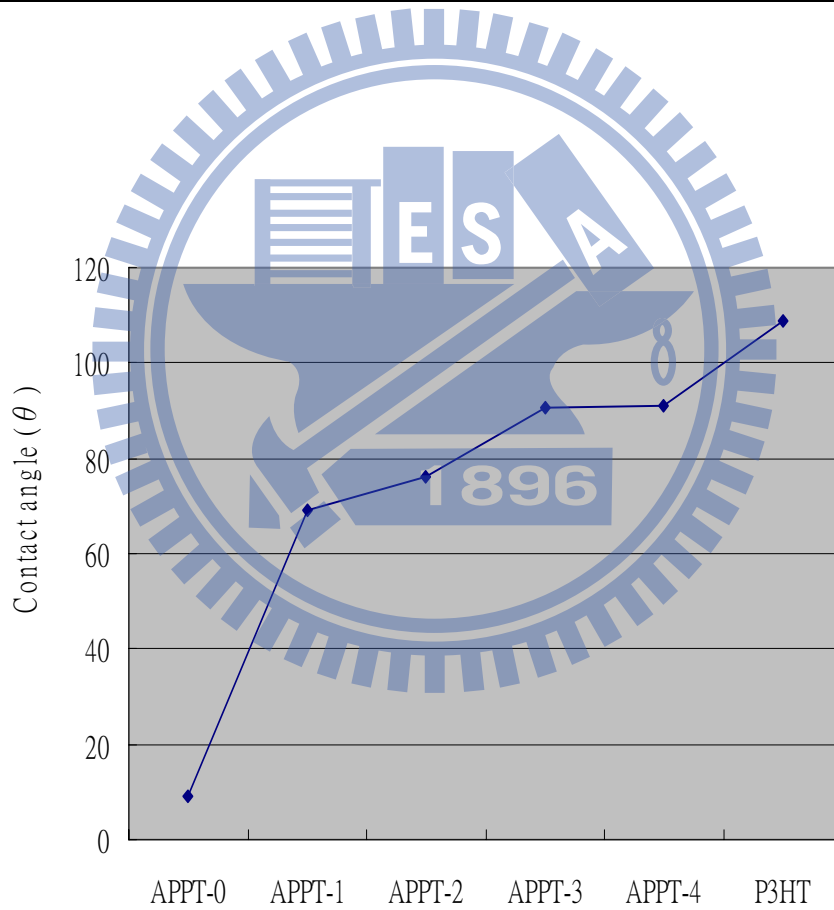
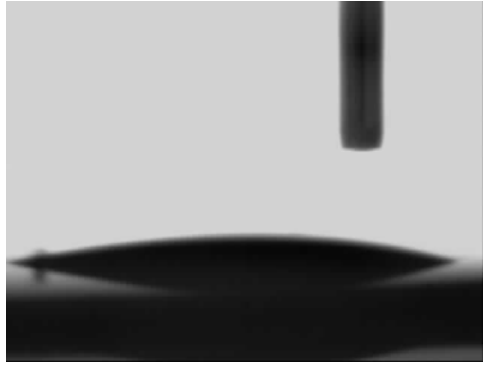


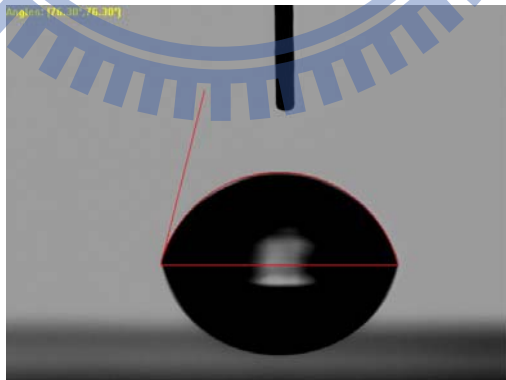
Figure 3-11: Contact angle vs. different scanning times by APPT



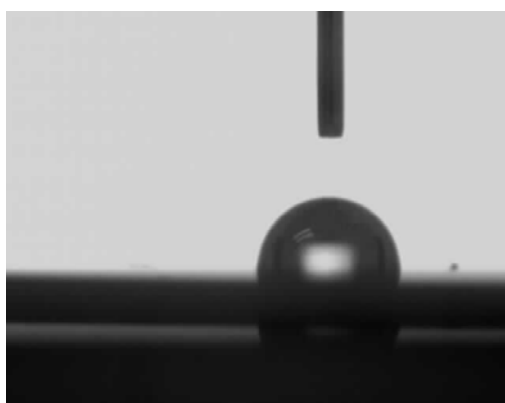
(a)



(b)



(c)



(d)



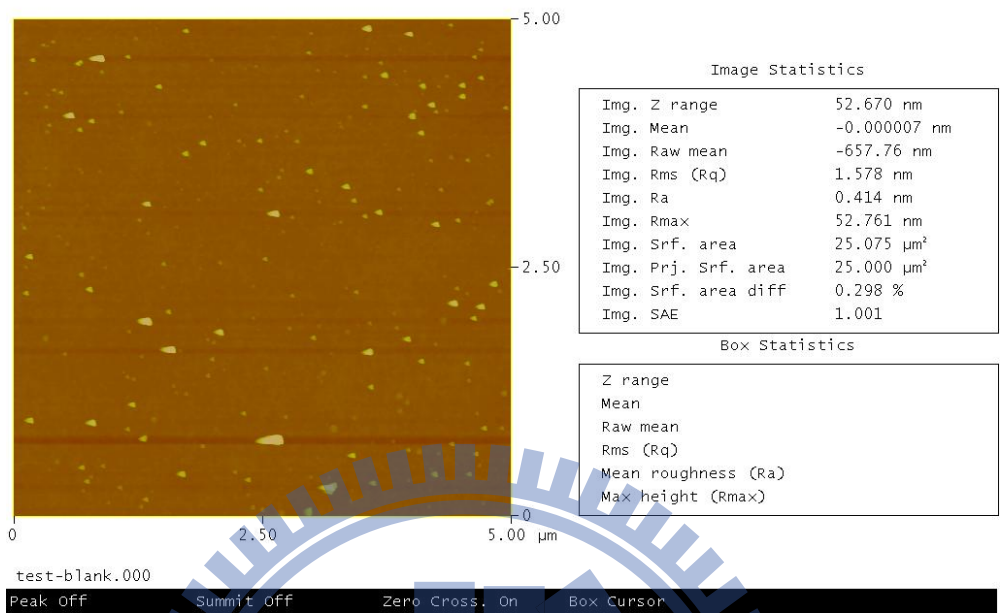
(e)

Figure 3-12: Contact angle of (a) No treatment ($<10^\circ$) (b) APP1(68.9°)

(c) APP2 (76.3°) (d) APP4 (90.5°) (e) APP8 (90.9°)

Peak Surface Area Summit Zero Crossing Stopband Execute Cursor

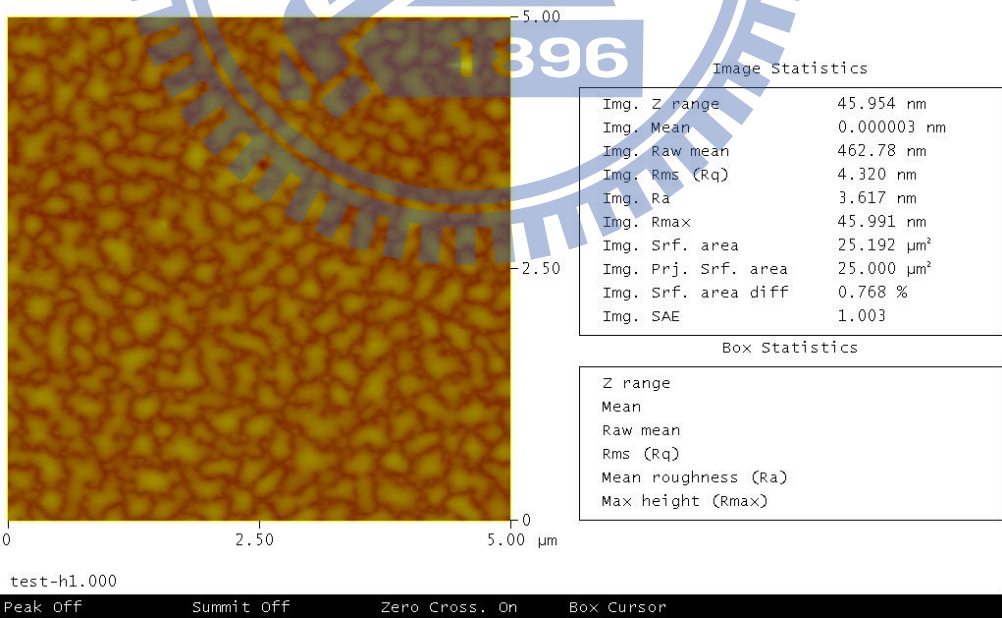
Roughness Analysis



(a)

Peak Surface Area Summit Zero Crossing Stopband Execute Cursor

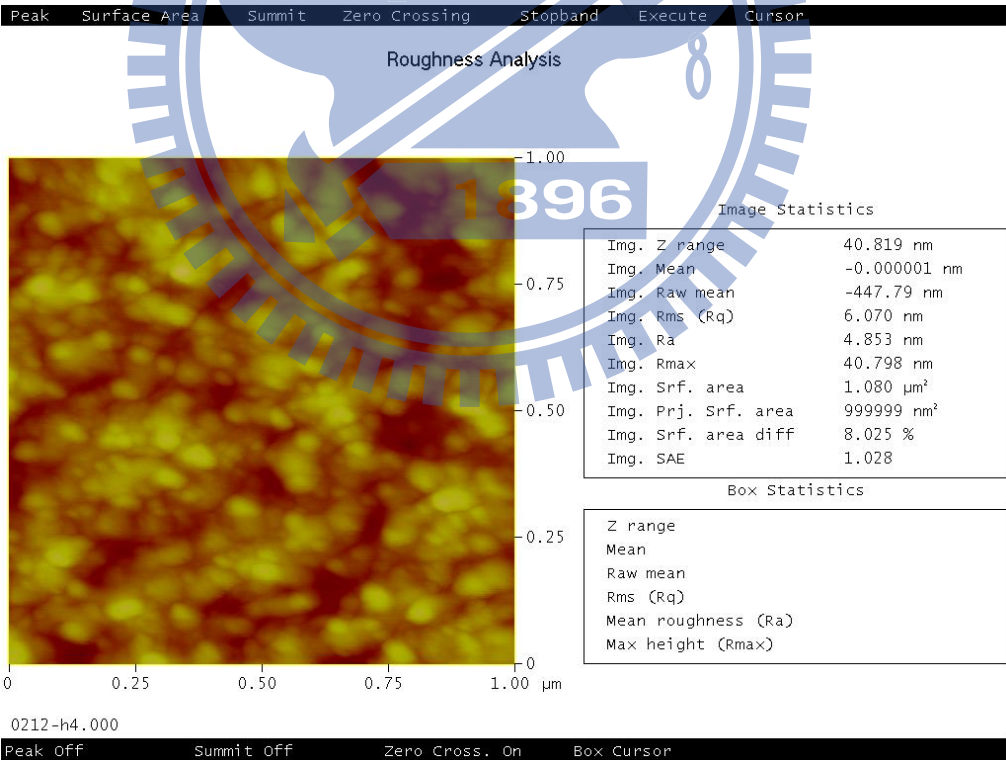
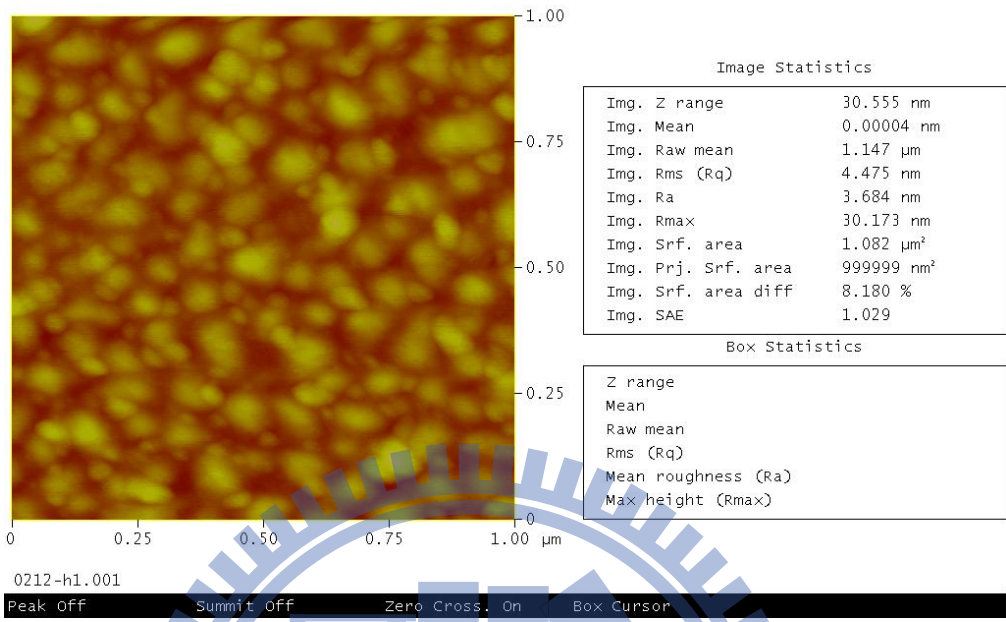
Roughness Analysis



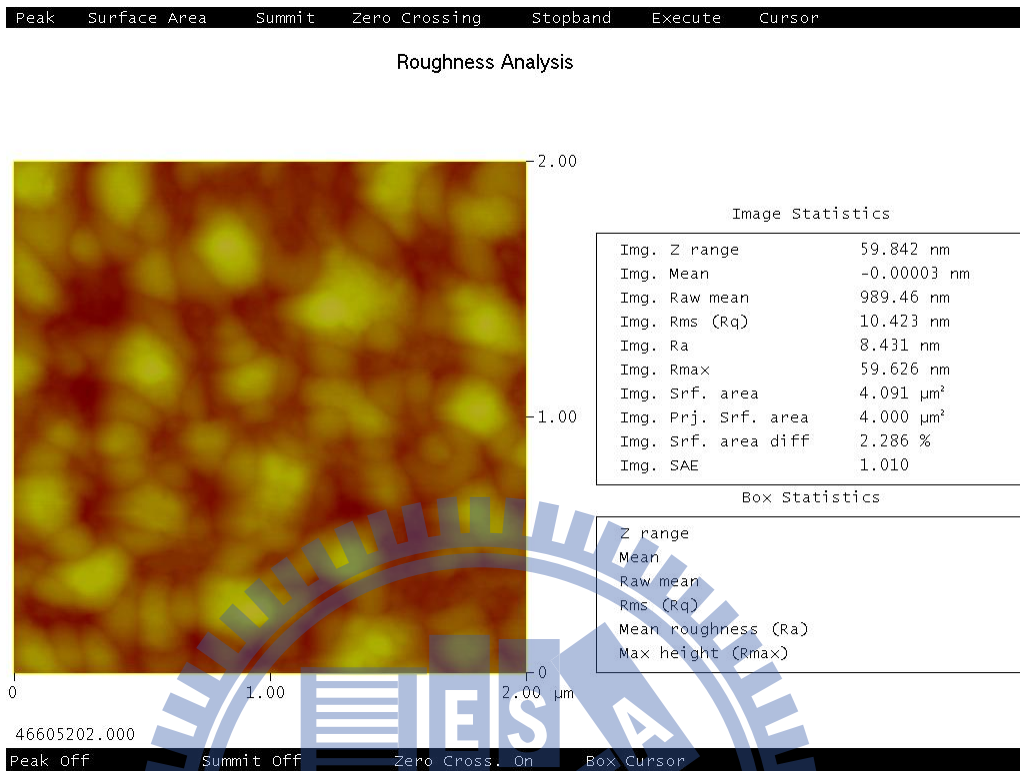
(b)

Peak Surface Area Summit Zero Crossing Stopband Execute Cursor

Roughness Analysis



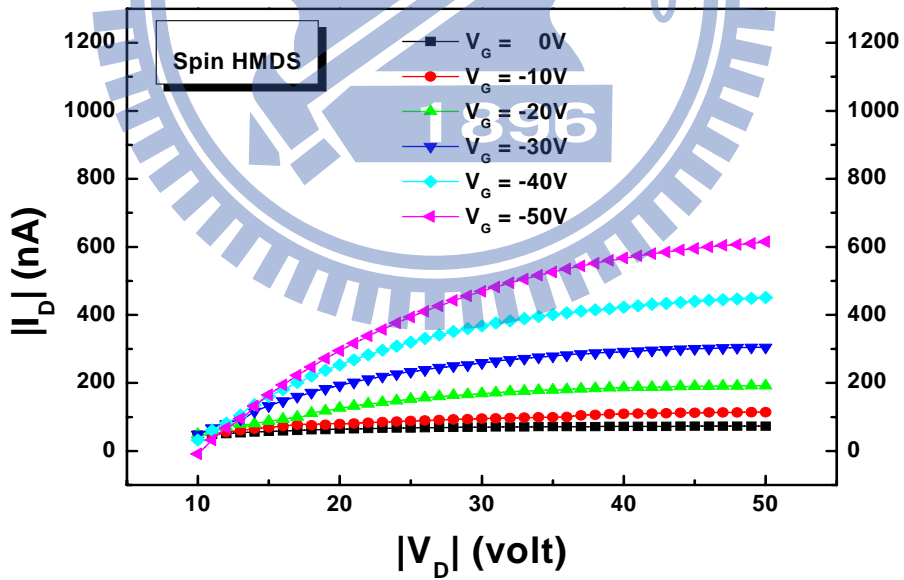
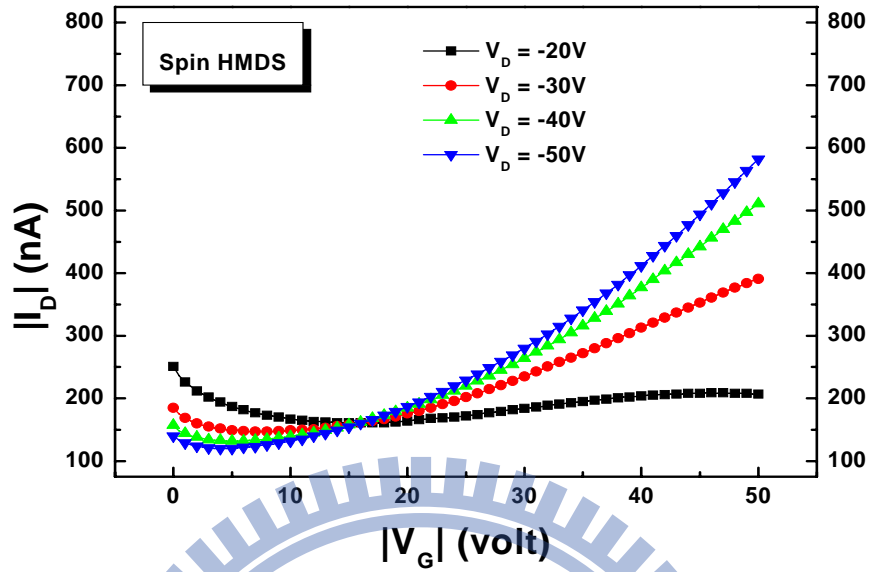
(d)



(e)

Figure 3-13: AFM micrography of (a) No treatment (b) APP1

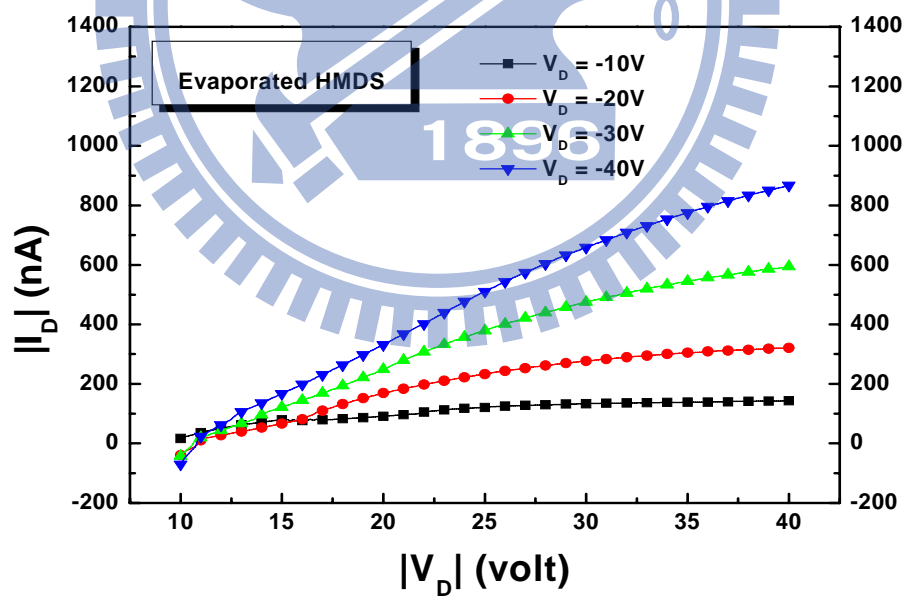
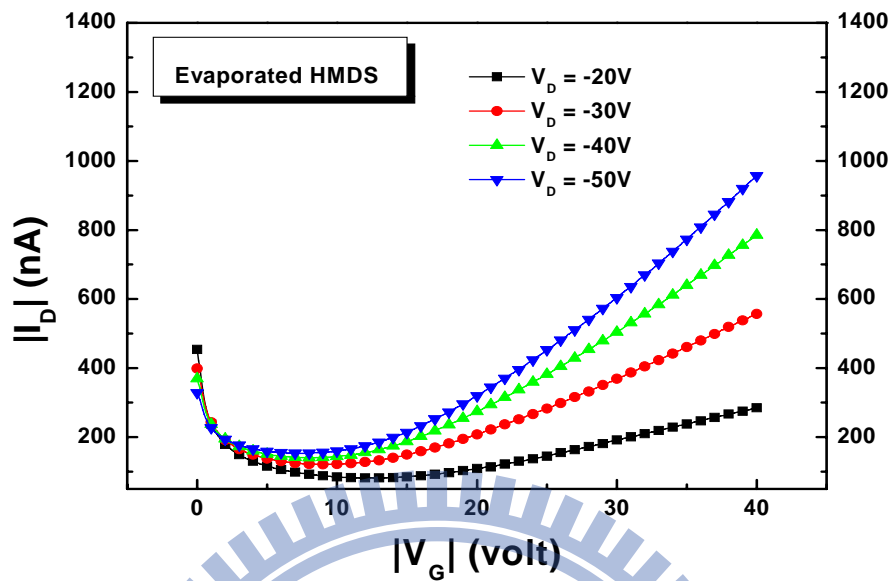
(c) APP2 (d) APP4 (e) APP8



(b)

Figure 3-14: (a) I_D - V_G curve (b) I_D - V_D curve with spin-coating HMDS

for OTFT



(b)

Figure 3-15: (a) I_D - V_G curve (b) I_D - V_D curve with evaporated HMDS

for OTFT

Table 3-3: The different methods of surface treatment

	u_{sat} (cm^2/Vs)	u_{lin} (cm^2/Vs)	V_{th} (Volt)	Surface roughness (nm)	Contact angle (degree)
No treatment	1.9E-3	1.2E-3	-21.7	1.580	<10
Spin-coating HMDS	7.8E-3	3.5E-3	-9.5	0.895	65.49
Evaporated HMDS	2.2E-2	4.2E-3	-12.0	0.890	75.28
APPT-HMDS-4	2.6E-2	1.7E-2	-8.3	6.07	90.46

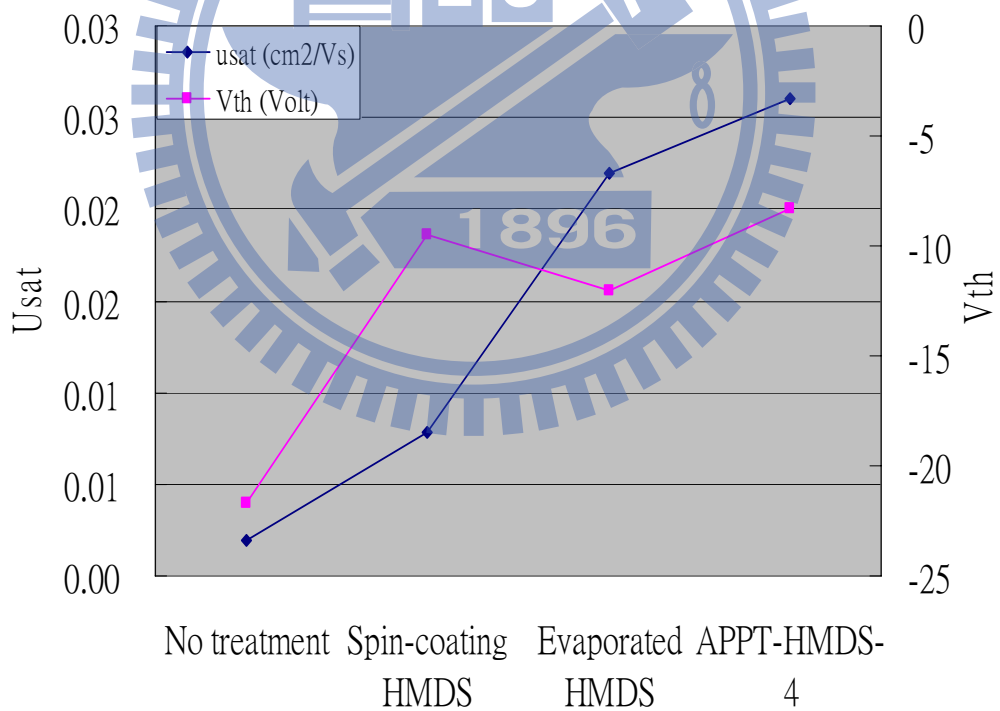
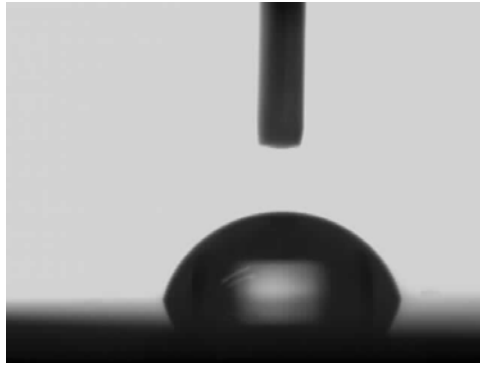
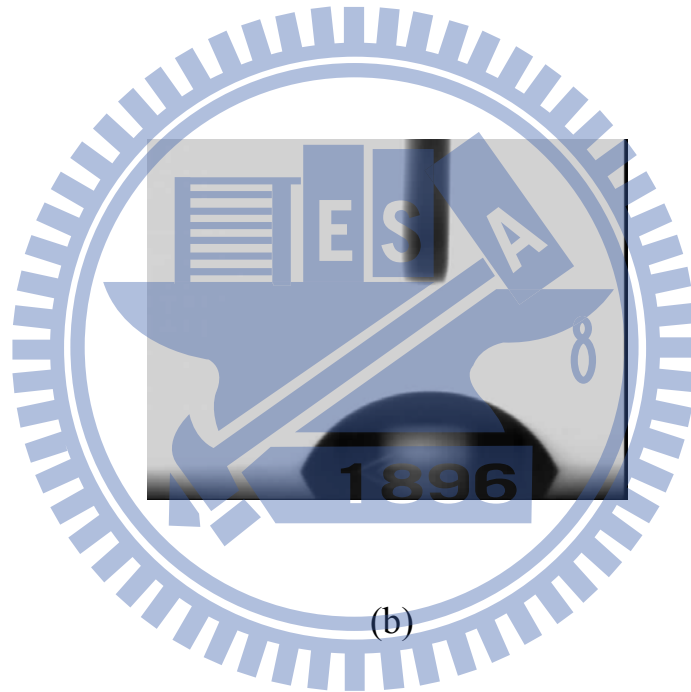


Figure 3-16: Comparison of threshold voltage and saturation mobility with different methods of surface treatment



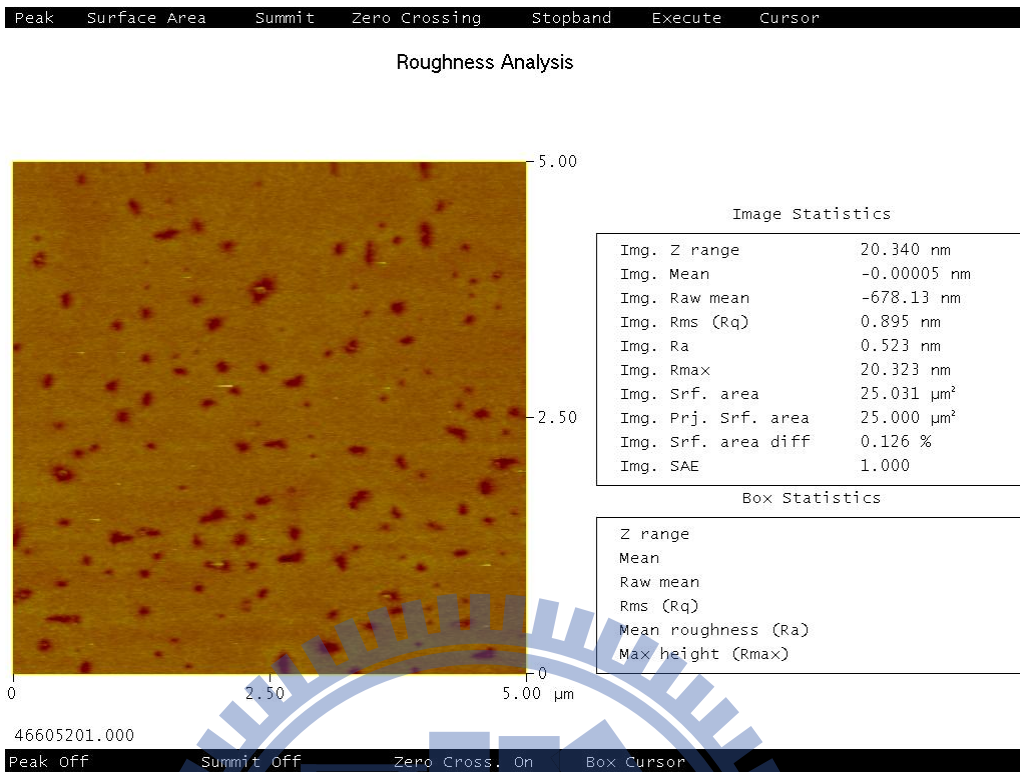
(a)



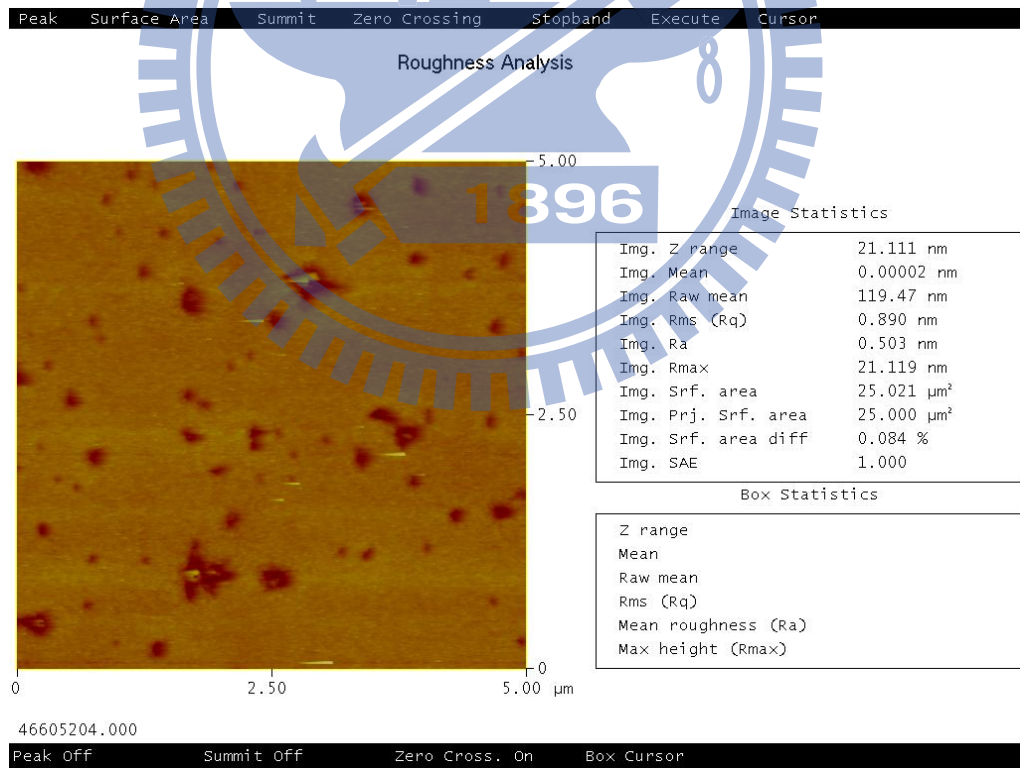
(b)

Figure 3-17: Contact angle of (a) spin-coating HMDS (65.49°)

(b) evaporated HMDS (75.28°)



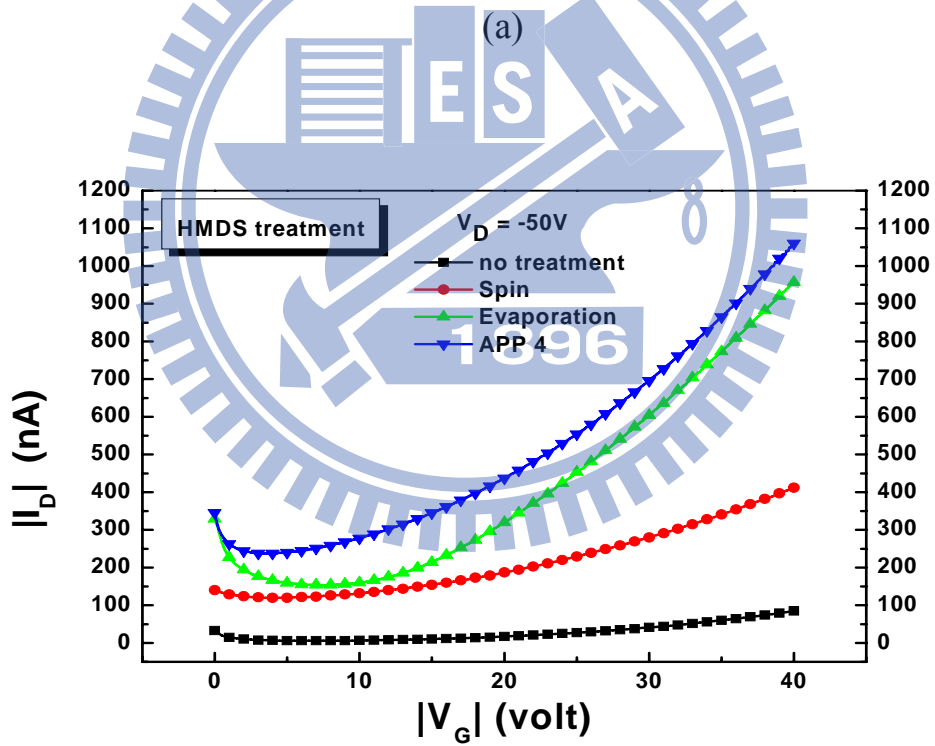
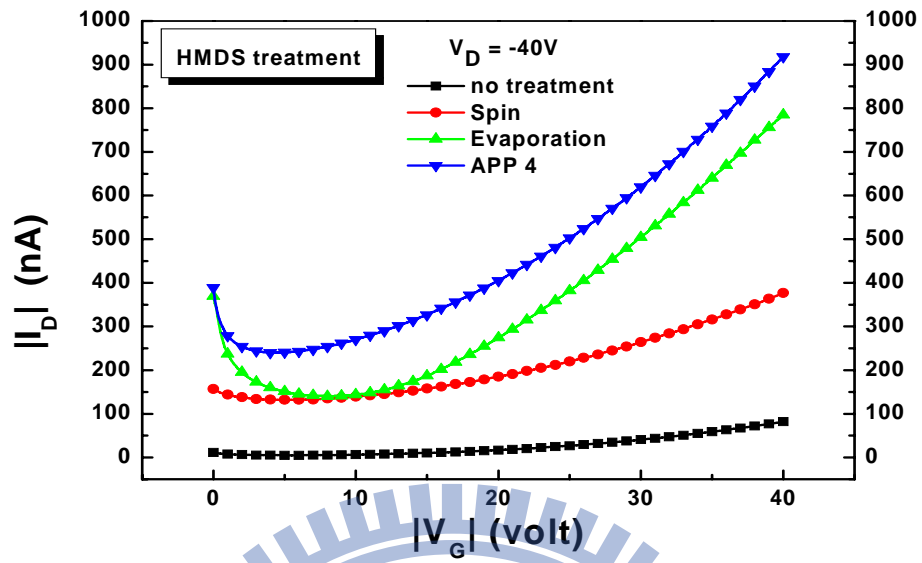
(a)



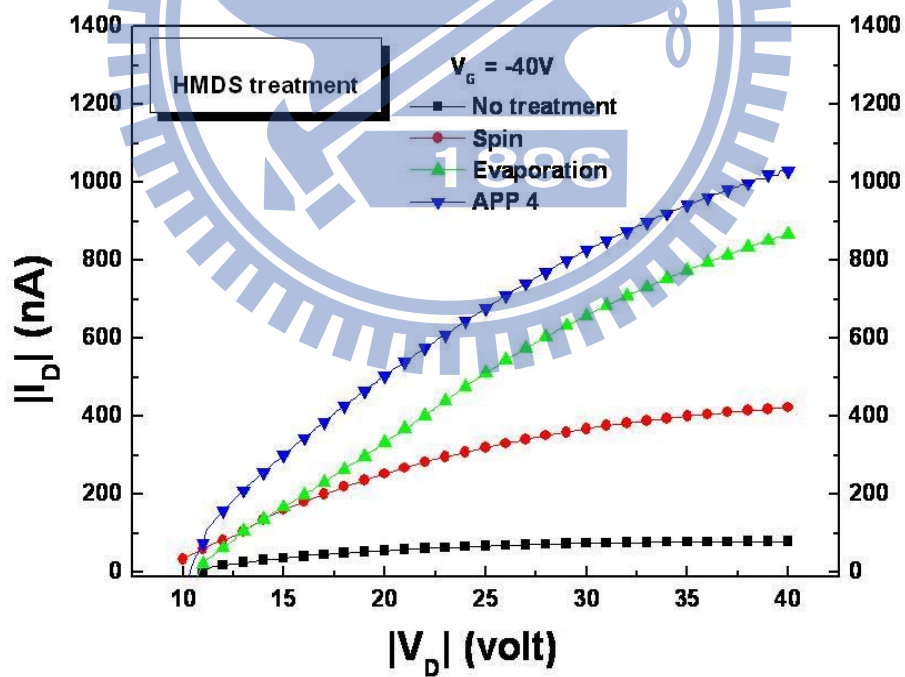
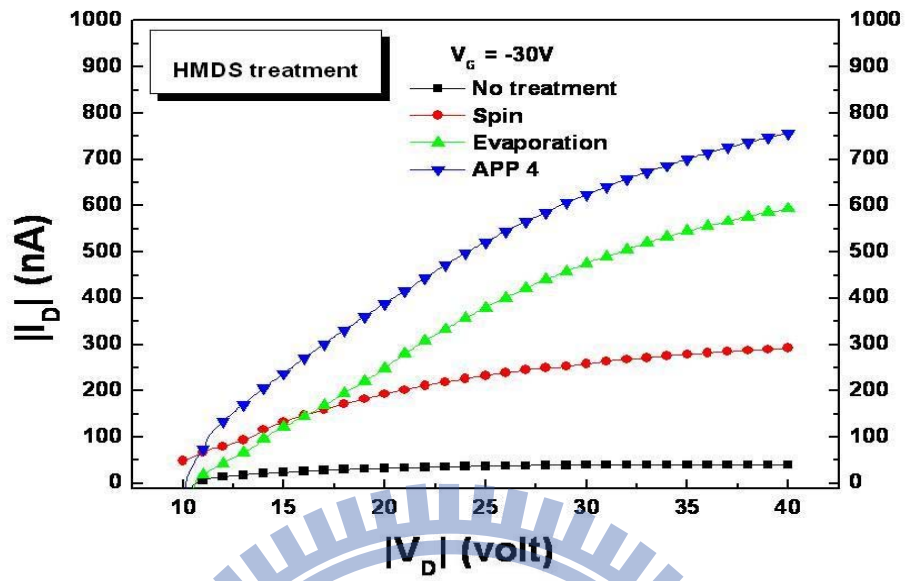
(b)

Figure 3-18: AFM photography of (a) Spin-coating HMDS

(b) evaporated HMDS



(b)



(d)

Figure 3-19: The comparison of (a), (b) I_D - V_G and (c), (d) I_D - V_D

with different methods of surface treatment

Table 3-4 The different methods of surface treatment

Surface treatment	$\mu_{sat}(cm^2/Vs)$	$V_{th}(cm^2/Vs)(Volt)$	roughness(nm)	Contact angle(θ)
No treatment	0.002	-21.7	1.58	<10
Spin	0.008	-9.5	0.895	65.49
Evap.	0.022	-12	0.89	75.28
APPT1	0.004	-7.8	4.47	68.9
APPT2	0.008	-8.3	6.07	76.3
APPT4	0.026	-8.3	6.07	90.46
APPT8	0.020	-7.7	10.42	90.9

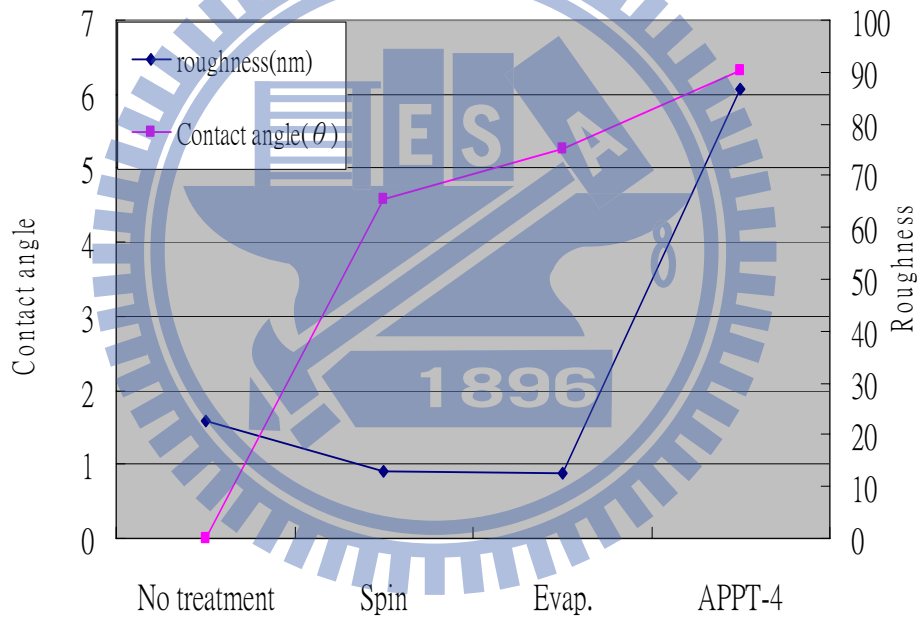


Figure 3-20: Comparison of contact angle and surface roughness with different methods of surface treatment

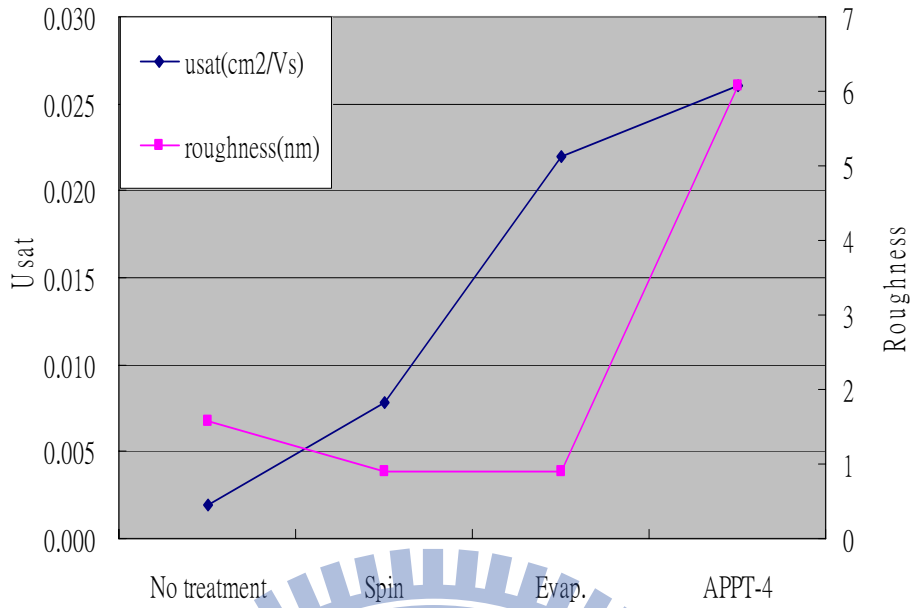


Figure 3-21: Comparison of surface roughness and mobility with different methods of surface treatment.

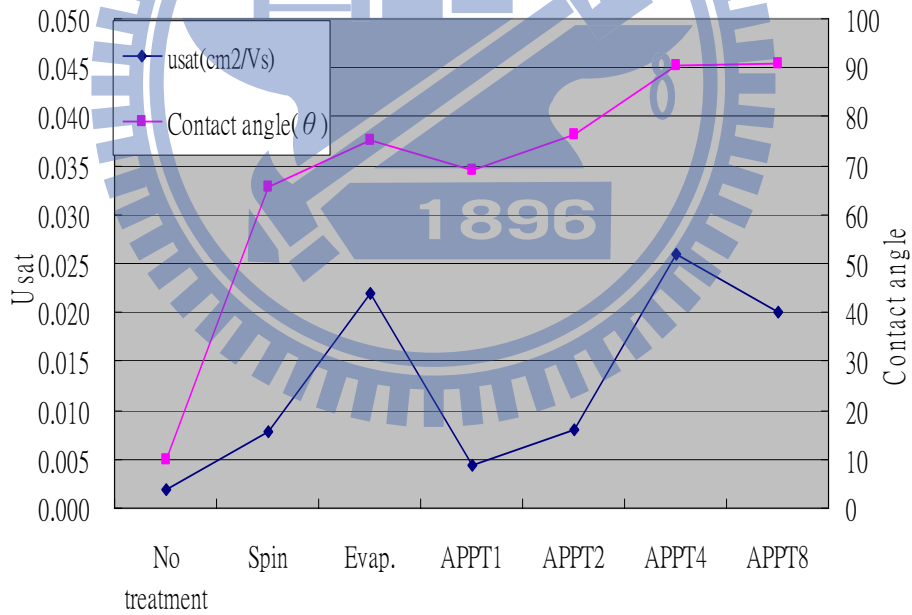


Figure 3-22: Comparison of contact angle and mobility with different methods of surface treatment and different scanning times by APPT

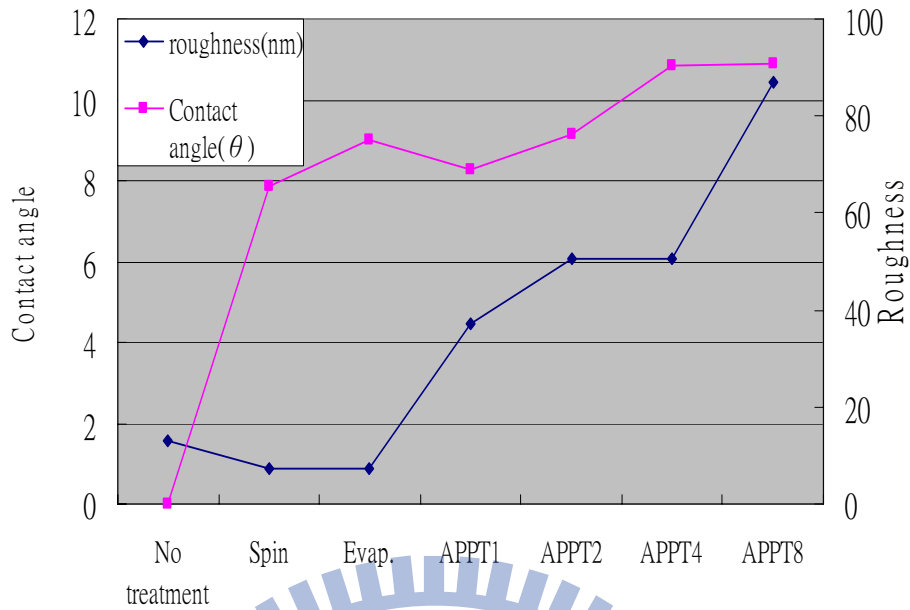


Figure 3-23: Comparison of contact angle and roughness with different methods of surface treatment and different scanning times by APPT.

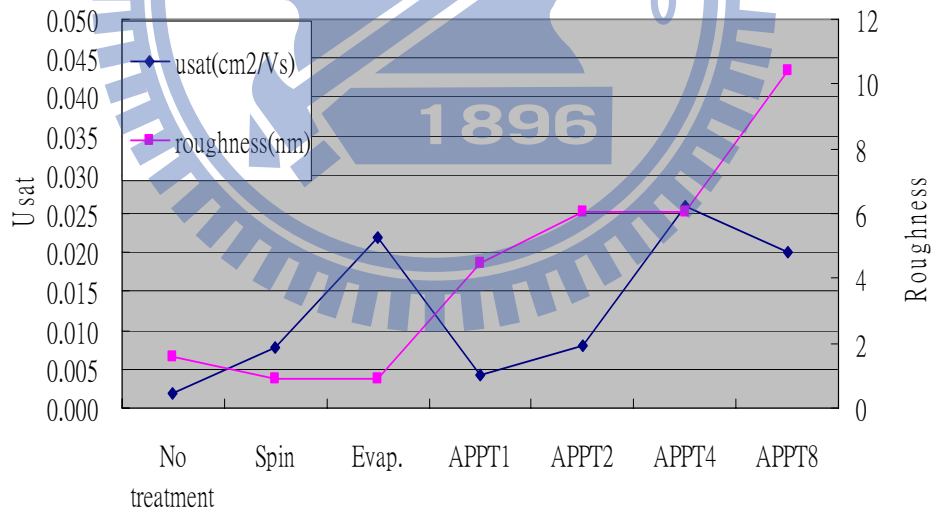


Figure 3-24: Comparison of roughness and mobility with different methods of surface treatment and different scanning times by APPT.

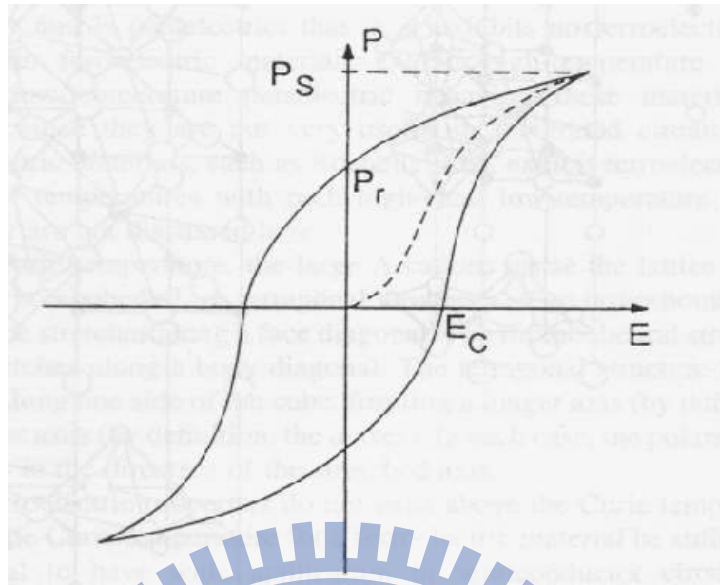


Figure 3-25: A typical hysteresis curve.

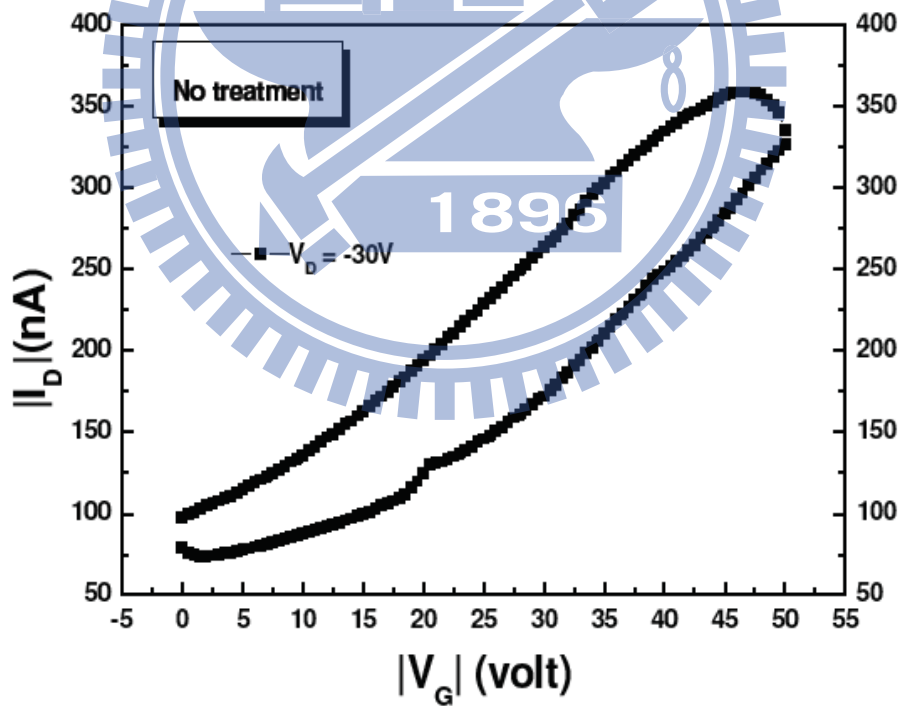


Figure 3-26: Hysteresis of P₃HT OTFTs with no surface treatment.

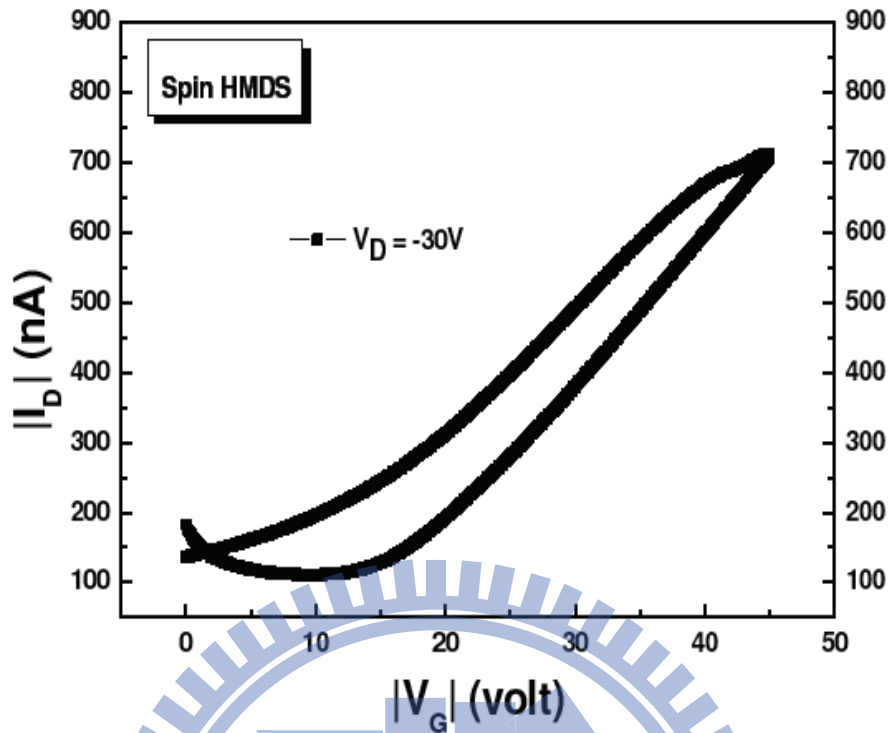


Figure 3-27: Hysteresis of P₃HT OTFTs with spin-coating surface treatment.

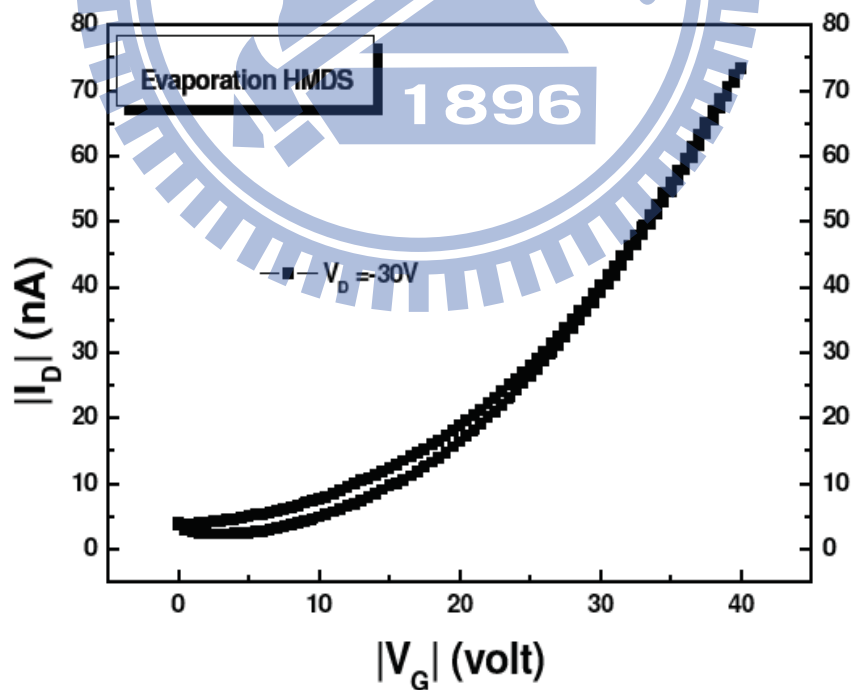


Figure 3-28: Hysteresis of P₃HT OTFTs with evaporation surface treatment.

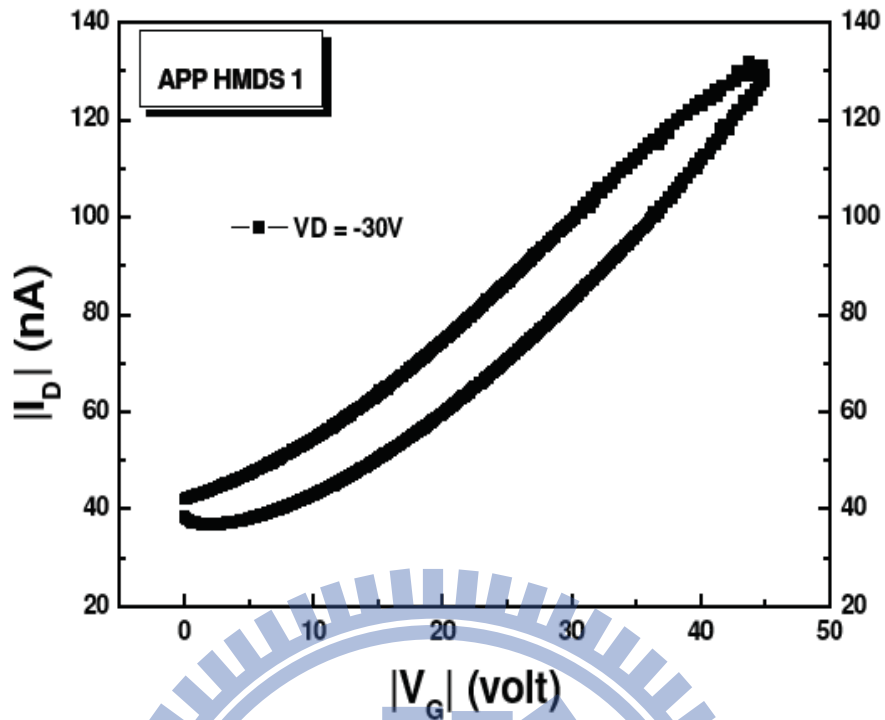


Figure 3-29: Hysteresis of P_3HT OTFTs with APP 1 time surface treatment.

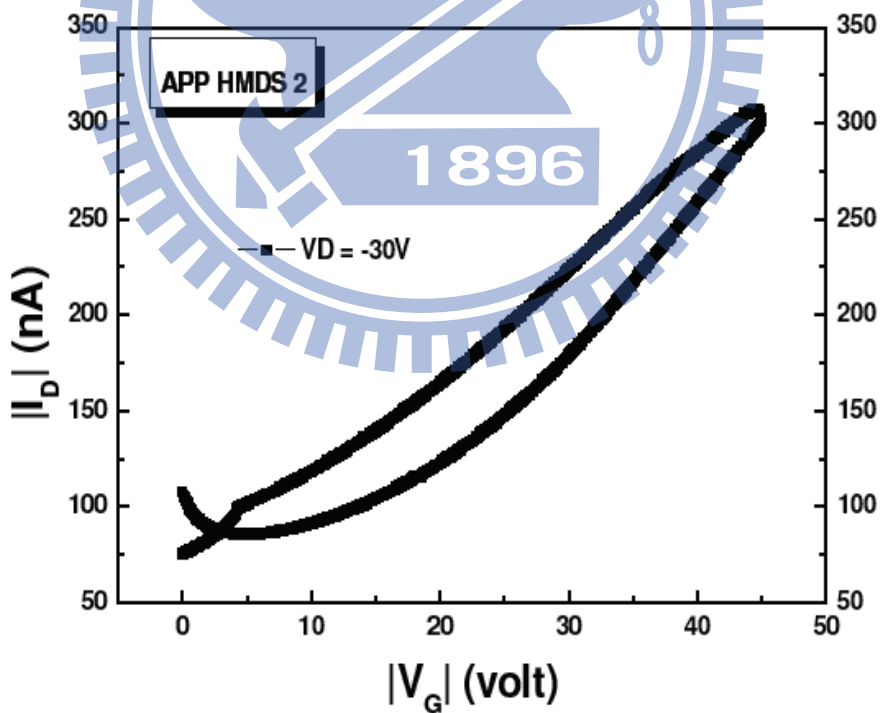


Figure 3-30: Hysteresis of P_3HT OTFTs with APP 2 times surface treatment.

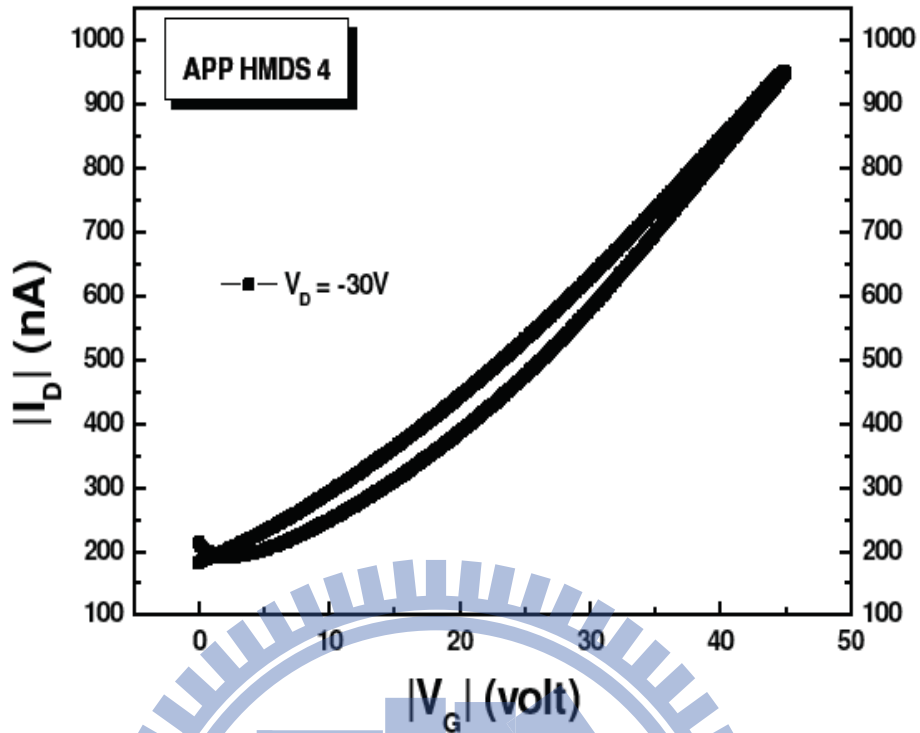


Figure 3-31: Hysteresis of P₃HT OTFTs with APP 4 times surface treatment.

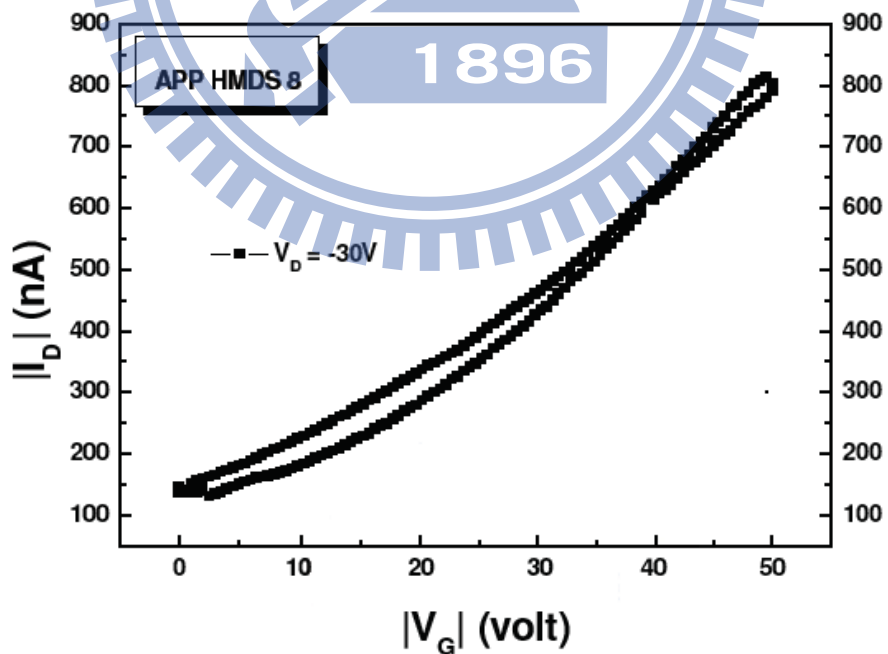


Figure 3-32: Hysteresis of P₃HT OTFTs with APP 8 times surface treatment.

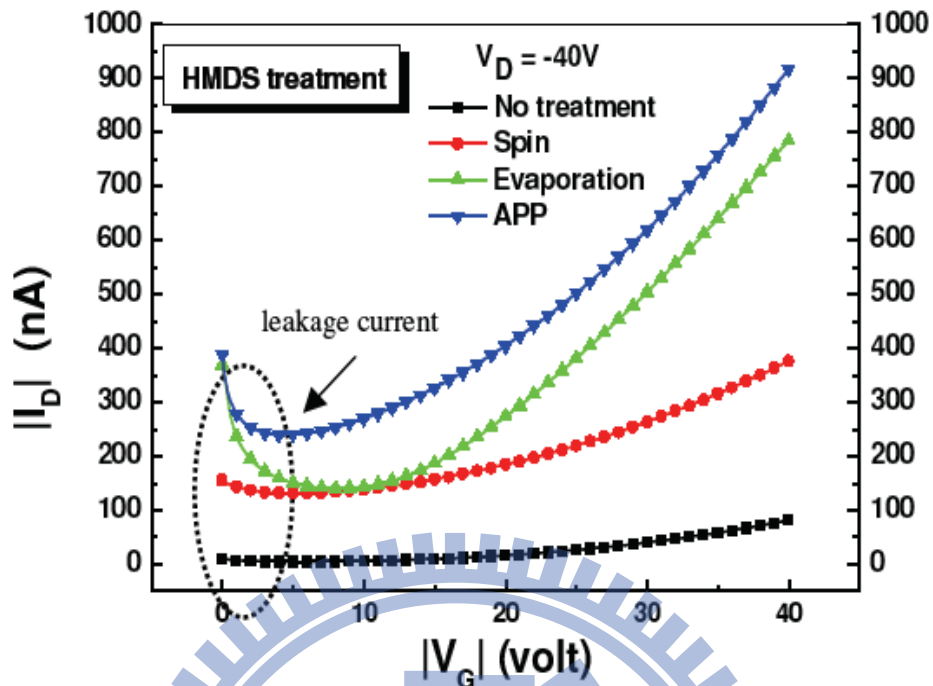


Figure 3-33: I_D versus V_G for various surface treatment processes and the gate leakage currents in V_G approaches 0 V.

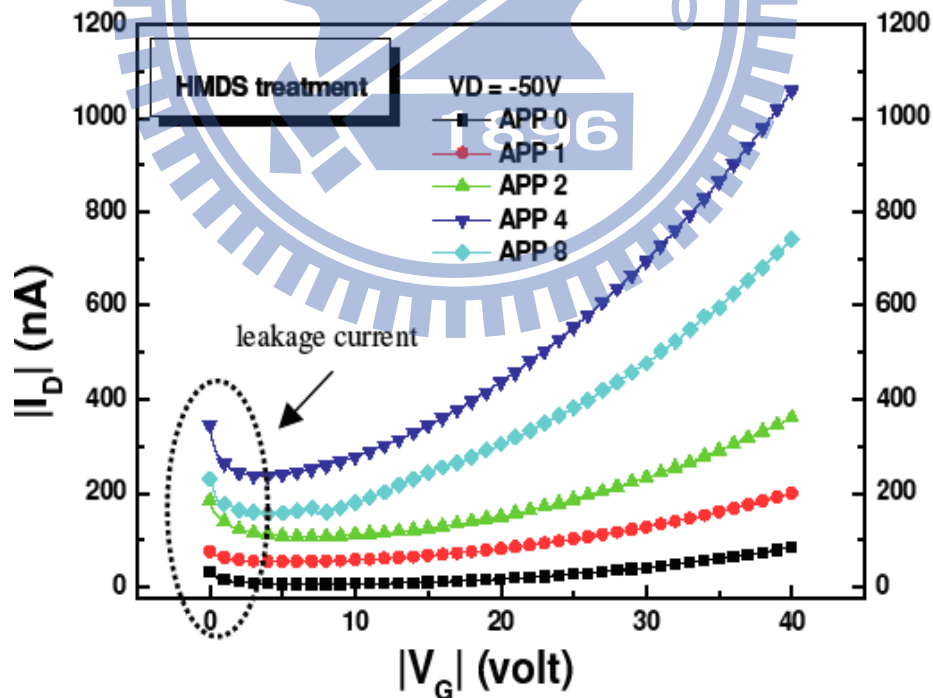


Figure 3-34: I_D versus V_G for different numbers of APP scans and the gate leakage currents in V_G approaches 0 V.

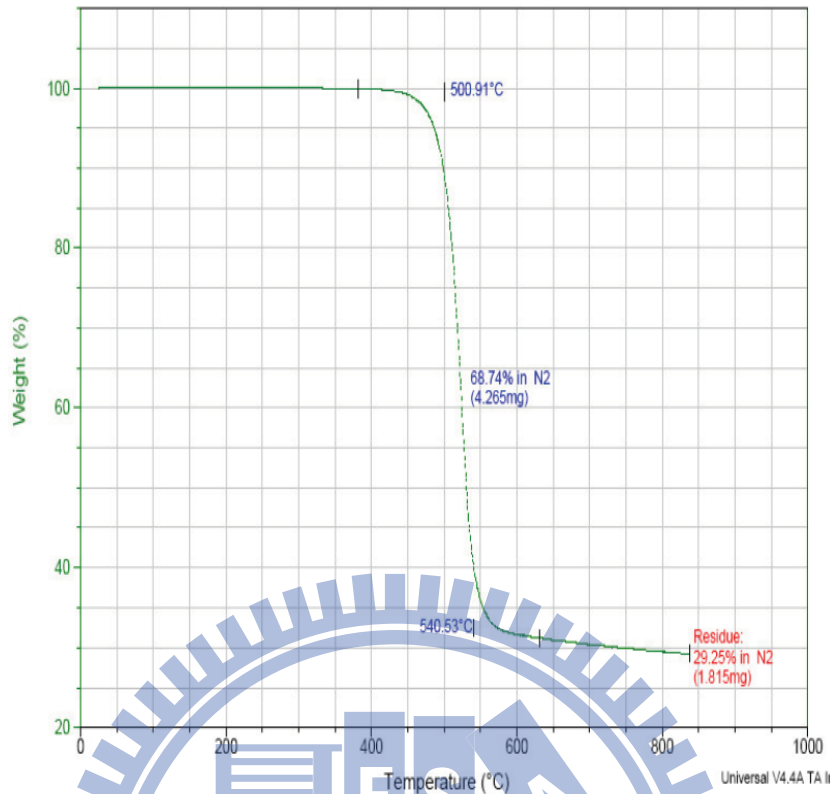


Figure 3-35: TGA thermograph of P₃HT 5 % weight loss is about 500°C .

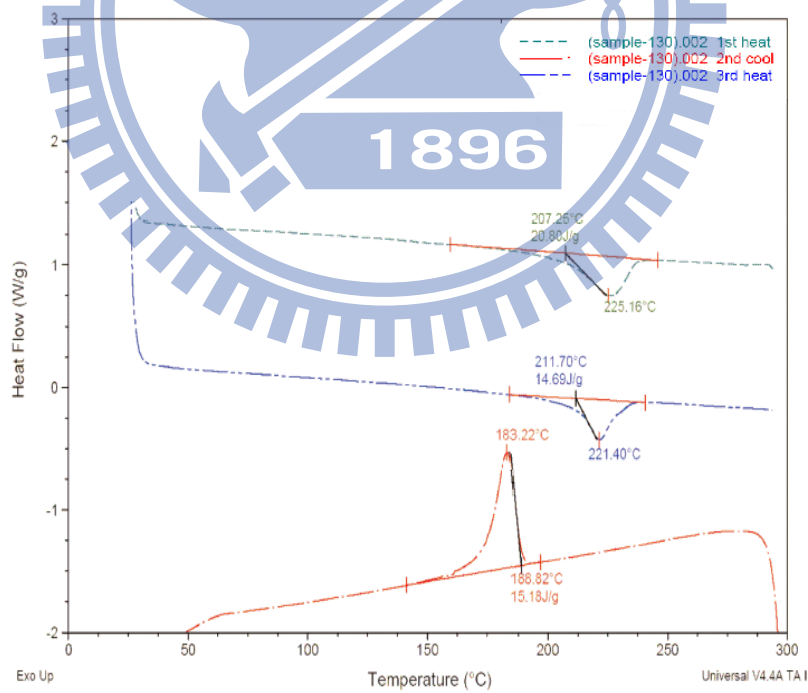


Figure 3-36: DSC thermograph of P₃HT was pre-heating at the temperature of 70°C for 3 min.

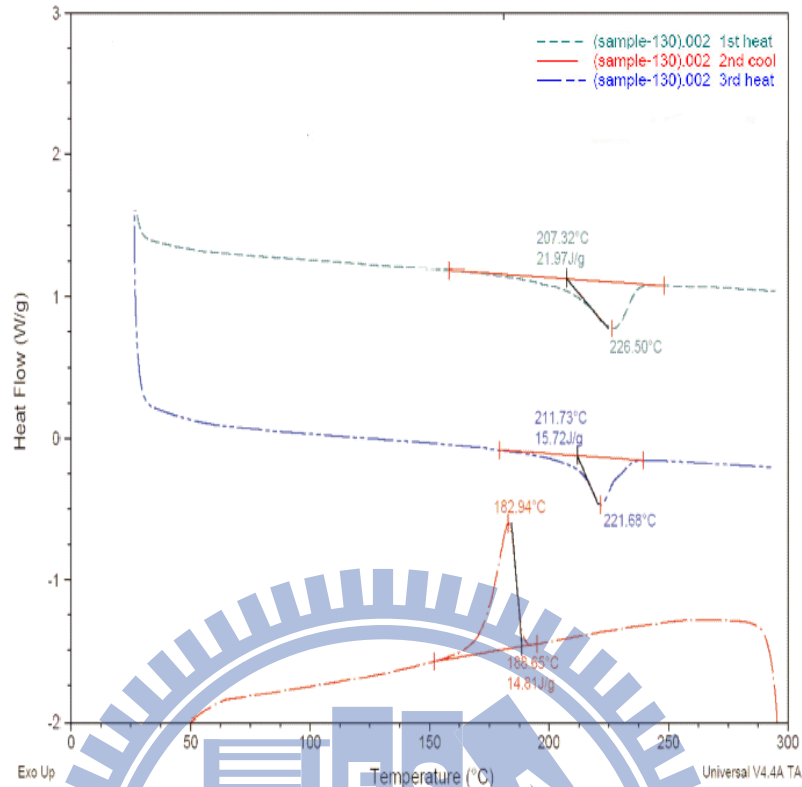


Figure 3-37: DSC thermograph of P₃HT was pre-heating at the temperature of 90°C for 3 min.

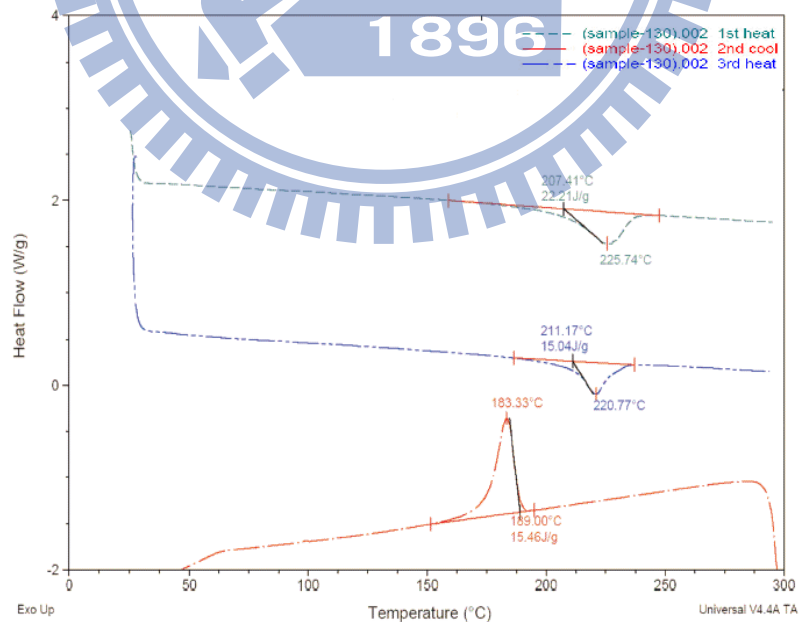


Figure 3-38: DSC thermograph of P₃HT was pre-heating at the temperature of 110°C for 3 min.

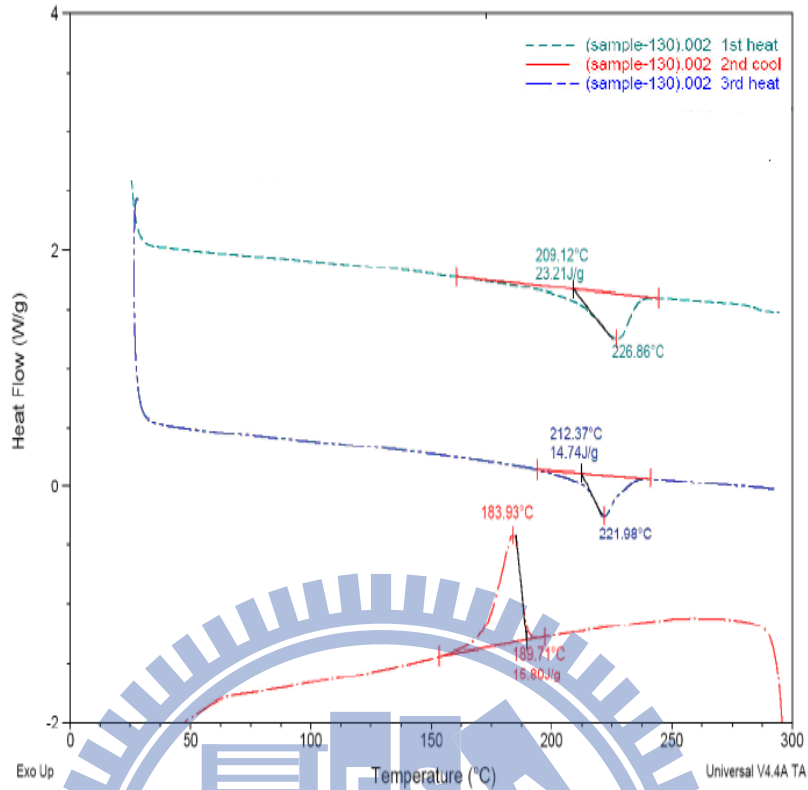


Figure 3-39: DSC thermograph of P₃HT was pre-heating at the temperature of 130°C for 3 min.

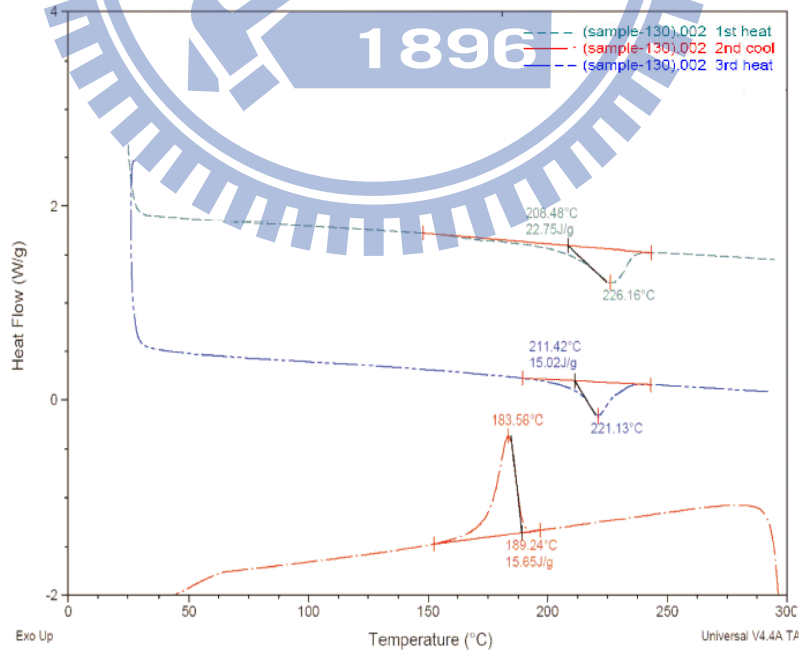


Figure 3-40: DSC thermograph of P₃HT was pre-heating at the temperature of 150°C for 3 min

Table 3-5 : T_m and ΔH of P_3HT in Run 1&2 with difference pre-heating temperature.

Pre-heating Temperature	Heat Run 1		Heat Run 2	
	$T_m(^{\circ}C)$	Entropy(J/g)	$T_m(^{\circ}C)$	Entropy(J/g)
70	225.16	20.81	221.41	14.69
90	226.51	21.97	221.68	15.72
110	225.74	22.21	220.77	15.04
130	226.86	23.21	221.08	14.74
150	226.16	22.75	221.13	15.02

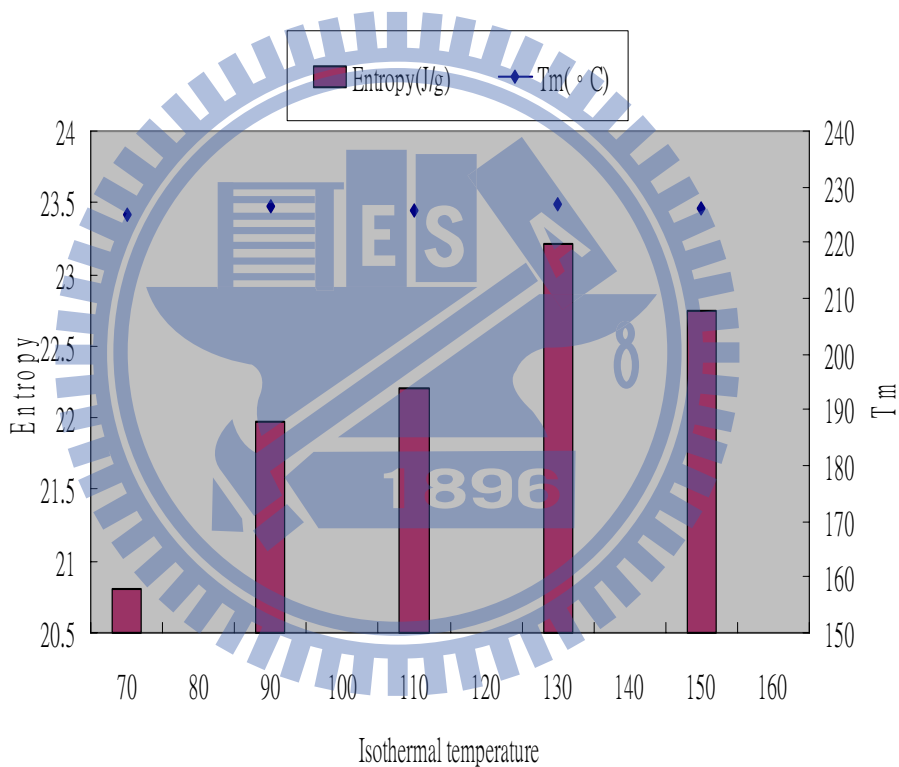


Figure 3-41: T_m and ΔH of P_3HT in Run 1 with difference pre-heating temperature.

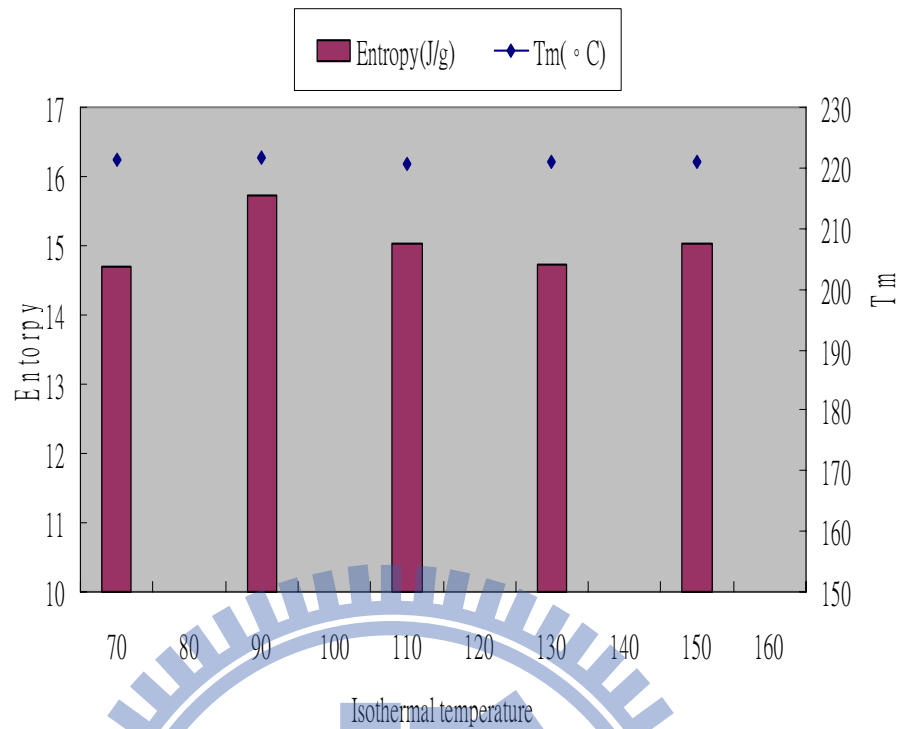


Figure 3-42 : T_m and ΔH of P₃HT in Run 2 with difference pre-heating temperature.

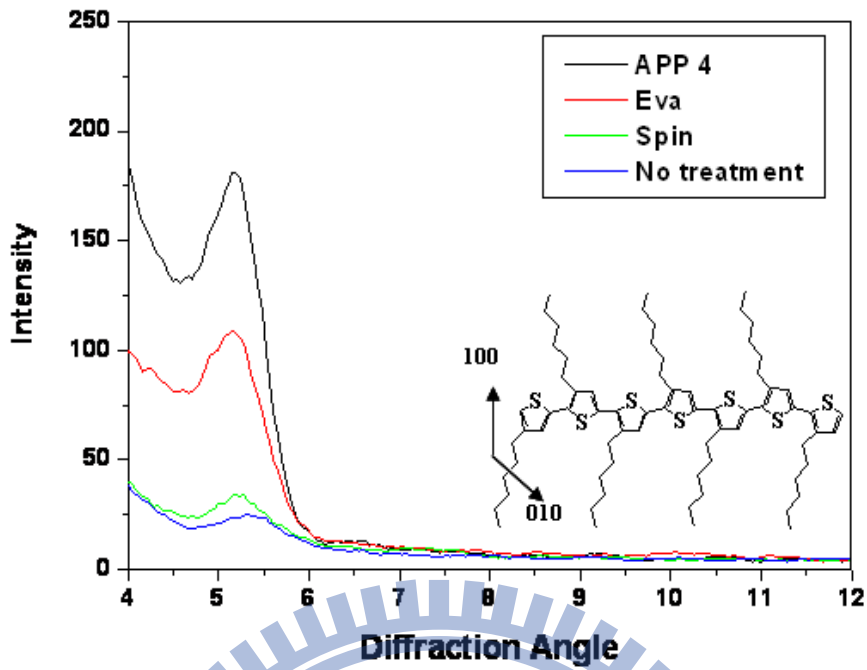


Figure 3-43: X-ray analysis of deposition of P₃HT on SiO₂ dielectric layer with various surface treatments.

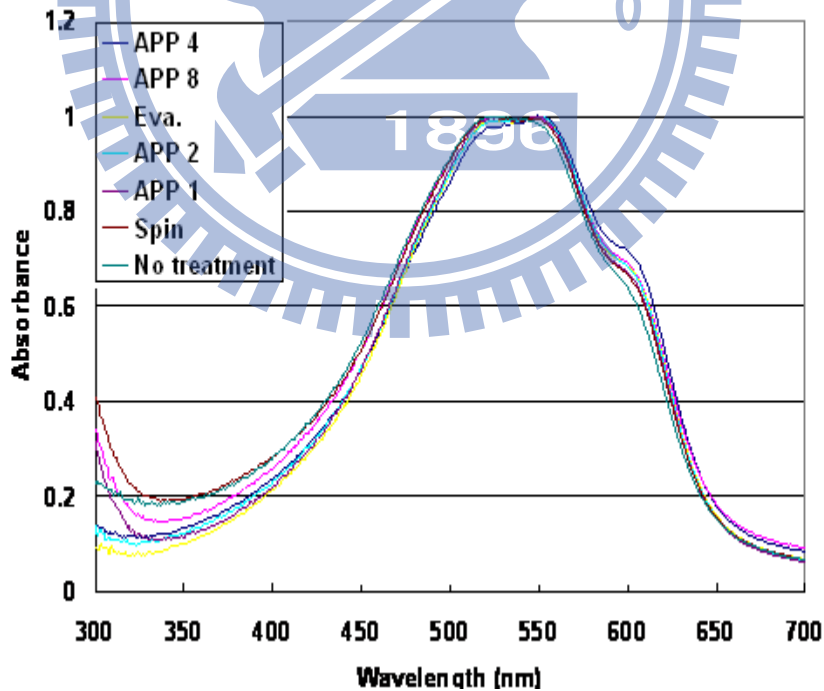


Figure 3-44: UV-VIS absorption spectra of P₃HT films that are deposited on SiO₂ dielectric layers following various surface treatments, normalized to the maxima of the spectra.

Chapter 4

Conclusions and Future Work

4.1 Conclusions

OTFT with P₃HT deposited as an active layer was fabricated on SiO₂ substrate. Electrical measurements yielded typical I-V characteristics of the TFT. In this work, APPT surface treatment methods were adopted to modify parts of the device to realize OTFTs that operate at low voltages with high mobility and good electrical stability. Surface treatment was employed to transform the hydrophilic surface to a hydrophobic surface, and to passivate surface hydroxyl groups, improving the orientation, enlarging the grains of the P₃HT films and increasing the field-effect mobility. The SiO₂ surface became hydrophobic upon the deposition of HMDS by APPT, and the field-effect mobility increased as the surface energy decreased. The highest mobility ($\sim 2.6 \times 10^{-2} \text{ cm}^2/\text{Vs}$) was associated with APP 4. The contact angles of APP 4 and APP 8 were similar, but the field-effect mobility of APP 8 was lower than that of APP 4. APP 8 may have been too rough to cause scattering. The surface roughness of the gate dielectric is generally an important parameter that determines device performance and the morphology of the deposited organic semiconductor film.

Increased roughness is associated with valleys in the channel region, which can act as carrier traps and scattering sites. The above demonstrates that the surface free energy (hydrophobic state) and surface roughness of gate dielectrics were

factors that affect the performance of the OTFT. The field-effect mobility is increased with the increment of hydrophobic state, but decreases as the surface roughness increases.

Two methods of surface treatment, spin-coating HMDS and evaporated HMDS, were performed. These two methods were associated with clear improvements in the experiments. The mobility in the saturation region was 4 times higher for spin-coating HMDS ($\mu_{\text{sat}} = 7.8 \times 10^{-3} \text{ cm}^2/\text{Vs}$) and 11 times higher for evaporated HMDS ($\mu_{\text{sat}} = 2.2 \times 10^{-2} \text{ cm}^2/\text{Vs}$) than without treatment ($\mu_{\text{sat}} = 1.9 \times 10^{-2} \text{ cm}^2/\text{Vs}$). HMDS-treatment of SiO_2 reduces the threshold voltage. The magnitude of the saturation current at a given operating voltage and mobility of the OTFTs follows the order APP4 > Evaporation > Spin-coating > No treatment. APPT is still better than the other methods of HMDS-treatment of SiO_2 in the experiment, perhaps because the APP uses chemical bonds to stack material on the SiO_2 surface, so the HMDS film becomes denser, and thus hydrophobic at the same deposited thickness, improving the performance of the OTFTs.

X-ray diffraction and UV-vis are adopted to provide direct evidence of highly oriented crystals at the interface between the polymer and the dielectric where the current flows in thin-film transistors. The degree of order of the lamellar structure follows the order APP 4 > Eva > Spin > No treatment, which was consistent with the mobility of OTFT, and demonstrated that high mobility requires an ordered structure. Furthermore, the formation of well-defined orientation of P_3HT grains markedly reduces the hysteresis by reducing the number of grain boundaries. Surface treatment by evaporation indicated was associated with better hysteresis than other methods of surface treatment; hence -OH groups, the orientation of P_3HT and the surface roughness of the gate dielectric surface were responsible for

the hysteresis behavior observed in OTFTs. Finally, according to the I_D-V_G plots, the current increased as V_G approached 0 V, especially when the surface was treated by APP. An anomalous leakage current may have been responsible for this phenomenon. The increase in the gate leakage current may have had two causes - one was weak points, and the other was the high channel conductance of the OTFTs.

This investigation has suggested an interesting direction for the preparation of high-performance OTFTs with high efficiency, involving low-temperature surface treatment by APPT. The low-temperature process and large area deposition associated with APPT surface treatment offer a great improvement in performance. Therefore, APPT has great potential for use at low-temperature and under atmospheric conditions.

4.2 Future work

The performance of P_3HT can be improved as described below.

4.2.1 In-situ passivation layer for protecting the P_3HT film

P_3HT OTFTs are sensitive to ambient conditions. Therefore, protection from the environment by encapsulation is essential to their stability. Hence, the use of a suitable material as passivation to protect the P_3HT film from environmental effects is an important topic.

4.2.2 Novel method for depositing P_3HT thin films

Three methods can be used to deposit P_3HT thin films: (1) spin-coating(2) dip-coating (3) drop-casting. The experiment in this work adopted the spin-coating

method to deposit P₃HT thin films. The best of these methods is drop-casting. Therefore, in the future drop-casting can be used in our experiment.

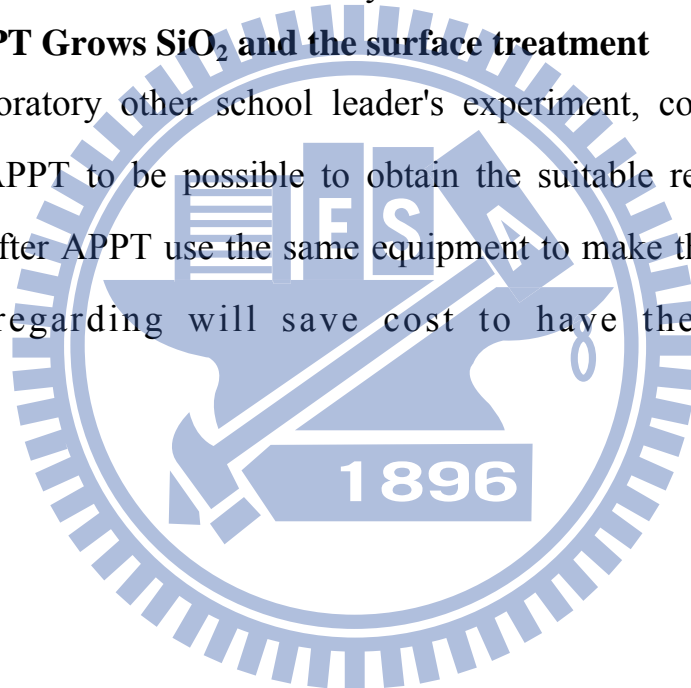
4.2.3 Thermal stability of P₃HT OTFT

Like the device lifetime and the stability of P₃HT in various ambients, thermal stability is an important topic, and for several OR numerous reasons.

For example, poly(3-hexylthiophenes) devices are likely to be exposed to high elevated temperatures during fabrication. Thermal cycling studies provide essential insights into device lifetime and stability.

4.2.4 Use APPT Grows SiO₂ and the surface treatment

In the laboratory other school leader's experiment, confirmed that grows SIO₂ using APPT to be possible to obtain the suitable result, we may unify grows SIO₂ after APPT use the same equipment to make the following surface treatment, regarding will save cost to have the suitable result.



References

- [1] C. J. Drury, C. M. Mutsaers, C. M. Hart, M. Matters and D. M. de Leeuw: Appl. Phys. Lett. 73 (1998) p108.
- [2] M. G. Kane, J. Campi, M. S. Hammond, F. P. Cuomo, B. Greening, C. D. Sheraw, J. A. Nichols, D. J. Gundlach, J. R. Huang, C. C. Kuo, L. Jia, L. H. Klauk and T. N. Jackson: IEEE Electron Device Lett. 21 (2001) p 534.
- [3] W. Fix, A. Ullmann, J. Ficker and Clemens: Appl. Phys. Lett. 81 (2002) p 1735.
- [4] C. D. Sheraw, L. Zhou, J. R. Huang, D. J. Gundlach, T. N. Jackson, M. G. Kane, I. G. Hill, M. S. Hammond, J. Campi, B. K. Greening, J. Francl and J. West: Appl. Phys. Lett. 80 (2002) p1088.
- [5] Y. Fujisaki, Y. Inoue, H. Sato, T. Kurita, S. Tokito and H. Fujikake: Proc. Int. Display Workshop (2003) (IDW'03), p291.
- [6] Y. Inoue, Y. Fujisaki, T. Suzuki, S. Tokito, T. Kurita, M. Mizukami, N. Hirohata, T. Tada and S. Yagyu: Proc. Int. Display Workshop (2004) (IDW'04), p 355.
- [7] Y. Taur and T. H. Ning, Fundamentals of Modern VLSI Devices, Cambridge University Press, New York, (1998), p 11.
- [8] H. E. Katz, Z. Bao and S. L. Gilat: Acc. Chem. Res. 34 (2001) pp359.
- [9] Y. Y. Lin, D. J. Gundlach, S. F. Nelson and T. N. Jackson: IEEE Electron Device Lett. 18 (1997) p606.
- [10] F. J. Mayer zu Heringdorf, M. C. Reuter and R. M. Tromp: Nature 412 (2001) p517.
- [11] D. J. Gundlach, H. Klauk, C. D. Cheraw, C. C. Kuo, J. R. Huang and T. N. Jackson: Electron Devices Meet., 1999, IEDM Tech. Dig., Washington, D.C., (1999), p. 111.

- [12] D. J. Cundlach, Y. Y. Lin, T. N. Jackson, S. F. Nelson and D. G. Schlom, IEEE Electron Device Lett. 18,(1997) 87
- [13] Zhenan Bao, a) ananth Dodabalapur, and Andrew J. Lovinger ; "Soluble and processable regioregular poly(3-hexylthiophene) for thin-film transistor applications with high mobility" Appl. Phys. Lett., Vol. 69, No. 26, (1996)
- [14] Bao, Z.; Lovinger, a. J, "Soluble Regioregular Polythiophene Derivatives as Semiconducting Materials for Field-Effect Transistors" Chem. Mater.(Article); 1999
- [15] Sirringhaus, Henning; Tessler, Nir; et al. "Integrated optoelectronic devices based on conjugated polymers", Science, 06/12/98, Vol. 280 Issue 5370, p1741
- [16] Sirringhaus, H.; Brown, P. J.; Friend, R. H.; Nielsen, M. M. ; Bechgaard, K.; Langeveld-Voss, B. M. W.; et. al. " Microstructure-mobility correlation self-organised, conjugated polymer field-effect transistor" Synth. Metals, Vol. 111-112, pp.129-132
- [17] Guangming Wang, Jmaes Swensen, Daniel Moses, and Alan J. Heeger, "Increased mobility from regioregular poly(3-hexylthiophene) at different length scales," Nanothechnology, Vol.93, no. 10, pp.6137-6141, 2003
- [18] H. Sirringhaus, P. J. Brown, R. H. Friend, M. M. Nielsen, K. Bechgaard, B. M. W. Langeveld-Voss, A. J. H. Spiering, R. A. J. Janssen, E. W. Meijer, P. Herwig & D. M. de Leeuw; "Two-dimensional charge transport in self-organized, high-moility conjugated polymers" Nature, Vol401,(1999)
- [19] T. A. Chen, X. Wu, and R. D. Rieke, J. Am. Chem. Soc. 117 (1995) pp233.
- [20] R. D. McCullough, R. D. Lowe, M. Jayaraman, and D. L. Anderson, J. Org. Chem. 58 (1993) p904 .
- [21] Prosa, T. J., Winokur, M. J., Moulton, J., Smith, P. Heeger, and A. J., Macromolecules 25 (1992) p4364.
- [22] Chrisos D. Dimitralopoulos, Parick R. Malenfant, " Organic thin film transistors for large are electronics" Adv. Mater. (2002)
- [23] A. Assadi. C. Svensson, M. Willander, O. Inganas, "Field-effect mobility of poly(3-hexylthiophene)" Appi. Phys. Lett. 53(3), (1988)

- [24] Howard E. Katz,* Joyce G. Laquindanum, and Andrew J. Lovinger ; “ Synthesis, Solubility, and Field-Effect Mobility of Elongated and Oxa-Substituted α, ω -Dialkyl Thiophene Oligomers. Extension of “polar Intermediate” Synthetic Strategy and Solution Deposition on Transistor Substrates” ; Chem, Mater. 1998,10, 633-638.
- [25] Giles Lloyd, Munira Raja, Ian Sellers, Naser Sedghi, Raffaella Di Lucrezia, Simon Higgins, Bill Eceleston ; “The properties of MOS structures using conjugated polymers as the semiconductor” ; Microelectronic Engineering 59(2001) pp323-328
- [26] Cheng Yang, FRANCESCO p. Orfino, and Steven Holdcroft, “A Phenomenological Model for Predicting Thermochromism of Regioregular and Nonregionregular poly(3-hexylthiophenes)” *Macromolecules*, Vol. 29, No. 20, 1996
- [27] Amundson, Karl r.; Sapjeta, B. Joyce; Lovinger, Andrew J.; Bao, Zhenan “An in-plane anisotropic organic semiconductor based upon poly(3-hexylthiophene)” Volume: 414, Issue: 1, July 1, (2002) p. 143-149
- [28] Hagen Llauk, Gunter Schmid, Wolfgang Radlik, Werner Weber, Lisong Zhou, Chris D. Sheraw, Jonathan A.Nichols, Thomas N.jackson; “ Contact resistance in organic thin film transistors”; *Solid-State Electronics* 47 (2003) pp297-301
- [29] Graciela B. Blanchet, C. R. Fincher, And Micheal Lefenfeld”Contact resistance in organic thin film transistors” *Appl. Phys. Lett*, Vol 84, no. 2, (2004)
- [30] Giles Lloyd, Munira Raja, Ian Sellers, Naser Sedghi, Raffaella Di Lucrezia, Simon Higgins, Bill Eccleston; “The properties of MOS structures using conjugated polymers as the semiconductor” ; *Microelectronic Engineering* 59 (2001) pp323-328
- [31] J. H. Lin”The Analysis of Process Improvement and Reliability Characteristic of Spin-On Organic TFT”, Graduate thesis
- [32] Y. Chen, I. Shin and S. Xiao, *Journal of Applied Physics*, vol. 96, no3 1, 2004
- [33] A.R. Brown, C. P. Tarrent, D.M. de Leeuw; “Field-effect transistor made from solution-processd organic semiconductors” ; *Synthetic Metals* 88 (1997) pp37-55
- [34] J. Veres, S. Ogier, G. Lloyd, and D. Leeuw, *Chem. Mater.* 16 (2004)pp4543.
- [35] A. Facchetti, M. H. Yoon, and T. J. Marks, *Adv. Mater.* 17 (2005) pp1705.

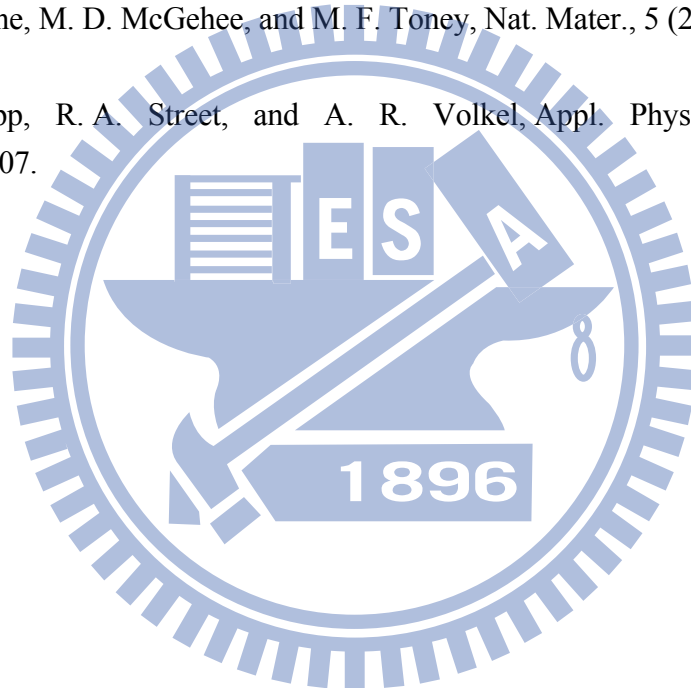
- [36] Y. Sun, Y. Liu, and D. Zhu, *J. Mater. Chem.* 15 (2005) pp53.
- [37] D. G. Oteyza, E. Barrena, J. Osso, and H. Dosch, *Appl. Phys. Lett.* 87 (2005) 183504.
- [38] I. Yagi, K. Tsukagoshi, and Y. Aoyagi, *Appl. Phys. Lett.* 86 (2005)103502.
- [39] S. Kobayashi, T. Nishikawa, T. Takenobu, S. Mori, T. Shimoda, T. Mitani, H. Shimotani, N. Yoshimoto, S. Ogawa, and Y. Iwasa: *Nat. Mater.* 3 (2004) pp317.
- [40] P. Too, S. Ahmed, B. J. Sealy, and R. Gwilliam: *Appl. Phys. Lett.* 80(2002) 3745.
- [41] H. J. Ahn, S. J. Rho, K. C. Kim, J. B. Kim, B. H. Hwang, C. J. Park, and H. K. Baik: *Jpn. J. Appl. Phys.* 44 (2005) 4092.
- [42] R.F. Gould (Ed.), "Contact Angle, Wettability and Adhesion", Proceeding of the 144th Meeting of the American Chemical Society, Vol.43, Washington, DC, 1964
- [43] R.J. Good, "Contact angle wetting and adhesion: a critical review", in:K.L. Mimal (Ed.), *Contact angle, Wettability and Adhesion*, USP, The Netherlands, 1993, pp. 3–36.
- [44] H. Klauk, D.J. Gundlach, J.A. Nichols, C.D. Sheraw, M. Bonse, T.N. Jackson, *Solid State Technol.* 43 (3) (2000) pp63.
- [45] H. Sirringhaus, N. Tessler, and R. H. Friend, "Integrated Optoelectronic-Devices Based On Conjugated Polymers,"*Science* 280, 1741 (1998).
- [46] H. Sirringhaus, N. Tessler, and R. H. Friend, "Integrated, High-Mobility Polymer Field-Effect Transistors Driving Polymer Light-Emitting Diodes," *Synth. Met.* 102 (1999). p85
- [47] S. C. Lim, S. H. Kim, J. H. Lee, M. K. Kim, D. J. Kim, T. Z., "Surface-treatment effects on organic thin-film transistors" *Synth. Met.*

148, (2005)pp75-79.

- [48] N. Karl in *Organic Electronic Materials*, Springer Series in Material Science, Vol. 41, edited by R. Farchioni and G. Grosso ~Springer, Berlin (2001).
- [49] R. J., M. D., M. L., and M.F. Toney “Highly oriented crystals at the buried interface in polythiophene thin-film transistors” *nature materials*, vol 5, March (2006).
- [50] C. Y. Chang, *ULSI Devices*, Wiley, New York, 2000.
- [51] C. S. Kim, S. J. Jo, S. W. Lee, and S. J. Lee, *Adv. Funct. Mater.* 17 (2007) p958.
- [52] S. Y. Park, M. Park, and H. H. Lee, *Appl. Phys. Lett.* 85 (2004) pp2283.
- [53] E. M. Muller, and J. A. Marohn, *Adv. Mater.* 17 (2005) pp1410.
- [54] A. Salleo, F. Endicott, and R. A. Street, *Appl. Phys. Lett.* 86 (2005)263505.
- [55] W. Kim, A. Javey, O. Vermesh, Q. Wang, Y. Li, and H. Dai, *Nano Lett.* 3 (2003) p193.
- [56] D. K. Schroder, *Semiconductor Material and Device Characterization*, 2nd ed., Wiley, New York 1998.
- [57] G. Wang, D. Moses, and A. J. Heeger, *J. Appl. Phys.* 95 (2004)p 316.
- [58] H. Jia, G. K. Pant, E. K. Gross, R. M. Wallace, and B. E. Gnade, *Organic*
- [59] T. A. Chen, X. M. Wu, and R. D. Rieke, *J. Am. Chem. Soc.* 117 (1995) p233.
- [60] E. J. Samuelsen and J. Mardalen, in *Handbook of Organic Conductive Polymers*, edited by H. S. Nalwa ~Wiley, Weinheim, 1997, Vol. 3, *Conductive Polymers: Spectroscopy and Physical Properties*, pp. 100-06.
- [61] P. J. Brown, D. S. Thomas, and J. S. Wilson, *Physical Review B*67 (2003) 064203.
- [62] Z. Bao, A. Dodabalapur, and A. J. Lovinger, *Appl. Phys. Lett.* 69 (1996)

p4108.

- [63] Y. Sun, Y. Ma, Y. Liu, Z. Wang, and Y. Wang, *Adv. Funct. Materials* 16(2006) p426.
- [64] Y. Kim, S. Cook, and S. M. Tuladhar, *Journal of Applied Physics* 93(2003) 6137.
- [65] G. Wang, J. Swensen, D. Moses, and A. J. Heeger, *Nat. Mater.*, 5 (2006) p197.
- [65] G. Wang, J. Swensen, D. Moses, and A. J. Heeger, "Increased mobility from regular poly(3-hexylthiophene) field effect transistor" *J. Appl. Phys.* 93 pp6137, 2003
- [67] R. J. Kline, M. D. McGehee, and M. F. Toney, *Nat. Mater.*, 5 (2006) 222.
- [68] D. Knipp, R. A. Street, and A. R. Volkel, *Appl. Phys. Lett.*, 82 (2003) 3907.



簡歷

姓 名:洪 柏 誠

性 別:男

出生日期:民國 67 年 12 月 4 日

住 址:屏東縣潮州鎮崙東里崙東路 437 巷 1-7 號

學 歷:省立屏東高中

私立大葉大學電機系

國立交通大學電機學院 電子與光電學程 碩士班

碩士論文:利用大氣電漿對有機半導體之介電層表面做改質研究

**Modify Surface of dielectric layer on polymer thin-Film
transistors by atmospheric-pressure plasma technology**

